A MEASUREMENT OF THE LIFE-TIME OF THE D MESON.

Lionel Edwin Sacks

Royal Holloway and Bedford New College

University of London

This Thesis is submitted in part fulfillment of the requirements for the degree of Ph.D. at the University of London

January 1987

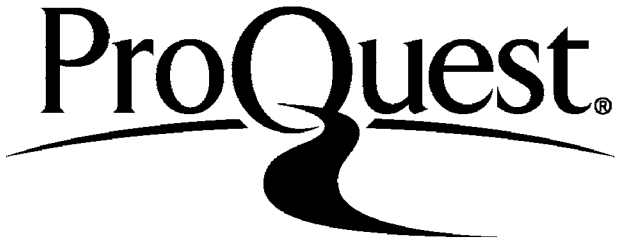

Contents

List of Tables

List of Figures

Abstract

A preliminary measurement is presented of the lifetime of the ground state neutral charm meson, the D^0. This study utilised data taken by the NA1 experiment running on the CERN SPS accelerator.

A tagged photon beam was used with energies between 70 and 175Gev and the FRAMM spectrometer provided final state particle identification. The D meson production and decay points were measured with an electronically read out monolithic germanium target followed by silicon strip detectors. Charm events were identified by the reconstruction of D^0 meson invariant masses where the D^0 originated from a D^* decay and decayed to final states containing charged kaons.

A sample of 90 $D^0/\bar{D}^0$ decay events was found. These were measured to have a lifetime of:

$$\tau_D = (3.7 \, ^{+0.6}_{-0.5} \pm 0.2) \cdot 10^{-13} s$$

Author's Contribution to the Experiment

During the setting up and physics runs of the experiment I assumed some responsibility for the vertex drift chamber Verginella and for some aspects of the trigger logic and monitoring. In addition I contributed to the general running of the data acquisition shifts.

For the data reconstruction I developed the analysis for the Verginella drift chamber and the new Pad Readout Streamer chamber in the SD1 calorimeter. For the target, I developed some of the analysis software, helped in writing the Monte Carlo simulation programme and in assessing its performance.

The analysis presented in Chapters Five and Six is entirely my own work.

Acknowledgements

The acknowledgement section of a thesis is the place to thank those people who have been helpful and encouraging during the period of study for the thesis. It is also the place for some compulsory acknowledgements of those people and organisations without whose assistance the thesis would not have been possible. I will try to make the distinction between those I must and those I want to thank the least unclear thing in this thesis.

I would like to thank Phil March and Ted Bellamy for inviting me to join their group in 1983 and for their advice and support in the subsequent years, especially teaching me that even professors pull wires. My thanks are also extended to the other members of the Royal Holloway HEP group John, Murah, Greg, Amire and more recently Jed for their help and company, especially Mike Green for his supervision and keen sense of statistics.

My period of study was financed by the SERC whom I thank not only for the money but for the support extended by that organisation through the liaison office staff at CERN.

I spent 14 months at CERN during which time I worked with a number of members of the FRAMM collaboration. I would like to thank all these people, especially Lorenzo Foa, for allowing me to work on their experiment and teaching me about so many of the problems which may be encountered in performing large experiments.

During this stay at CERN I met a number of my peers from whom I learned a great deal about the world of physics, especially the manipulation of ethanol. Among others I note particularly Daniella, Ian, Sarah, Tim, John, Tex, Phil, Steve, Neil and Nigel for making my stay that much more interesting. Omitted from this list is Chris Bee to whom I owe special thanks for his inspiring skiing. Special thanks also to Graham Beck for his inspiring consumption of Cognac.

During the last year I have been working at Liverpool University on both my thesis and a new experiment. This combination undoubtedly degraded my performance on both counts. I owe a special thanks to Erwin Gabathuler for tolerating this situation and for his support and the support of the other members of the Liverpool physics department. In the last year I have also made a friend, Katherine Murray, whose support has been invaluable and whom I would like to thank.

That's now, but maybe I would have not come this far without: Ross, Sylvia, Lyn or Martin. This I gratefully acknowledge.

Finally, without the platitudes, my parents Benny and Becky....Thank You.

In Memoriam

For
Goldie Lan
and
Tilly Sacks

WHEN THE GOING GETS WEIRD,

THE WEIRD TURN PRO.

Hunter. S. Thompson

and

Ralph STEADman

The Curse of Lono

Introduction

The systems of elementary particles carrying the charm quantum number provided one of the first experimental verifications of the modern quark model theory of hadronic matter. This thesis constitutes a preliminary report on a measurement of the lifetime of the D^0 meson, the lowest lying mesonic state of the family of particles carrying open charm. The measurements reported here were made by the NA1 experiment using the FRAMM spectrometer equipped with an active target and using a high energy, high flux tagged photon beam with an energy range of 75Gev→170Gev produced by the 450Gev protons of CERN's SPS.

The active target, a combination of a monolithic germanium target and silicon strip detectors, was read out electronically at a high rate, allowing a large amount of data to be recorded. This contrasts with other high resolution vertex detectors such as bubble chambers and photographic emulsions, which limit the quantity of data taken because of both their operational rates and by the amount of work and time required for analysis.

The FRAMM target measured multiplicities of relativistic charged particles along the beam direction, allowing measurements of decay distances by the detection of changes of charge multiplicity. The use of the neutral photon beam allowed production of the hadronic systems of interest, without extraneous charged matter swamping the signals in the target due to other charged beam particles.

The FRAMM spectrometer has large acceptance for charged particle detection and for calorimetry. Two Čerenkov counters provided some discrimination between $K^{\pm}$, $\pi^{\pm}$, $e^{\pm}$ and $p^{\pm}$, with further particle identification from the calorimetry which, in addition to π^0,η and photon identification, distinguished between charged hadrons and electrons. The calorimetry of FRAMM was also used as part of the data acquisition trigger to distinguish between electromagnetic and hadronic interactions of the photon. Thus the data written to tape was highly enriched with hadronic events and the overall data acquisition was not swamped by the high rate of events due to electromagnetic pair production of e^+e^- by the beam.

The NA1 experiment was first proposed in 1974 [AMENDOLIA74] for hadronic interaction studies. It was updated in 1979 [AMENDOLIA79] for charm lifetime studies and took data in 1981. This data yielded a lifetime for the $D^{\pm}$ [ALBINI82]. Following the runs of NA7 and NA29 using the FRAMM spectrometer, NA1 was reapproved with an upgraded target, spectrometer and trigger configuration [AMENDOLIA82]. Further data was taken from May 1983 through to September 1984 covering SPS running periods; 5A, 5B and 5C in 1983 and 1B, 2A, 2B and 2C in 1984. Preliminary results

from these data have already been presented [AMENDOLIA86/1] for the D^0 lifetime. The presented result was produced independently of the analysis given in this thesis.

The results presented here are based on the data taken in the periods 5A and 5C (the active target was not used during period 5B). Selection of charmed events may be made by either reconstructing totally the event to detect all produced charmed particles - the exclusive analysis - or by detecting evidence for charm - the inclusive analysis. Due to expected problems with acceptance and efficiency, the former technique required considerable time to develop. As a first approach I selected to make an inclusive analysis using the channel of $D^{*\pm} \rightarrow D^0 \pi^{\pm}$ to provide a clear sample of events.

A review of important theoretical and experimental results related to measurements of the D^0 lifetime is given in Chapter One. A description of the apparatus is given in Chapter Two and its use for event reconstruction and particle identification in Chapter Four. The trigger and data acquisition are discussed in Chapter Three. A description of the analysis technique and final lifetime measurement are given in Chapters Five and Six.

Chapter One

Charm Physics

This chapter contains a review of the physics materially related to the production and decay of the neutral D meson. An outline of the theory related to these subjects is presented with little mention of the other charmed particles or new heavy particles containing top or bottom quarks. A short review of interesting measurements of the D^0 lifetime, decay modes and production mechanisms is given.

1.1. Theory of Charm Physics

Historically, the charm quantum number holds a special place in the development of the present theories of elementary particles - the standard model. Its introduction in 1970 by Glashow, Iliopolos and Maiani (GIM) [GLASHOW70] as part of the mechanism for suppressing strangeness-changing neutral currents in weak decays of hadrons preceded the first detection of a charmed particle, the J/Ψ, by 4 years [AUBERT74, AUGUSTIN74] although this was not the first occurrence of the charm quantum number in a theory. It is now accepted that there is a charm quantum number which may only be changed in weak interactions and that it is carried by the charm quark.

1.1.1. The Charm Quantum Number

A discussion of the charm quantum number c requires some understanding of group theory as used in the standard electro-weak model of fundamental interactions[¶]. The charm quark c extends the $SU(3)_F$ quark field with base vector q = (u,d,s) (where u=up, d=down and s=strange) to $SU(4)_F$ with q = (u,d,s,c). The subscript F is for flavour to distinguish these groups from other special unitary (SU) groups. The principal quantum numbers of each member of q are given in Table 1.1.

The elements of q preserve their identity under (*i.e.* represent conserved quantum numbers of) strong and electromagnetic (em) interactions. For weak interactions the vector q can be decomposed into two doublets of the weak lagrangian:

$$q' = \begin{pmatrix} c \\ s_c \end{pmatrix} \text{ and } q = \begin{pmatrix} u \\ d_c \end{pmatrix}$$

[¶] For the following discussion I have found the following particularly useful [AITCHISON, LEADER, PALMONARI84 and PERKINS].

with both left and right handed (negative and positive helicity) states. Here s_c and d_c are the Cabbibo mixtures:

$$d_c = d\cdot\cos\theta_c + s\cdot\sin\theta_c \quad \text{and} \quad s_c = s\cdot\cos\theta_c - d\cdot\sin\theta_c.$$

The angle θ_c is the Cabbibo or weak mixing angle and it has been measured to be 28.4°. With these quark fields, the standard model of electro-weak interactions describes the conserved currents which mediate in the interaction of elements of q, and between the elements of q and the leptonic doublets: $\binom{e}{\nu_e}_L$, $\binom{\mu}{\nu_\mu}_L$ and $\binom{\tau}{\nu_\tau}_L$. These currents are combined in the electro-weak lagrangian to calculate the interaction couplings between elementary particles. The hadronic terms of the electro-weak lagrangian are three-fold; the em current J^α_{em} and the neutral weak J^α_3, and charged weak currents J^α_+ and J^α_- (for charge raising and lowering interactions).

Quark Symbol	Electric charge (Units of e^-)	Isospin I_3	Flavour Number
u	$+\frac{2}{3}$	$+\frac{1}{2}$	-
d	$-\frac{1}{3}$	$-\frac{1}{2}$	-
s	$-\frac{1}{3}$	0	-1 (Strangeness)
c	$+\frac{2}{3}$	0	+1 (Charm)

Table 1.1. The Principal Quark Quantum Numbers

The elements of the electro-weak hamiltonian describe the coupling of quarks to the quanta of a gauge field. These quanta are the intermediate gauge vector bosons, the $W^\pm$ and Z^0, which mediate the charged and neutral weak interactions respectively, and the photon, γ, which mediates the em interactions. The $W^\pm$ and Z^0 are known to be heavy, of the order of 80Gev. For the small momentum transfers involved in charm decay the propagator of the gauge bosons is not important. In this case the original assumptions of the Fermi theory of weak interactions are good approximations to the full Weinberg-Salam model. The Fermi Lagrangian has the form:

$$L_F = \frac{G}{\sqrt{2}} J^\alpha(x)\, J^\dagger_\alpha(x) + \text{h.c.} \qquad (\alpha = 1,....,4) \qquad (1.1)$$

The factor $\frac{G}{\sqrt{2}}$ is the Fermi coupling constant and has a value of $1.1 \cdot 10^{-5} Gev^{-2}$. The original nucleon fields of the Fermi theory may be replaced by the quark fields q with the Cabbibo mixing described above. Further terms must be introduced to allow for the "handed" nature (Left or Right above) of the quarks and leptons (chirality). This requires the introduction of the operators $(1 \pm \gamma_5)$ which project out left and right handed states, together with the 4 vector Dirac matrices γ^μ in the explicit space time structure of $J^\alpha(x)$.

The em current term of (1.1) has the form:

$$J^\alpha_{em} = \bar{q}\gamma^\alpha \tfrac{1}{2}(\tau_3 + \tfrac{1}{3} I)q + \bar{q}' \gamma^\alpha \tfrac{1}{2}(\tau_3 + \tfrac{1}{3} I)q' \qquad (1.2)$$

where the γ are 4×4 matrices, composed of the Pauli 2×2 matrices, associated with the flavour quantum numbers. The element τ_3 is a 2×2 matrix associated with the isospin quantum number and I is the identity matrix. The neutral weak current has the form:

$$J^\alpha_3 = \bar{q}\,\gamma^\alpha \tfrac{1}{2}(1-\gamma_5)\,\tau_3\, q + \bar{q}'\,\gamma^\alpha \tfrac{1}{2}(1-\gamma_5)\,\tau_3\, q \qquad (1.3)$$

Using the q and q' of $SU(4)_F$ above, expanding (1.2) and (1.3), and suppressing the Dirac γ matrices gives:

$$J_{em} = \tfrac{2}{3} u\bar{u} + \tfrac{2}{3} c\bar{c} - \tfrac{1}{3} d\bar{d} - \tfrac{1}{3} s\bar{s} \qquad (1.4)$$

and

$$J_3 = u\bar{u} + c\bar{c} - d\bar{d} - s\bar{s} \qquad (1.5)$$

The interactions of equations (1.4) and (1.5) can be seen to conserve all flavours in neutral interactions. Without the c quarks in q, terms of the form: $Cos\theta_c Sin\theta_c(\bar{d}s + \bar{s}d)$ would appear, giving rise to predictions of interactions without charge exchange ($\Delta Q=0$), but which change the total strangeness ($\Delta S=\pm 1$). The fact that no such interactions have been observed at the rates that would be predicted [CLINE86] was the motivation for the GIM mechanism. Equation (1.4) also shows that in electromagnetic interactions, charm (u, s and d also) must be pair produced, *i.e.* the total charm content must be preserved. This will be discussed further in Section 1.3.

The charge exchange part of the weak current part of the lagrangian can change the flavour quantum numbers (u, d, s and c) of the system. This current has the form:

$$J^{\alpha}_{+} = 2\,\bar{q}_L\,\gamma^{\alpha}\,\tau_{+}\,q_L + 2\,\bar{q}'_L\,\gamma^{\alpha}\,\tau_{+}\,q'_L \qquad (1.6)$$

where the "+" subfix indicates that this is a charge raising current, and there is a conjugate charge lowering current J^{α}_{-}. Expanding the vector q gives:

$$J^{\alpha}_{+} = \bar{u}\,\gamma^{\alpha}\,(1 - \gamma_5)\,(\cos\theta_c d + \sin\theta_c s) + \bar{c}\,\gamma^{\alpha}\,(1 - \gamma_5)\,(\cos\theta_c s - \cos\theta_c d) \qquad (1.7)$$

The charged current can be seen to be flavour changing. Thus it is only through this term of the weak interaction Lagrangian that charm quarks can decay.

The quarks may be combined into multiplets to describe most of the observed elementary particles by treating them as group elements within a broken special unitary symmetry. The four quarks each constitute a degree of freedom in the $SU(4)_F$ group. With the additional degrees of freedom of spin, isospin and other symmetries, we may be led to higher order groups [CLOSE]. Higher order groups are also required to incorporate the new particles, heavier than charm, which contain the beauty quark (and it is believed top quarks also). However $SU(4)_F$ serves well to understand and classify a large number of observed particles and phenomena. In the quark model baryons are considered to be composed of sets of three quarks in a totally anti-symmetric wave function. With the empirical observation for some baryons to be symmetric in both spin and isospin, it is necessary to introduce the colour quantum numbers (y,r,b) and assign these to constituent quarks. Thus, for the colour quantum numbers, the baryon wave function has the form:

$$B_c = \frac{1}{\sqrt{6}}\,(ybr + ryb + bry - yrb - rby - byr) \qquad (1.8)$$

Mesons are considered to contain quark anti-quark pairs and the mesonic colour wave function has the form:

$$M_c = \frac{1}{\sqrt{3}}\,(\bar{y}y + \bar{r}r + \bar{b}b) \qquad (1.9)$$

Considering just the flavour degrees of freedom for mesons in q we can derive the multiplet structure for $q\bar{q}$ pairs from:

$$SU(3)_F: \quad 3 \otimes \bar{3} = 8 \oplus 1 \qquad (u, d, s) \qquad (1.10)$$

$$SU(4)_F: \quad 4 \otimes \bar{4} = 15 \oplus 1 \qquad (u, d, s, c) \qquad (1.11)$$

that is, an octet and a singlet for $SU(3)_F$ and a 15-tuplet and a singlet for $SU(4)_F$. The 15-tuplet of $SU(4)_F$ contains the octet and singlet of $SU(3)_F$. These are the mesons of a given spin parity (J^P) which contain the u d & s quantum numbers with c = 0. In addition, the 15-tuplet contains a c = -1 doublet, symmetric in isospin with $J^P = 0^-$ and identified with the D mesons s = 0, and an isospin singlet the D_s (the F) meson with strangeness s = 1 (again for $J^P = 0^-$).

The organisation of the mesons into the above multiplets is illustrated in Figure 1.1. The lines joining meson states represent transformations which may be performed by the flavour changing currents. Such interactions are seen in this context to be kinds of symmetry transformations within an $SU(4)_F$ group.

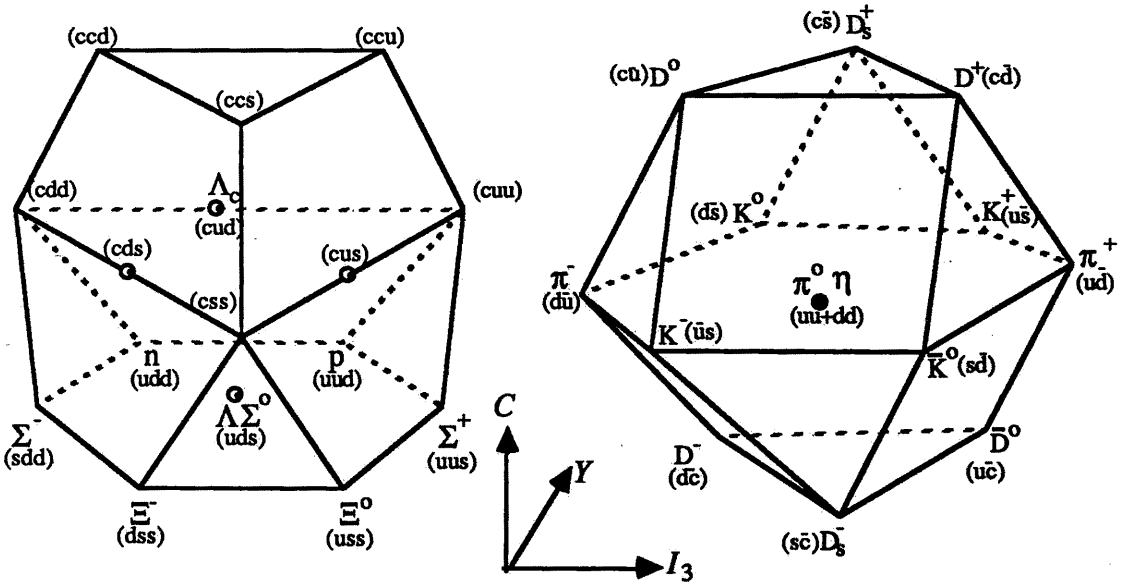

Figure 1.1. SU(4) Multiplet Structure

1.1.2. Charm Meson Decay Channels

For the D^0 decay there are no channels open for strong or em decays since it is the lightest of the charmed mesons. Thus all D^0 decays must occur through weak, charged current channels. The second term in equation (1.7) describes the transition of the c quark to the s quark as proportional to $Cos\theta_c$ and to the d proportional to $Sin\theta_c$ giving a ratio for the transition matrix elements of 8 : 2 ($Cos^2\theta_c$: $Sin^2\theta_c$). The transition of the c quark to the d is suppressed relative to its transition to the s. To understand the final states of charm particle decay the possible decays of the $W^{\pm}$ boson must also be considered. These final states are summarised in Table 1.2 below with the relative rates arising from the weak mixing angle. Figure 1.2 shows the Feynman diagrams for the c quark transforms. The decay rate of the c quark to s = 1 states is by far the largest among the hadronic decays so far as the weak mass mixing factors are concerned.

	Channel	Weak Mixing Factor	
i)	$c \rightarrow su\bar{d}$	$3Cos^4\theta_c$	1.797
ii)	$c \rightarrow su\bar{s}$	$3Cos^2\theta_c Sin^2\theta_c$	0.525
iii)	$c \rightarrow d\bar{d}u$	$3Cos^2\theta_c Sin^2\theta_c$	0.525
iv)	$c \rightarrow du\bar{s}$	$3Sin^4\theta_c$	0.153
v)	$c \rightarrow sl_+\nu$	$Cos^2\theta_c$	0.774
vi)	$c \rightarrow dl_+\nu$	$Sin^2\theta_c$	0.226

Table 1.2. Weak Mixing Factors

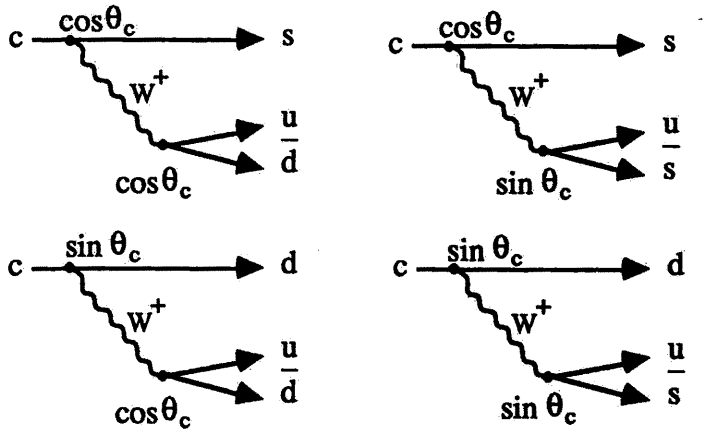

Figure 1.2. Feynman Diagrams for c Quark Weak Transforms

The final states of decays of particles containing charm depend on the hadronisation of the quarks both from the c decay, and from those already present in the decaying particle. Figure 1.3(a) shows the decay of a D^0 to a $K^-\pi^+$ final state. This is a spectator diagram for D^0 decay since the $\bar{u}$ quark is passive.Similar diagrams exist for the decays of the $D^{\pm}$ and $D_s^{\pm}$ mesons. An additional non-spectator diagram exists for the D^0 decay shown in Figure 1.3(b). Here the W^+ interacts with the $\bar{u}$ quark to transform it to a $\bar{d}$ through the first term in equation (1.7). The existence of these extra decay channels implies that the D^0 willhave a shorter lifetime than the $D^{\pm}$.

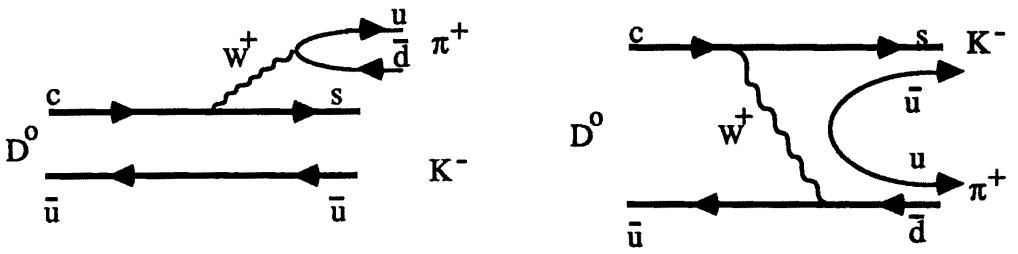

a) Spectator b) non-Spectator

Figure 1.3. D Decay Diagrams

The decay branching ratios (Br) of the charm mesons have been measured with good accuracy by experiments at e^+e^- colliders studying the decay of the Ψ'' to $D\bar{D}$ pairs, principally the MARK II and MARKIII experiments. There has been a shift of over 2s.d. in the values of the branching ratios measured by MARK III in 1985 [COWARD85, BALTRUSAITIS85] from those published by MARK II in 1981 [SCHINDLER81]. The 1981 results were found from measurements of the quantity $\sigma \cdot Br$ for each decay channel of the D meson. The cross-section was factored out between all the measurements to give the branching ratios.

The MARK III results were obtained from events in which both the D and $\bar{D}$ mesons are reconstructed. In this way branching ratios may be directly measured for each decay mode without inefficiencies from one channel influencing other channels. The branching ratios for the dominant hadronic decays of the D^0 are shown in Table 1.3 from MARK II, MARK III and from the current world averages given by the PDG [AGUILAR86] (The branching ratios for the $K^-\pi^+$ channel is an upper limit).

Channel	Branching Ratios (%)		
	MARK II	MARK III	World Average
$D^0 \rightarrow K^-\pi^+$	3.0±0.6	5.1±0.4±0.4	5.4±0.4
$D^0 \rightarrow K^-\pi^+\pi^0$	8.5±3.2	18.5±1.3±1.6	17.3±1.7
$D^0 \rightarrow K^-\pi^+\pi^-\pi^+$	8.4±3.5	11.5±0.8±0.8	10.9±1.0

Table 1.3. The Hadronic Branching Ratios for Neutral D Decay

There is substantial evidence that the three and four body decays above proceed via intermediate hadronic resonances to their final states. The measured branching ratios for these intermediate states are summarised in Table 1.4.

Channel	Branching Ratios For Resonance (%)		
	MARK III	TPS	World Average
$D^0 \rightarrow K^-\pi^+\pi^0$			
$K^-\rho$	13.7±1.3±1.5	$3.2^{+2.3}_{-1.8}$	9.9±3.5
$K^{*-}\pi^+$	7.1±1.6±1.3	$3.4^{+3.8}_{-2.8}$	7.1±2.5
$\bar{K}^{*0}\pi^0$	2.1±0.9±0.6	$0.9^{+1.4}_{-0.9}$	2.3±2.1
$D^0 \rightarrow K^-\pi^+\pi^-\pi^+$			
$\pi^+\rho^-$			$9.3^{+1.5}_{-2.6}$

Table 1.4. Branching Ratios for Intermediate States

These intermediate states are worth noting since they provide an interesting check on the quality of reconstructed D^0 particles. A full account of the hadronisation of the charm mesons is more complex than the process illustrated in Figure 1.3. A full description of the hadronisation of D decay should eventually be given by a theory of strong interactions like QCD.

1.1.3. The D^* Decays

The D mesons have a higher mass resonant state the $D^*(2010)$ with $J^P = 1^-$. This particle occurs in both neutral and charged states. Decays occur through strong interactions to the D ground states and a pion (Figure 1.4.), or radiatively to a D and a photon.

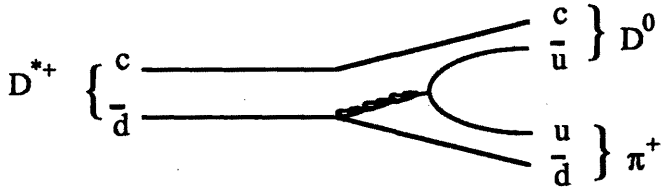

Figure 1.4. Strong Decay Diagram of the D^*

The branching ratios for these decays are summarised in Table1.5. from the particle data group [AGUILAR86].

Resonance	Decay Channel	Branching Ratio
D^{*+}:	$D^0\pi^+$	49 ± 8
	$D^+\pi^0$	34 ± 7
	$D^+\gamma$	17 ± 11
D^{*0}:	$D^0\pi^0$	51.5 ± 7.6
	$D^0\gamma$	48.5 ± 7.6

Table 1.5. The D^* Decay Branching Ratios

1.1.4. Charm Meson Lifetime

For decays through the spectator diagrams the lifetime (τ_c) of charm carrying particles may be estimated by relating the weak coupling vertices to the corresponding vertices in μ decay shown in Figure 1.5. The decay widths of the D and μ may be related by the widths (Γ_c) of the charm carrying particles [KALMUS82]:

$$\frac{1}{\tau} = \Gamma_c = 5\,(M_c / M_\mu)^5\,\Gamma_{(\mu \to e\nu\bar{\nu})} \qquad (1.12)$$

with $\Gamma_{(\mu \to e\nu\bar{\nu})} = 4.5 \cdot 10^5$ and $M_\mu = 0.105$ Gev/c^2

Both the mass of the muon and its decay width are well measured. The mass of the c quark is however speculative and values between 1.25 Gev/c^2 and 1.75 Gev/c^2 are used. Some values of τ_c with differing values of M_c are:

$M_c = 1.25$ Gev/c^2 gives $\tau_c \approx 1.8 \cdot 10^{-12}$ s
$M_c = 1.50$ Gev/c^2 gives $\tau_c \approx 7.6 \cdot 10^{-13}$ s
$M_c = 1.75$ Gev/c^2 gives $\tau_c \approx 3.5 \cdot 10^{-13}$ s

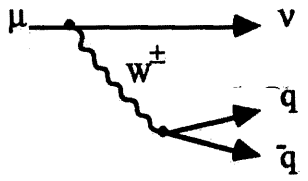

Figure 1.5. Feynman Diagram for μ Weak Transform

These numbers only give an approximate idea of the lifetime of particles containing charm. The factor of 5 before the mass term in (1.12) is given by the number of flavour doublets into which the virtual $W^\pm$ may decay, 3 hadronic colours, and 2 leptonic. For the c quark in a hadron, additional QCD effects must be considered. They amount to short distance gluon corrections and strong radiative corrections giving rise to strong coupling terms in addition to the factor of 5 in equation 1.12 [GAILLARD75, ELLIS75]. In the specific case of the D^0 there are non-spectator diagrams for which (1.12) does not apply.

A number of experiments have measured the lifetime of the charmed particles. A brief discussion of the principal lifetime measurements and a summary of the measured lifetimes is given in the next section.

1.2. Measurements of Charm Lifetimes

With a lifetime τ_c of the order of $5 \cdot 10^{-13}$ seconds, highly relativistic charm particles travel approximately 15mm in one τ_c. Experiments trying to measure such lifetimes must be capable of measuring decay and production vertices with precision better than 150μm to resolve such decays with 1% accuracy, comparable with the resolution of most spectrometers. This precision is also required to enable decay and production vertices to be clearly distinguished against track background.

A number of techniques have been employed to measure τ_c including the use of high resolution bubble chambers, emulsion targets, and more recently solid state active targets. Measurements have also been made in e^+e^- storage rings. The quality of results in these experiments depends not only on the method used to measure decay distances, but on the particle detection apparatus used to identify decay products of charm and on the beam used to produce charmed events. Up to the inception of NA1 the lifetime measurements were from small samples of events. Some of these results from experiments measuring the lifetime of the D^0 are discussed below and summarised in Table 1.6.

1.2.1. Early Measurements

The expected lifetime for the D mesons was clear early in the development of the quark theory [GAILLARD75, TRILLING81]. The first experimental tests of these predictions provided some surprises in 1978 - 1979 [NIU78, SACTON78, REEDER79] with results for lifetimes around $4 \cdot 10^{-14}$s, one order of a magnitude lower than expected. The results were based on only a few observed decays. With experimental upper limits being set above the predicted lifetimes by, for example, the Gargamel bubble chamber [ARMENISE79] at $\tau_D < 8 \cdot 10^{-13}$s from nonobservation of charm decays in 126 events, clear indications of the range of sensitivity to be searched for by dedicated charm experiments was established. The first charm lifetime experiments used emulsion or bubble chambers to measure the production and decay vertices of the charm mesons. Some method for detecting decay products of the interaction and measuring the momenta was also available.

1.2.2. Emulsion Detectors

Photographic emulsion can be used to observe decay vertices with a resolution of a few microns depending principally on the configuration in which it is employed [VOYVIDIC79]. A number of difficulties with emulsion detectors result in most experiments yielding low statistics:

- Finding decay vertices requires a large amount of film scanning (often little help in this process can be given by external detectors).
- Associating a decay vertex with particles found in external detectors. Most emulsion experiments employ some hybrid vertex detector to help the combination of the emulsion target and the spectrometer.
- Emulsion experiments must operate at low rates to avoid clouding the decays with background charged tracks. For this reason they are best suited for use in neutrino beams which have low flux, low interaction rate and, being neutral, do not cloud the films.

An early observation of D decays by an emulsion experiment used the wide band ν beam at FNAL. The experiment, E531, used an emulsion target followed by dispersed planes of emulsion to enable charged tracks to be followed back to the production and decay vertices. A first lifetime of

$$\tau_D = (1.0^{+0.5}_{-0.3}) \cdot 10^{-13}\text{s}$$

was published [USHIDA80] from 10 events. Later results were published with higher statistics [USHIDA82 1&2] giving a lifetime of:

$$\tau_D = (3.2^{+1.0}_{-0.7}) \cdot 10^{-13}\text{s}$$

from 19 events.

A measurement of the D lifetime has been made without a spectrometer using an emulsion target by the NA15 collaboration.The target had 21 layers of emulsion coated polystyrene of 450μm each, followed by an "analyser" of 62 similar films interleaved with lead giving a total thickness of 650μm for each layer [FUCHI81]. This apparatus was placed in a 340Gev π^- beam. Tracks from decays were followed through the analyser and an estimate of their momenta derived from coulomb scattering effects. 16 D events were found with a mean lifetime, with efficiency corrections, of:

$$\tau_D = (3.1^{+2.0}_{-1.6}) \cdot 10^{-13}\text{s}.$$

The problem of tracking back to the decay vertices has been tackled by combining an emulsion stack and the Big European Bubble Chamber (BEBC) [ALLASIA80]. A muon beam was used. The magnetic field of BEBC provided some momentum

measurement, although particle identification was minimal and there was no neutral particle identification. This experiment gave a lifetime of:

$$\tau_D = (0.5^{+0.6}_{-0.3}) \cdot 10^{-13}s$$

from 3 events.

One of the more powerful spectrometers to be used in lifetime experiments was the Omega spectrometer. A tagged photon beam was used with an emulsion stack. Early results by the WA58 collaboration gave a lifetime of:

$$\tau_D = 0.58 \cdot 10^{-13}s$$

from 5 events. A number of results with low statistics have been announced by this collaboration. This may be due to the small length over which they scan the emulsion ~500μm, which we now believe to correspond to only one lifetime.

Recently new results have been published by the WA58 group. A final sample of 52 neutral charm decays with approximatly 50% of events having two decays observed in the target have been presented [ADAMOVICH84]. A lifetime for these D^0 events was measured to be:

$$\tau_D = (3.91^{+2.3}_{-2.2}) \cdot 10^{-13}s.$$

1.2.3. Bubble Chamber Experiments.

Bubble chamber experiments tend to have poorer resolution (~50μm) than emulsion detectors. However, they can operate at a higher rate relative to emulsion detectors and they enable the target (the chamber itself) to be triggered by the spectrometer allowing film frames to be associated with detected decays thus easing the burden on scanning. They may also operate with any beam since they suffer less from the clouding problems of emulsion.

A neutrino beam was used with the FNAL 15ft bubble chamber [BALLAGH80]. The low interaction rate of neutrinos is not suited to bubble chambers. Of 89 charged weak current events found, only two proved to be D^0s giving a lifetime of:

$$\tau_D = (3.5^{+3.5}_{-1.7}) \cdot 10^{-13}s.$$

A 340Gev π^- beam was used with the Bern Infinitesimal Bubble Chamber (BIBC) by the NA18 collaboration [BADERTCHER83]. A streamer chamber provided the particle momentum measurement with good acceptance. No neutral particle identification was available and only fully constrained events were used in the final sample. The optical system could resolve bubbles to 30μm. This experiment found 9 useful D^0 events with an estimated background of 1.4 events and lifetime of:

$$\tau_D = (4.1^{+2.6}_{-1.3} \pm 0.5) \cdot 10^{-13}\text{s}.$$

Higher production rates were achieved by the NA16 collaboration using π^- and p^+ beams, the Lexan Bubble Chamber (LEBC) with a resolution of ~40μm and the European Hybrid Spectrometer (EHS). The early publications from this experiment did not give very high statistics [ADEVA81] but illustrated the ability of this equipment to reconstruct complicated events. Later results from NA16 [AGUILAR82] reported a lifetime measured with 14 events of:

$$\tau_D = (3.9^{+1.4}_{-0.9}) \cdot 10^{-13}\text{s}.$$

The experiments BC72-73 [ABE84/1] and the upgrade experiment BC75 [ABE84/2] used a 1m bubble chamber in a monochromatic photon beam of 20Gev and the SLAC Hybrid Facility (SHF). The cameras of the bubble chamber could resolve bubbles of 50μm. Charged tracks were measured to have a width around 55μm giving the basic precision for measured lengths. There was high resolution charge track spectroscopy with Čerenkov counters and a lead glass wall to give pion / electron discrimination, with no neutral particle reconstruction. The combined yield of these experiments was 42 D^0 events. A number of corrections were made for background processes, momentum and position measurement precision giving a final lifetime of:

$$\tau_D = (6.4^{+1.1}_{-0.9} \pm 0.5) \cdot 10^{-13}\text{s}.$$

1.2.4. Recent Measurements

A number of experiments started data taking at about the same time as NA1. These second generation experiments utilised the experiences of the earlier collaborations either in upgrading or designing detectors. A primary concern was to increase the yield of charm events without introducing background or losing precision.

The equipment used by the NA16 experiment was upgraded and used by the NA27 group with both π^- and p^+ beams. The precision of the LEBC optical system was improved to give a resolution of approximately 7μm. With the EHS spectrometer capable of good e-π and π-K separation and of giving a mass resolution of D's for 5-10Mev/c^2 NA27 has yielded some of the most highly constrained results to date. From a total D^0 yield of 114 events 29 decays were acceptable to "V4" fits giving a lifetime of :

$$\tau_D = (3.9^{+0.9}_{-0.7}) \cdot 10^{-13}\text{s}.$$

This result is achieved using kinematic fits. A new measurement [ROBERTS86] from 145 events has been made using transverse momentum fits to the data, of:

$$\tau_D = (4.6^{+1.0}_{-0.7}) \cdot 10^{-13}\text{s}.$$

The detection of charm decays with visual detectors - emulsion or bubble chambers - gives high resolution results with good fits to vertices. However the amount of work required to obtain these results is large. In NA27, for example, over 100 film scanners in 20 laboratories took $1\frac{1}{2}$ years to process the ~$2 \cdot 10^6$ bubble chamber pictures. The amount of manpower required to analyse visual detectors eventually sets a limit on the amount of data they can process and their final statistics. For this reason a number of experiments have used purely electronic techniques, which only require computer time, to find the decay vertices.

A number of experiments devised *ad hoc* methods of measuring decay points of charm particles using existing tracking equipment. The most notable of these were experiments running on e^+e^- storage rings (MARK II, DELCO, HRS, MAC, JADE and TASSO) These lifetimes are summarised in Table 1.6. The loss in resolution in these measurements was compensated for by high yield of charm events in high centre of mass energy e^+e^- interactions.

For fixed target experiments the complicated topologies boosted strongly in the forward direction of charm decay make the use of conventional proportional and drift wire chambers to resolve decay points and distances impractical. Two experiments, NA11 and E691 have used high resolution silicon strip detectors and heavy targets to provide very high precision tracking of the charm decay products.

The NA11 experiment used the ACCMOR spectrometer with three Čerenkov counters and neutral calorimetry. A 100Gev π^- beam was used with a thin 20mm long beryllium target. Eight silicon strip micro strip detectors (MSDs) were used for high precision tracking close to the target. A set of MSDs were located upto 20mm before the target to

give a high precision beam track. Another three pairs of MSDs were set starting ~29mm after the target to track the interaction products for ~100mm. The silicon strips had a granularity from 4.5μm in the central region, to 7.8μm in the outer area. The primary interaction vertex was measured with a precision of 150μm along the beam line and the difference in position between the primary vertex and a given track could be measured with a precision of 20μm [SEEBRUNNER84]. From $4.4 \cdot 10^6$ single electron triggers 26 D^0 particles were reconstructed with purely charge decay modes. These events gave a lifetime of [BAILEY85]:

$$\tau_D = (3.7^{+1.0}_{-0.7}) \cdot 10^{-13} \text{ s}$$

One of the most recent results has been presented by the E691 collaboration. This experiment used a photon beam and the Tagged Photon Spectrometer (TPS) for decay product reconstruction. The target configuration was similar to that used by NA11 except for the upstream tracking silicon strips. The target was 5cm Be with the MSDs covering 25cm along the beam line. Only preliminary results have been given to date [ANJOS86]. The distinguishing feature of these results is the high statistics with 675 D^0 events in the $K^-\pi^+$ and $K^-\pi^+\pi^-\pi^+$ channels, from 15% of their total data sample and with a lifetime of:

$$\tau_D = (4.4 \pm 0.2 \pm 0.2) \cdot 10^{-13} \text{ s}$$

Such high statistics were achievable because of the high flux photon beam and the purely digital form of the data. The latter factor was enhanced by the use of a very powerful computer system (the ACP - Advanced Computer Project) which allowed the data to be thoroughly analysed within a reasonable amount of time.

Some problems occur in common between the E691 and NA11 experiments with finding primary and decay vertices. The inert target and forward nature of the events make the error in resolution along the beam axis critical. New experiments using silicon strip detectors with finer spacial precision or CCDs with good spacial precision and no tracking ambiguitys, should overcome some these problems (for example NA14 and NA32 [DAMERELL86]).

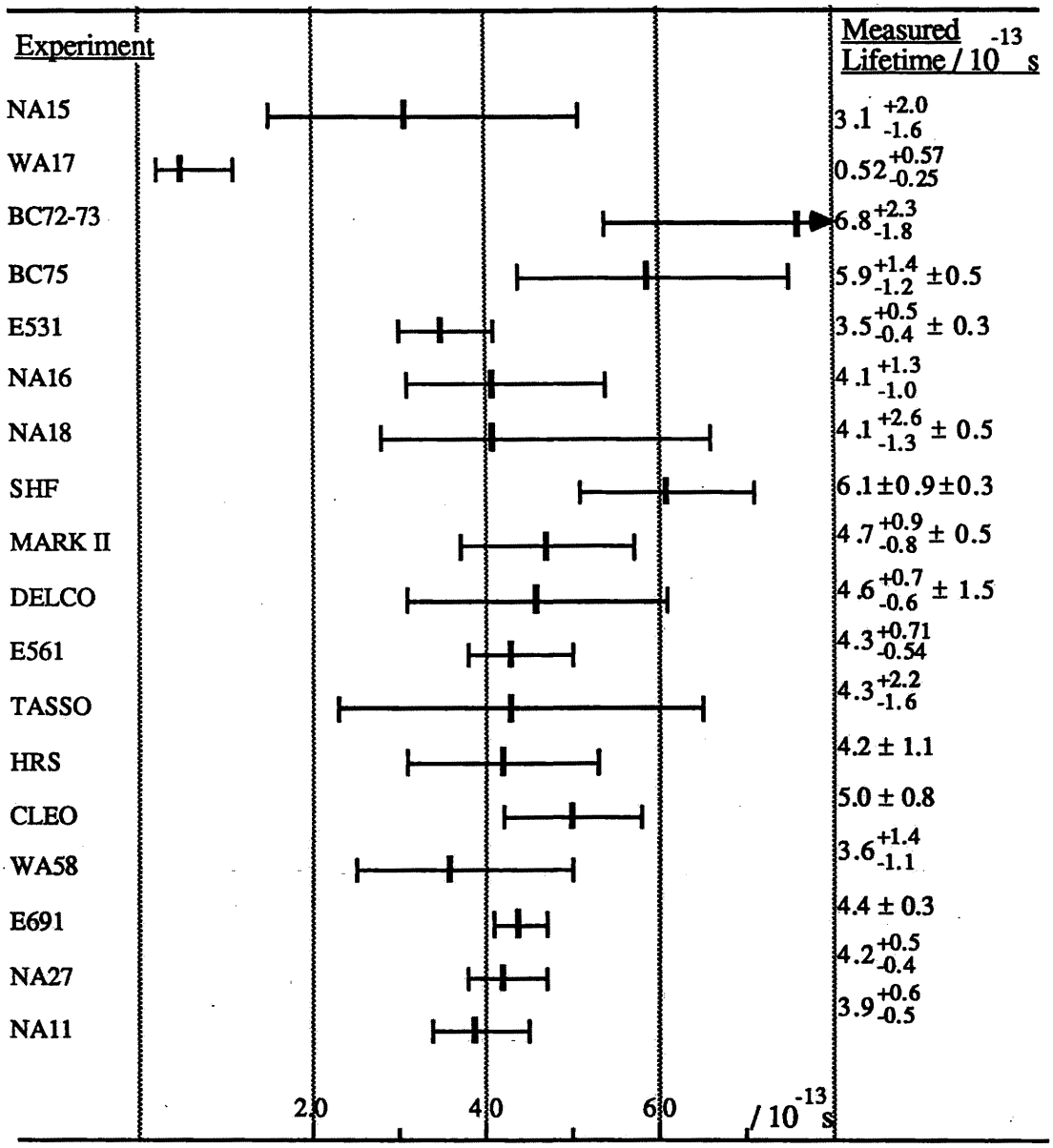

Table 1.6. List of Lifetime Measurements

1.2.5. Summary of Present Lifetime Measurements

The calculation of the "world average" lifetime by combining measurements from any or all of the above results is a complicated statistical exercise. The complications arise from:

- Correct treatment of the - asymmetric - statistical errors
- The variations in the number of events from each measurement
- Decisions about omitting results which deviate substantially from the standard mean measurement.

A number of reviews and summaries exist giving such averages the most recent of which are summarised in Table 1.7. The last, from the Berkeley conference, is heavily influenced by the E691 results which are still preliminary. The result from the Particle Data Group is in some ways the most reliable, with a reasonable treatment of the errors, consideration of a large number of experiments and - most important - an explanation of their derivation of the result reached.

Reference	Date	Quoted $\tau_D/10^{-13}$s
[KALMUS82]	1982	$4.0^{+1.2}_{-0.9}$
[AGUILAR84]	1984	$4.4^{+0.8}_{-0.6}$
[LÜTH]	1985	$4.38^{+0.36}_{-0.31}$
[CASO85]	1985	4.1 ± 0.3
[AGUILAR86]	1986	$4.3^{+0.5}_{-0.4}$
[GILCHRESE86]	1986	$4.3^{+0.20}_{-0.19}$

Table 1.7. Summary of Review Lifetimes

1.3. Photon Interactions And Charm Particle Production

Charm particle production has been observed in several experiments using a number of different beams of high energy particles. The use of a photon beam is essential for the NA1 experiment due to the operational features of the active target:

- Photons have a large production cross section for charm within hadrons.
- Pair production with few extra particles enables easy detection of decay points within the target.

The photon beam also has some advantages with respect to the relative cross-section of hadronic production channels. Substantially above charm threshold coupling of the photon to charm quarks becomes close to the coupling to the lighter quarks.

1.3.1. Atomic Number Dependence

A number of measurements and theoretical predictions of the charm photo-production cross section (σ_c) have been made. The measurements are often from hydrogen or other light targets and the theoretical results are normally expressed in terms of photon-proton (or neutron) cross sections ($\sigma_{\gamma p}$). The effect of heavy nuclei, as in an active target, must be considered properly when discussing both production cross sections and mechanisms in the NA1 target. For reactions in which the photon interacts with the nucleon as a whole - coherent interactions - it is usual to scale the values of $\sigma_{\gamma p}$ by a factor close to $A^{2/3}$ for a nucleus of atomic number A [LOHRMANN, STODOLSKY67]. The $\frac{2}{3}$ power is derived from integrating the cross section over all nucleons and considering shielding effects.

The $A^{2/3}$ factor was derived within the theory of Vector Dominance (see below) which is a long range phenomenological theory. For "harder" processes involving higher momentum transfer the individual nucleons should become more important and the heavy nucleus factor for scaling σ will then become proportional to A [BAUER78].

1.3.2. Photo-production: Theory

The distinction between "hard" - high momentum transfer - and "soft" - coherent - processes is important when considering both the theories and measurements of photoproduction processes. Not only do the nuclear effects tend to vary between these interactions, but there is much evidence that different interaction processes must be considered. Experimentally, the coherent processes are distinguished either by observation of the recoil target nuclei, or by the ratio of the momentum of the charm

system to the photon energy (z) being close to one. The selection for such events is not always possible for experiments which either do not reconstruct the full charm system produced, or which cannot detect the recoil target nuclei.

Currently there are two theories of the production of charmed hadrons from real and virtual (γ^*) photons [FONTANNAZ81, HOLMES85]. The Vector Dominance Model (VDM) and the Photon Gluon Fusion (PGF) theory. These theories should not necessarily be considered as mutually exclusive, but may describe different aspects of photon interactions.

The phenomenological VDM theory [BISWAL81, LIKHODED81, PAUL85] relates the production characteristics of the lighter vector mesons, *e.g.* ρ, ω & ϕ, to those containing charm, the J/Ψ, Ψ' and Ψ''. In VDM the cross section is related to the real part of the interaction amplitude describing a diffractive process. Such processes are taken to interact coherently with the nucleon with small momentum transfer, via exchange of some intermediate particle with zero quantum numbers, so that no change of state is induced in the nucleus (Figure 1.6b).

The PGF theory relates to the production of quark anti-quark pairs, says little about hadronisation to final state particles and is not restricted to vector meson production. The interaction proceeds via the coupling of virtual $q\bar{q}$ states of the photon with gluons in the nucleus [AFEK80, JONES78] (Figure 1.6a). The "hard" / "soft" distinction is made in PGF by considering the order of the interaction in the strong coupling constant α_s. First order interactions (with only soft secondary gluon exchange) involve little momentum transfer and are considered to be "soft" processes. Higher momentum transfer interactions involve higher order QCD terms with more important secondary gluon couplings. For this reason the ratio of "soft" to "hard" interactions should be of the order of α_s [NASH83]. For the "scale" involved in charm physics (set by ~m_c) α_s is around 0.3.

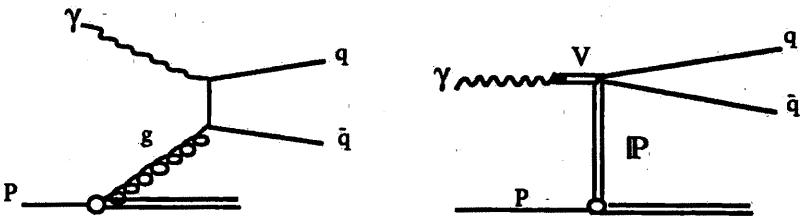

a) Photon Gluon b) VDM

Figure 1.6. Photon Nucleon Interaction Diagrams

1.3.3. Photo-production: Measurements

A number of experiments have measured the cross section for charm production from photons. The photons used may either be real, or virtual from lepto-production. In the latter case, the cross sections used are derived by extrapolating the data to $Q^2 = 0$ where Q^2 is the invariant mass of the photon. Note that in lepto-production the energy transfer ν will not be zero and thus these experiments may produce both hard and soft reactions. Figure 1.7. shows a plot of a number of recent measurements. The measurements quoted here have not only been derived from real or virtual photons, but have been made using different kinds of targets. Each experiment has extrapolated their data to give the cross section on a proton. The curve shows a prediction from the photon-gluon fusion theory.

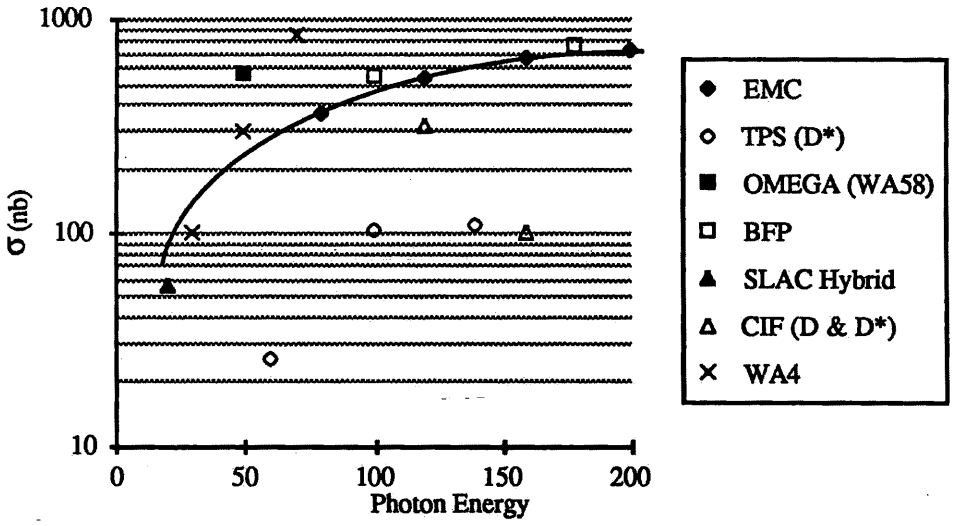

Figure 1.7. Measured Photo-Production Cross Section

Given the above discussion, it is clear that the cross section for charm photo-production on protons is somewhere between 100nb and 500nb for photon energies above 50Gev. There is some further uncertainties in these measurements due to the branching ratios used. Most of the results quoted were made before the publication of the MARK III results (Section 1.2). The measured values of a number of the main decay mode branching ratios have increased by a factor of 2 since 1984. This would produce a corresponding decrease in the measured cross sections.

1.3.4. Pair Production

Charm production with photons occurs completely through the electromagnetic coupling. In soft diffractive processes there is no exchange of quantum numbers with the nucleus and either charm mesons or baryons must be pair produced taking up the c and $\bar{c}$ quarks.

In the case of the D it is possible to produce the combinations: $D\bar{D}$, $D^*\bar{D}+D\bar{D}^*$ or $D^*\bar{D}^*$. The threshold for charm production is at 4.028Gev centre of mass energy (E_{cm}), corresponding to a photon energy of 9Gev. At this energy phase space factors are important giving the ratios of 65:25:1 for these channels [IWASKI77]. Counting spin states gives ratios of

$$D\bar{D} : D^*\bar{D}+D\bar{D}^* : D^*\bar{D}^* \equiv 1 : 4 : 7 \qquad (1.13)$$

[GEORGI76] indicating a preference for $D^*\bar{D}^*$ over $D^*\bar{D}+cc$ production. A method for calculating these ratios in terms of the c quark mass and available energy has been suggested [IWASKI77] giving the formula;

$$D\bar{D} : D^*\bar{D}+D\bar{D}^* : D^*\bar{D}^* \equiv 1 : \frac{4E^2}{m_c^2} : 3+\frac{4E^2}{m_c^2} \qquad (1.14)$$

where m_c is quark mass and E is the energy of the c quark. The value of m_c is not well known. However from (1.14) it can be seen that well above threshold at high E_{cm} the ratio of $D^*\bar{D}$ to $D^*\bar{D}^*$ production will tend to 1 and to dominate $D\bar{D}$ production.

The ratios (1.14) were predicted within the context of e^+e^- production and are equivalent to (1.13) in the limit $E = m_c$. At this limit the ratios of (1.13) are the sum of contributions from longitudinally polarised photons:

$$D\bar{D} : D^*\bar{D}+D\bar{D}^* : D^*\bar{D}^* \equiv 1 : 0 : 3 \quad (\sigma_L) \qquad (1.15)$$

and transversely polarised photons:

$$D\bar{D} : D^*\bar{D}+D\bar{D}^* : D^*\bar{D}^* \equiv 0 : 4 : 4 \quad (\sigma_T) \qquad (1.16)$$

Strictly, only the ratios of (1.16) hold for real photons. With experimental evidence for $D\bar{D}$ production from real photons some contribution from (1.15) was expected with

the photon gaining a longitudinal polarisation component during its interaction with the target.

Few experiments studying charm physics can measure the production cross sections of D and D^* particles with equal acceptance. Often the particular kinematics of D^* production or particular D decay channels are used as signatures of charm either in a trigger or in event reconstruction. Thus it is not easy for any experiment to measure the relative production ratios of (1.13) and little data on this has been produced.

The production of other particles in association with the two charm mesons has been observed. Little is said about this by the theory of the gluon fusion model, except for particles arising from the hard component of the nuclear interaction. Recent results from the TPS experiment [NASH83] give the ratios:

$D^*\bar{D}^*$	11%
$D^*\bar{D}^*+\pi^+\pi^-$	44.5%
$D^*\bar{D}^*+\pi^+\pi^-\pi^0$	44.5%

These statistics were derived from data that was believed to contain coherently produced charm particles.

This indicates that a substantial number of D^* events should be accompanied by at least two extra charged particles not arising from charm particle decay.

Chapter Two

Experimental Apparatus

This chapter contains an account of the apparatus used in this experiment. An account is given of all the equipment used for the production of charm particles, the observation of their decays and the detection of their decay products. Some detail is given of the operational features of this equipment, but an assessment of the overall quality of the apparatus is postponed until Chapter Four. Some attempt is made for completeness since no account of the equipment used has yet been published.

2.1. The Overall Apparatus

The layout of the apparatus is shown in Figure 2.1 Electrons, produced from protons of the SPS, were used to produce bremsstrahlung photons. The momentum of the scattered electron was measured in a tagging system to determine the photon energy.

Non-interacting photons reached a shower detector at the back of the apparatus (SD5) as did photons from secondary bremsstrahlung of the beam electrons. If the photon interacted, the particles produced entered the spectrometer FRAMM, in which their momentum (for charged particles) or energy (for photons) was measured. Each part of the apparatus produced an electronic signal in response to a particle entering it. These signals were amplified close to the originating apparatus, and transmitted to the data acquisition system (Chapter Three). The signals were encoded to digital form and recorded on computer tape for later analysis. The data acquisition required a trigger signal to tell it when to write the encoded data to tape. There were some parts of the apparatus specifically installed to provide parts of the trigger signals. Other signals were taken from the shower detectors for use in the trigger.

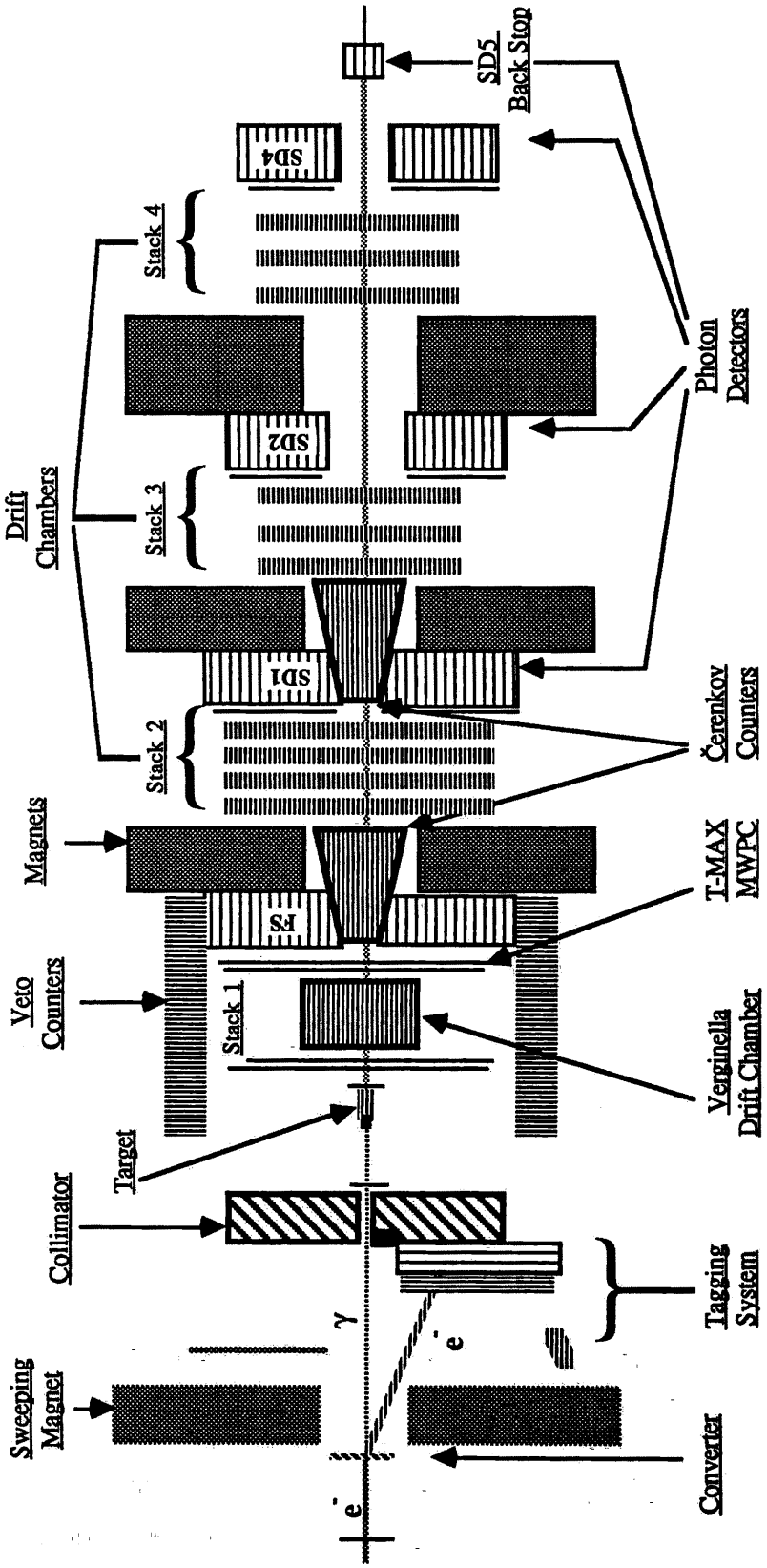

Figure 2.1. The FRAMM Spectrometer

2.2 The H4 Beam Line

The photon beam had an energy range of 70 to 170Gev. The photons were produced from the bremsstrahlung interaction of electrons. These electrons were produced from the 450Gev protons of the CERN SPS. The method of producing the electrons is illustrated in Figure 2.2. The H4 beam line could supply electrons in the momentum range of 100 - 200Gev/c, and a momentum resolution of:

$$\frac{\delta P}{P} = 1.4\%.$$

It will be seen that this error is of the same order as the error of measuring the bremsstrahlung photon energy in the tagging system (Section 4.3).

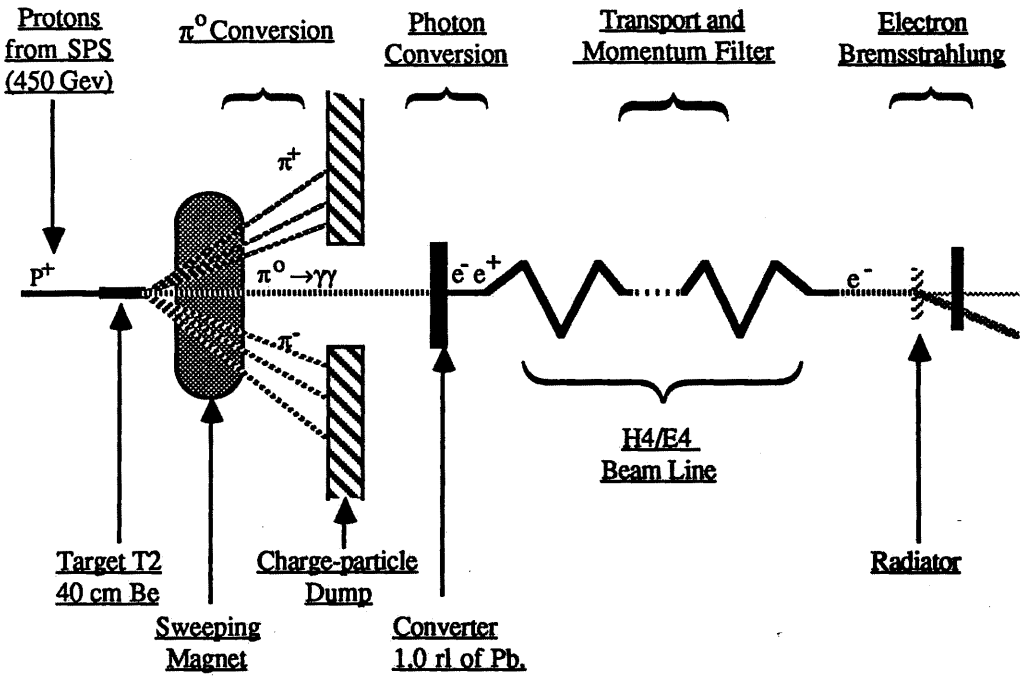

Figure 2.2. The H4 Beam Line

The active elements of the beam line were controlled by the computers of the SPS. Access to these computers for control of the beam was available from the experiments control room. Apart from providing bremsstrahlung photons, the beam line could be controlled to provide beams of either electrons or π^+ particles. These beams were highly monochromatic, the π^+ beam had a momentum spread of the order of 0.2%. The pion and unconverted electron beams were used to calibrate the shower detectors, and find the operational parameters of the tracking chambers. Control of the beam line could also be exercised to steer the electrons, and thus the photons, so as to ensure a finely

collimated beam of photons on the target. By controlling collimators in the beam line, the number of electrons reaching the electron / photon converter could be adjusted. This adjustment depended on the absolute rates of electrons produced and the rates with which the experimental apparatus could cope.

2.2.1. Photon Flux

The rate at which electrons and thus photons were produced was important in constructing the trigger for the data acquisition. The SPS delivered protons in bursts of 1.2s with around 10^{13} particles per burst. The time between bursts was 14s; this was long compared to apparatus and data acquisition recovery times. Thus the rates during one burst are discussed here since complete recovery was possible between bursts.

Calculations of the numbers of electrons produced for a burst of $3 \cdot 10^{12}$ protons were made by the SPS staff shown in Figure 2.3 [DOBLE76]. Our normal running conditions were with a beam target of 400mm beryllium, taking electrons of 175Gev/c. Thus the maximum rate under these conditions should have been $9 \cdot 10^{7}$ electrons per burst. In practice the SPS delivered about $2 \cdot 10^{11}$ protons per burst and we detected a rate of $2 \cdot 10^{6}$ electrons per burst in counter BØØ (Section 3.4.1) which was consistent with expectations.

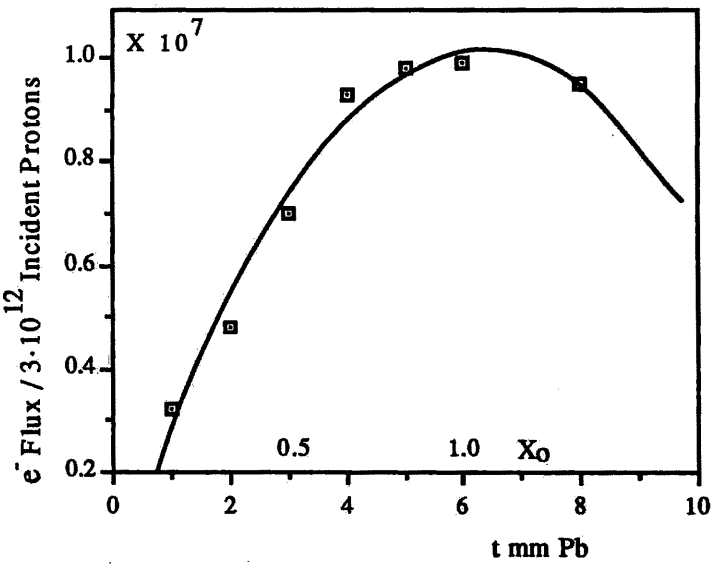

Figure 2.3. The Electron Flux as a Function of Converter Thickness

The final step in the production of photons was the conversion of electrons to photons in a 0.35mm (0.1 radiation length X_0) lead converter. The probability of an electron producing a photon with energy between E_{thresh} and E_{max} by bremsstrahlung in x cm of lead may be calculated by the approximate formula:

$$P(E_\gamma > E_{thresh}) = \frac{x}{X_0} \int_{E=E_{thresh}}^{E=E_{max}} \frac{1}{E}\, dE \qquad (2.1)$$

which holds for high values of E_γ [ROSSI52]. The final rate of producing photons above an energy of 75Gev was approximately $6 \cdot 10^5$ per spill of the SPS.

2.2.2. The Tagging System

The purpose of the tagging system was to measure the energy of electrons which have undergone bremsstrahlung in the electron / photon converter. Since the electron beam momentum was known to good accuracy, a measurement of the deflected electron energy can be used to determine the energy of a photon entering the apparatus.

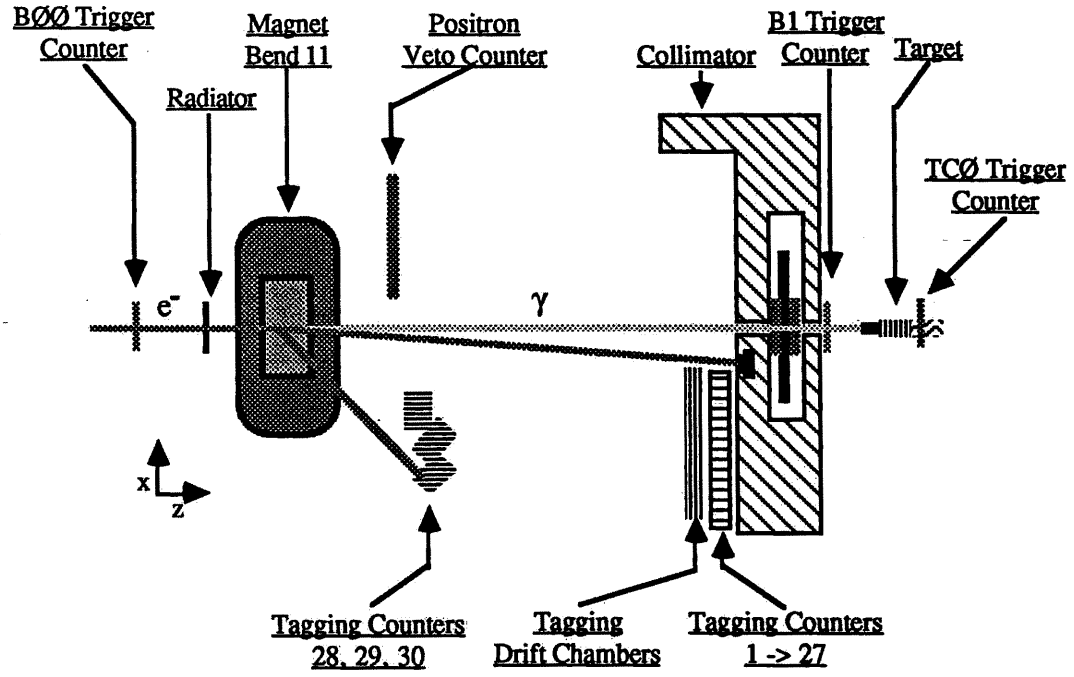

Figure 2.4. The Photon Tagging System

Figure 2.4 shows the detailed layout of the tagging system. The tagging magnet of 4.4 tesla meter swept charged particles into tracking chambers and calorimeters. Any positively charged particles such as positrons were swept into a veto counter of scintillator used in the trigger. The electron then passes through a set of drift chambers and into a set of lead glass Čerenkov shower detectors TT 1->27. Low energy electrons are swept into tagging counters TT 28,29 and 30. These electrons were associated with high energy photons. Electrons with a momentum greater then 160Gev/c entered a beam dump next to the collimator. These electrons were associated with low energy photons, and were not of interest in the experiment.

The combination of tracking chambers and calorimeters provided redundancy in the measurement of the electron energy since the energy of the electron could be measured by both its angle of sweep, and the amount of energy it deposited in the tagging counters. The position resolution of the drift chambers was typically 0.5mm. The position resolution of the shower detectors was around 34 mm. The average distance between electron converter and tagging detectors was 3.6m. The energy resolution from the drift chambers was expected to be less than 0.01% and of the order of 1% from the calorimetry.

2.3. The Vertex Region

The vertex region of the experiment was that area in which the photon beam interacts with the target (Figure 2.5). There were two sets of multi-wire proportional chambers. These were used both in the event reconstruction and contributed to the trigger (Section 3.5). The target was located in a cryostat, details of the operation of the target will be given below. Above and below the target were scintillation counters for detection of slow neutrons (not shown). These contributed to the event trigger. Downstream of the target was a high resolution drift chamber called Verginella. This drift chamber provided the link between the charged tracks leaving the target, and those reconstructed in FRAMM.

The target region ended at the front shower detector. All apparatus thereafter was considered to be part of the FRAMM spectrometer. For convenience, the front shower detector will be discussed below with the other shower detectors.

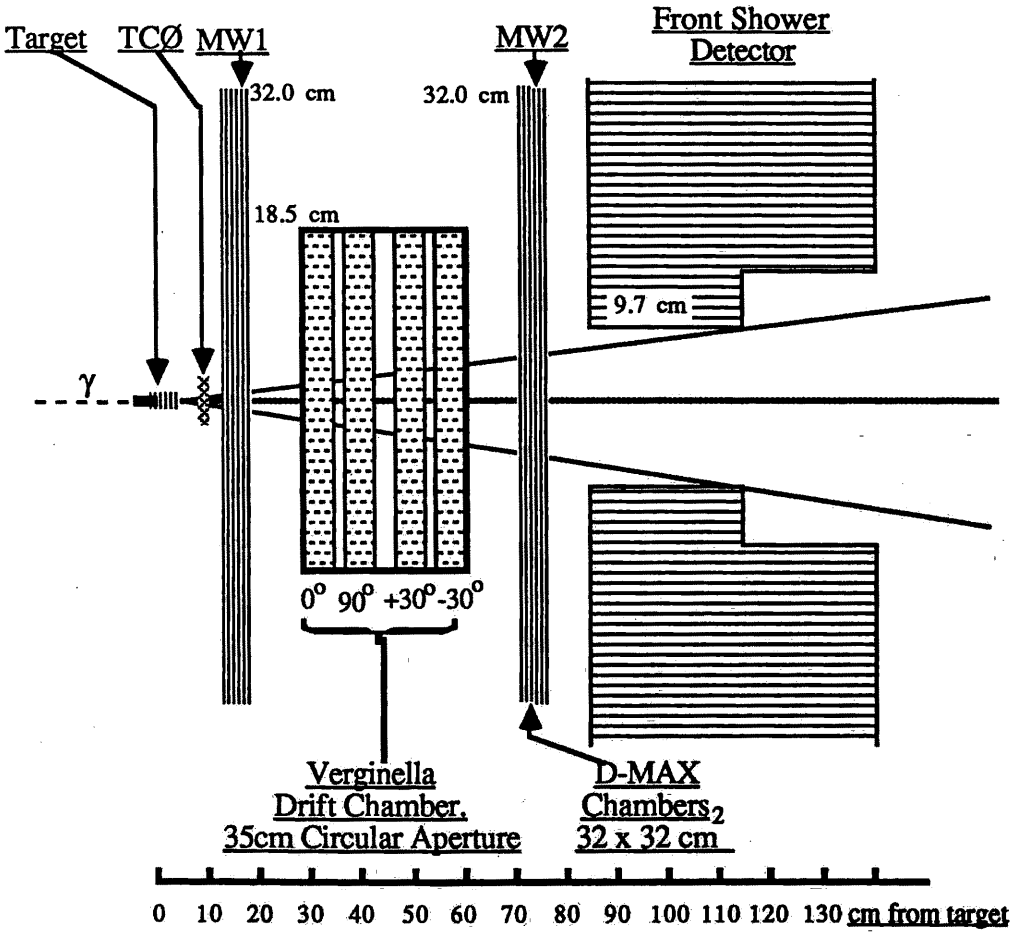

Figure 2.5. The Vertex Region

2.3.1. The Vertex Drift Chamber: Verginella

A high resolution drift chamber was located 30cm after the target. This drift chamber had 24 planes of sense wires and field shaping wires. These planes were grouped in 4 sets of 6 wire planes, each plane being oriented at different angles, 0°, 90°, 30° and 150° (Figure 2.6) to allow reconstruction of charged tracks originating from the target. Each wire plane contained 20 sense wires. Consecutive planes of wires were staggered by 0.5mm to aid in track finding. The drift cell sizes in Verginella increased in from 5.0mm at the center where the particle flux was highest to 20mm at the edge of each chamber.

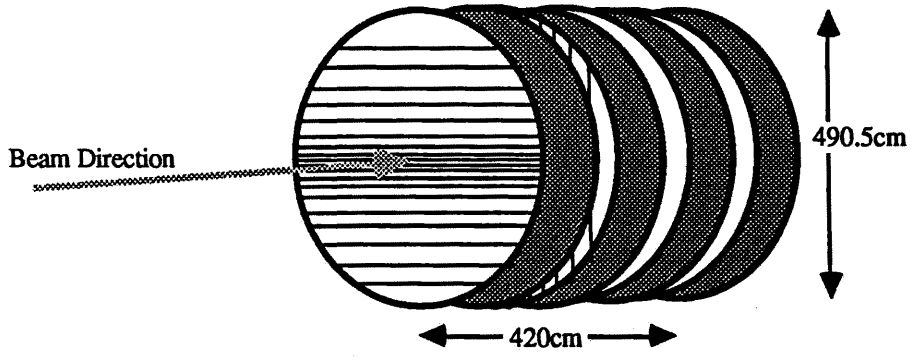

Figure 2.6. An Illustration of Verginella Drift Chamber Geometry

2.3.2. The Multi-Wire Proportional Chambers

Two pairs of multi-wire proportional chambers, with x and y oriented planes, were located before (MW1) and after (MW2) the Verginella drift chamber at 15cm and 70cm from the vertex. There were four wire planes in each chamber with 100 readout wires per plane. The chambers had a spatial resolution of 0.5mm.

2.3.3. The Surrounding Anti-Coincidence Counters

The target region was surrounded by a layer of scintillation counters to detect wide angle charged particles and neutrals. This equipment is primarily used in the trigger to veto nuclear breakup in photon interactions or evaporation neutrons. Together with the front shower detector it presented an effective constraint on forward production.

2.4. The Target

The target in NA1 consisted of a system of semiconducting solid state devices [BELLINI82]. The target was constructed in two parts. The front part was a monolithic germanium target. The back part consisted of a silicon wafer telescope (Figure 2.7). Both parts of the target were located in a cryostat containing liquid nitrogen at a temperature of 90K. The dimensions and operational parameters of the targets are summarized in Table 2.1.

	Silicon	Germanium
Atomic number Z	14	32
Atomic weight A	28.06	72.60
Density (3000K)	2.33 g/cm^3	5.33 g/cm^3
Ionization Energy	3.66 eV	2.69 eV
Radiation Length X_0	9.8cm	2.2cm
Nuclear Interaction Length for High Energy Pions	24cm	10.5cm
Probable Energy Loss for MIP	285 Kev/mm	584 Kev/mm
Dimensions	200×20×20mm^3	5×5×20mm^3
Pitch	200 and 400μm	50 or 100μm
Number of Active Strips	15	48 or 96

Table 2.1. Operational Parameters and Dimensions of the Target

The target allowed detection of short decays by measuring the development of ionization of particles produced by the photon interaction and / or their decay products (Figure 4.11). Changes in the amount of ionization along the target indicating points of production or decay. For highly relativistic particles the amount of ionization per particle reaches a minimum constant level, these are minimum ionising particles (MIP). For the solid state targets to clearly distinguish the number of MIPs at any point, the ratio of the ionization signal to ambient noise had to be as large as possible. For a given energy loss for MIP, the amount of signal produced was proportional to the thickness of material transversed by the particle. The noise originated from the readout electronics and the target itself. The noise from the target was proportional to the capacitance and the capacitance was inversely proportional to the thickness of material. For the fine granularity detectors the signal from ionising particles becomes small and the noise

large. Thus the requirement for measuring short lived particles was in conflict with the requirement of a low signal to noise ratio and the resolution of the decay points.

Further constraints on target design arose from problems of accurately mounting thin planes of material within small distances. A number of approaches to constructing solid state detectors have been pursued before and after the inception of NA1 [AMENDOLIA84]. The silicon detectors were the original target used by the FRAMM collaboration. This device was used in concert with the germanium target for the data considered here.

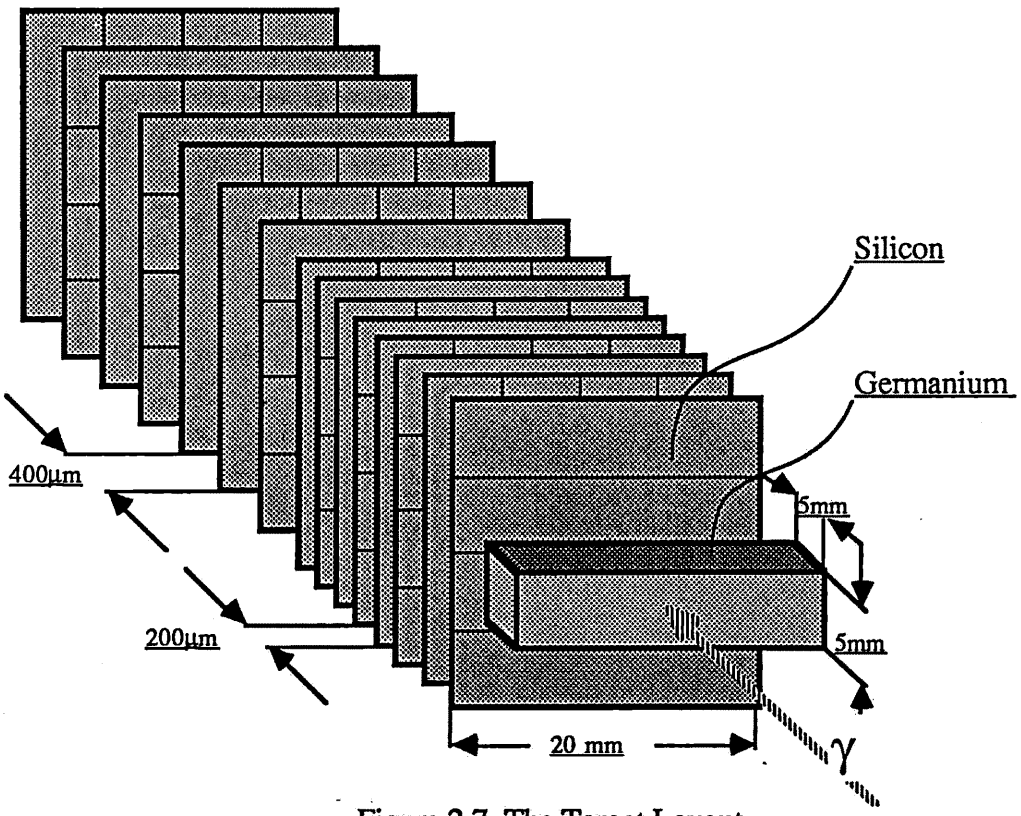

Figure 2.7. The Target Layout

2.4.1. The Germanium Target

The main target was composed of a single block of germanium with electrodes etched along the upper surface. Six such germanium blocks were constructed, three with 96 electrodes [AMENDOLIA84] one of which was used for the 1983 data taking and three with 48 electrodes [AMENDOLIA83] one of which was used in 1984.

The use of germanium was determined by engineering considerations. It also had the advantage of having a signal for MIP 2.5 times that of silicon. The construction of a monolithic device, rather than individual strips, allowed the segmentation of charge detection to be very fine while overcoming the problems of capacitance discussed

above. Ionization in the target was detected by drifting the energized electrons to anodes on the top surface of the germanium.

The upper surface of the germanium was doped with a 500Å layer of boron and the 96 or 48 strips etched away (Figure 2.8). Contacts of gold were deposited on the boron to allow good contact for the preamplifiers. The target was operated with a reverse bias of approximately 300V to deplete the germanium-boron boundary and provide the drift potential. A current of approximately 9μA was detected for single minimum ionising particles with a rise time of around 200nsec. The width of this signal was four times that of the fluctuations due to noise. This was due to the statistical characteristics of the ionising processes. The first germanium strip was not read out and served to provide a uniform field for the later strips.

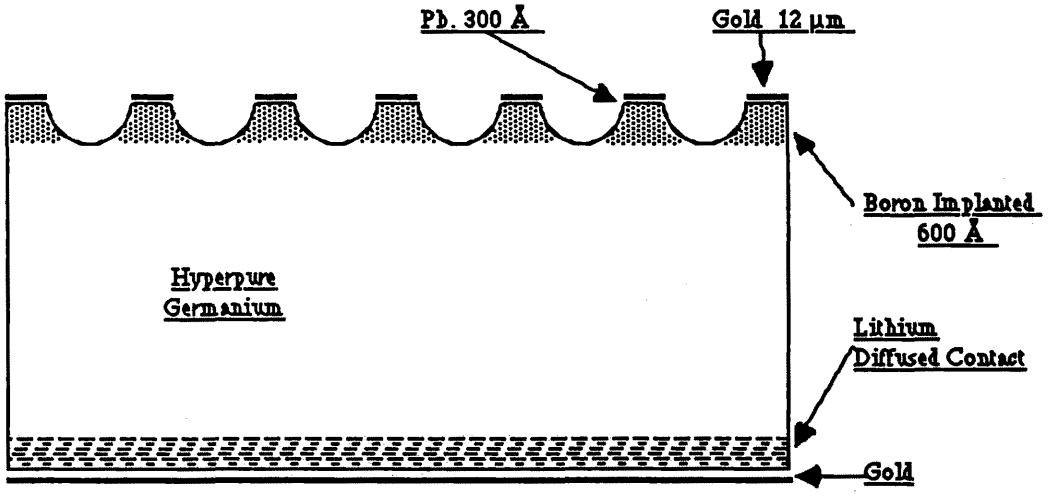

Figure 2.8. The Germanium Target Construction

2.4.2. The Silicon Strips

The silicon strip detectors [AMENDOLIA80/4] followed the germanium target with an intervening gap of 1.2mm. The 15 strips were organised in two regions, the first eight with a spacing of 200μm and the last seven with a spacing of 400μm. This provided a compromise between good resolution and a large decay volume.

Each silicon strip consisted of a 200μm thick slice with a coating of 500Å of gold on one side and 2000Å of aluminium on the other for electrical contact. The contacts were divided laterally into four strips to reduce capacitance. Total depletion was found with a potential bias of 16V.

2.5. Tracking In FRAMM

Charged particles were tracked through the FRAMM spectrometer by stacks of drift chambers [AMENDOLIA80/1] located between the magnets as in Figure 2.1. The layout of each stack of DC's and the salient parameters are described in Table 2.2. Each chamber was read out from both sense and delay wires, the sense wires measuring position in a plane orthogonal to that of the delay wires. Note that stack numbering started at 2, the vertex region tracking was counted as stack 1.

Stack name	Number of chambers	Start position from target	length /cm
ST 2	10	320.0	176.0
ST 3	8	768.	84.0
ST 4	6	1285.8	205.8

Overall dimensions	50 × 70cm
Sensitive area	38.4 × 57.6cm
Drift space	24mm
Gap	11mm
Sense wire (SW) resolution	0.2mm (fwhm)
Delay line (DL) resolution	5.0mm (fwhm)
Step between shaper and field wires	2mm
Distance between SW and DL	1mm
Delay lines propagation velocity	6 ns/cm
Positive bias (SW)	1680 - 1730 V
Negative bias (field wires)	3500 - 4000 V
Number of sense wires per chamber	16

Table 2.2. Drift chamber parameters

An assessment of the momentum resolution in FRAMM was complicated by the geometry of three magnets. In general, for an apparatus with tracking chambers located either side of a magnet, the error on a measure of momentum is not linearly dependent on the momentum. The original principle of the design of FRAMM was to vary the amount of magnetic field a particle sees, depending on its momentum. The original design of FRAMM had five magnets, set in such a way that the error on the momentum

was almost linearly dependent on the momentum. The number of magnets had been decreased, to ease reconstruction, and reduce the number of electronic channels required.

2.6. The Čerenkov Counters

Two multi-cell threshold Čerenkov counters [AMENDOLIA80/3] were located in the apertures of the first and second magnets of FRAMM. The specifications of these counters are shown in Table 2.3. The Čerenkov counters were divided into a number of small cells in order to be able to cope with the high multiplicity resulting from charm particle decays as illustrated in Figure 2.9.

	$\check{C}_1$	$\check{C}_2$
Number of cells	22	10
Number of planes	11	5
Plane spacing (mm)	30 to 77	53
Gas	CO_2	dry air
$\mu = (n - 1) \times 10^4$	4.1	2.73
Pion threshold (Gev/c)	4.87	5.97
Kaon threshold (Gev/c)	17.2	21.1

Table 2.3. Čerenkov Counter Parameters

The Čerenkov counters were found to have an efficiency for discriminating between pions and kaons of 98% in test conditions.

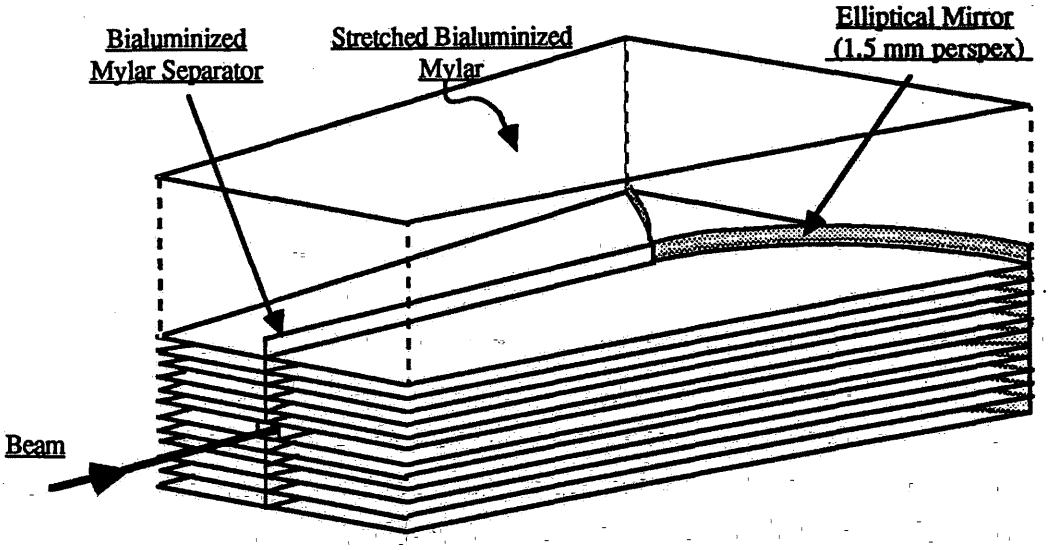

Figure 2.9. The Čerenkov Construction

2.7. The Shower Detectors

FRAMM was designed so that all particles produced at the vertex, and their decay products, entered a shower detector. Photons and electrons or hadrons produce differing responses in shower detectors. The shower detectors thus served to distinguish hadrons from electrons as well as to detect photons for π^0 reconstruction (Section 4.4). The different responses of the shower detectors were used in both the trigger and event reconstruction.

There were two types of shower detector used in FRAMM; SD2 SD4 SD5 were homogeneous devices (SD3 was removed after the NA7 runs). These detectors covered a cone of ±20mr. The front shower detector (here after FS) and SD1 were sampling calorimeters. These covered a cone of ±30° except for a hole through the centre of ±20mr. The salient features of the shower detectors are given in Table 2.4.

Detector Name	Start Position / cm	Type
FS	84.2	pb/scint
SD1	528.9	pb/scint
SD2	942.6	pb-glass
SD4	1521.3	pb-glass
SD5	1677.0	pb-glass

2.4. The Shower Detector Geometry

2.7.1. The Front Shower Detector - FS.

The front shower detector (FS) was located downstream of the vertex region. Particles produced in the target passed through a hole in the centre of the front shower detector and entered FRAMM. This detector was a sampling calorimeter composed of layers of scintillator and lead. The FS was not used in event reconstruction, but contributed a veto against nuclear breakup of the target, in the trigger. As illustrated in Figure 2.5, the inside lip of the FS defined the maximum geometrical acceptance of the FRAMM spectrometer. The diameter of the hole at this point was 196mm giving a maximum angle of 86mr from the target. This was the acceptance for particles to be detected in the event reconstruction. To contribute to the trigger, particles would have to enter the front of the FS.

2.7.2. The Sampling Shower Detector - SD1

SD1 was a shower detector located before the second magnet in FRAMM. The particle flux on this detector was large with possibly ≥4 charged particles and ≥2 photons per event. It was a sampling calorimeter composed of planes of lead and lucite plexiglass scintillator. The strips of scintillator were 10mm by 32mm and of varying length. The whole of SD1 had a size of $1.22 \times 1.22 m^2$, a hole of 196mm square, and was located 84 cm from the target. SD1 was 17.7 radiation lengths in total with 20 active strips of scintillator oriented at 0°, 90° and one at 45°.

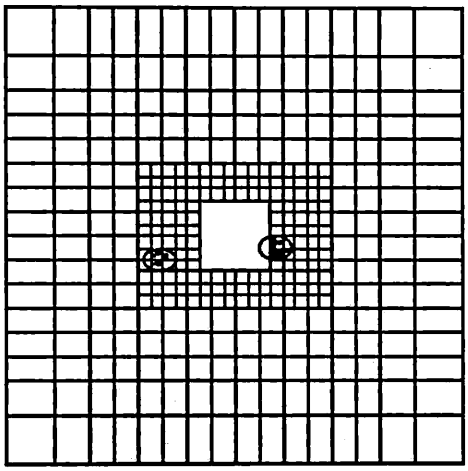

Figure 2.10. An Illustration of a PAD Chamber Event

For read out purposes, the scintillator was grouped in strips of five elements, one from each plane, per orientation. Light generated by scintillation was channelled by light guides to photomultipliers, amplified and passed on to the data acquisition. To help in the reconstruction of showers, a pad chamber was inserted after the first x and y views, 5.6 rl's into SD1.

The pad chamber consisted of a plane of limited streamer tubes operating in saturation mode. The tubes had 3 walls of aluminium each 1.5cm long. The fourth wall of the streamer tubes was provided by the pad read out. The pad read out consisted of a mylar sheet with copper squares etched onto it. The geometry of the pads is illustrated in Figure 2.10. The pad sizes ranged from $3.2 \times 3.2 cm^2$ (the size of the scintillator fingers) at the centre, to $12.8 \times 12.8 cm^2$ on the outer region.

The electromagnetic field produced by a streamer generated by a charged particle traversing a tube, was picked up by the pad read out, amplified and passed to ADC's on the data acquisition. The pad chamber provided absolute x and y position information for showers.

2.7.3. Lead Glass Shower Detectors - SD2, SD4 and SD5

The shower detectors located at the ends of stacks 3 and 4 and the backstop shower detector were constructed with a system of lead glass blocks [AMENDOLIA80/2]. Each shower detector was composed of a front part lead glass block (FLG) and a back part (BLG). The specifications of the lead glass blocks used are shown in Table 2.5. The lengths and positions of the FLGs were such that one FLG completely covered a row of BLG blocks. The energy resolution of the lead glass block calorimeters was measured in test beam conditions to be:

$$\frac{\sigma_E}{E} = \left[\frac{14}{\sqrt{E}} + 1 \right] \%$$

Detector name	length /cm	length /X_o	length /l_o	Number of blocks
SD2 back	40	15.7	1.24	140
SD4 back	50	19.7	1.55	108
SD5 back	50	19.7	1.55	4
FLG	10	3.9	0.3	25
	Back Lead Glass (BLG) area		$3.2 \times 3.2 cm^2$	
	Front Lead Glass(FLG)		height 6.4cm	
	Radiation length of (X_0)		2.45cm	
	lead glass (type SF 5)			
	Nuclear interaction length (l_0)		32.3cm	
	Density		$3.9\ gm/cm^3$	

Table 2.5. Shower detector parameters

In front (up beam) of SD2 and SD4 were scintillation counter hodoscopes called T-counters. Each finger of the T-counters corresponded to one FLG, and these could be used in the trigger, to identify charged particles entering the SD's. The layout of the BLGs and relative positions of the FLGs are illustrated in Figure 2.11.

2.7.4. Electrons, Photons and Hadrons in the Shower Detectors

Use of the shower detectors for discrimination between electrons and hadrons was based on the differences in shower profiles between these two kinds of particles. Electrons (and photons) were expected to start showering in the FLG's, depositing over 50% of their energy there, the remainder of the particles energy being absorbed in the BLG's. There was only a 30% chance that a hadron would shower in the FLG's, and were only expected to deposit around 60% of their energy in the whole shower detector if they showered at all. Hadrons were characterised by only a small amount of the deposited energy being present in the FLG's, and the total deposited energy being a small fraction of that of the charged track. The use of these features in the trigger is described in Section 3.5. and for particle identification in the event reconstruction in Section 4.5.

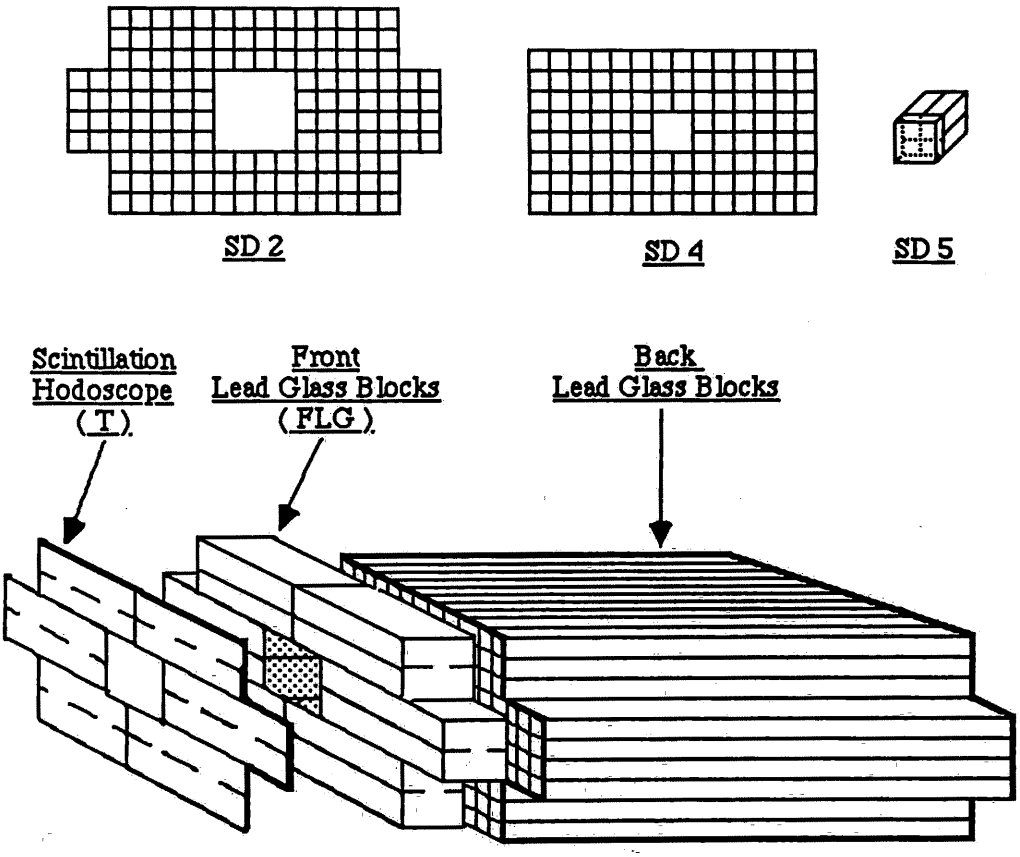

Figure 2.11. The Lead Glass Shower Detectors

Chapter Three

Data Acquisition & Trigger

The method of recording the responses of the experimental apparatus is discussed here. Due to restrictions in the amount of computer time available to analyse events and the rate at which data may be read out a method was required for filtering events "on line" as they were produced. This filter - the trigger - set the limits on the final data in so far as there was no means of recovery from mistakes made in its implamentation *post facto*.

3.1. Overview of the Data Acquisition

The data acquisition was that part of the apparatus which records the signals from the detection apparatus on magnetic computer tape, for later analysis. These signals were amplified close to the detectors, and passed to a system of electronics where they were converted to digital signals, and passed on to the computer. The electronics used was, for the most part, housed on a system of CAMAC crates [PETERSON]. This facilitated easy control and monitoring of the electronics, as well as fast transfer of digital signals between the electronics and the computers. In addition to supporting the standard CAMAC protocols, part of the data acquisition system had been augmented with the ROMULUS system [POINTING]. The ROMULUS system facilitated the fast transfer of large amounts of data from CAMAC electronic units to the computer system.

The data acquisition was under the control of two PDP 11/34a's. These computers were named FPUØ and FPDA. FPDA was primarily responsible for collecting data from CAMAC and transferring it to magnetic tape. FPUØ ran programmes for monitoring the apparatus. The PDP's were equipped with 5 RL01 disk drives, a line printer, and a variety of consoles.

The basic trigger of NA1 was a request for hadrons in the events. The presence of hadrons was determined by assessing the states of the shower detectors. There were over 70 signals from the SD's which required processing by the trigger logic. A trigger constructed of standard AND($\wedge$) and OR($\vee$) gates for this number of signals would prove too complex and impossible to maintain or amend. For this reason the bulk of the trigger logic was handled by programmable logic units. The configuration of these units is shown in Figure 3.1. and details of the elements of which are described below.

A limiting factor of the data acquisition was the rate at which it could transfer data to tape. Figure 3.2 shows the results of a test made to find these rates. The plot shows the number of events successfully written to tape along the y-axis, and the length of the

events along the x-axis. The two curves are for the conditions when the computer was required to transfer the data to magnetic tape, and when the computer was merely required to read the data into its memory. The length of the events was expected to be around 1500 words. This means we could write a maximum of 100 events per burst. This statistic provided a basis for tuning the trigger and was above the final data rate used.

The electronic units used were, for the most part, standard analog to digital converters (ADCs) time to drift converters (TDCs), delay units, and scalers. The electronics used by the trigger is less well known, and I will describe their characteristics in some detail here.

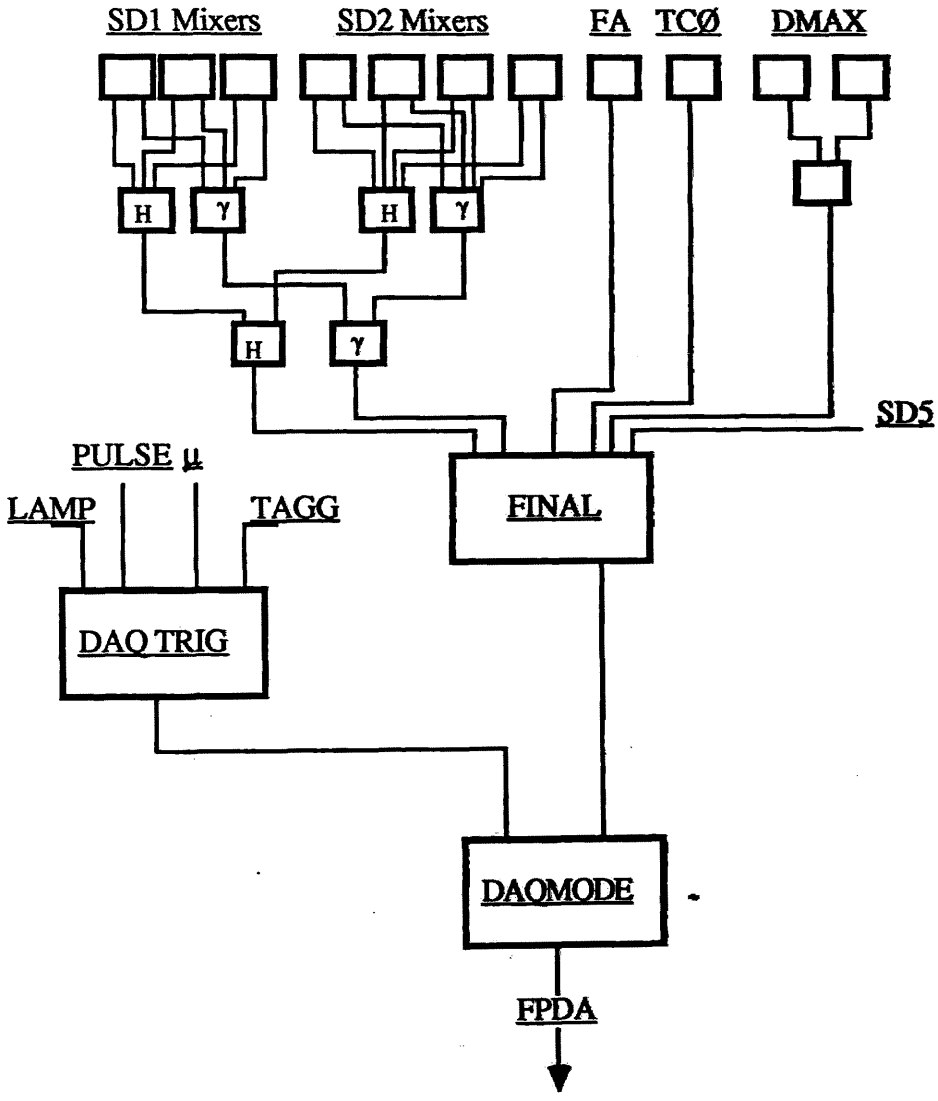

Figure 3.1. The Main Trigger Logic Chain

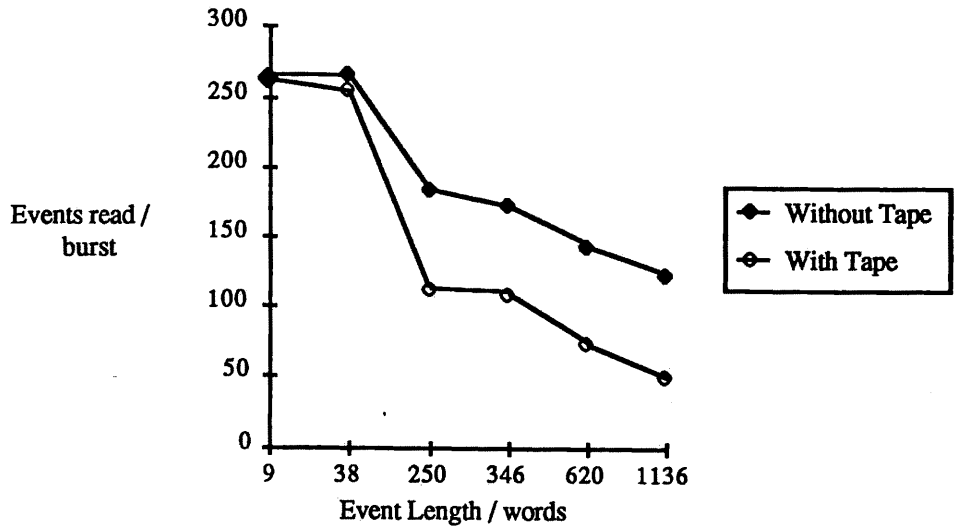

Figure 3.2. Rates for Reading Events to Tapes

3.1.1. The Spill Data Taking Structure

A signal was sent from the SPS control system indicating that a spill of particles from the SPS had started (SOB) or ended (EOB). This signal set a LAM (Look At Me) flag on the CAMAC data way. The computer system could then react to the presence of the LAMs to prepare for or end the data taking. The following operations were performed at the start or end of each spill of the SPS:

At Start of Burst:

- Reset the romulus processors and flags.
- Initiate and read the SD lamp system.
- Read the ADC pedestals.
- Record the electronically made position measurements of the SD's.
- Zero event statistics scalers.

At End of Burst:

- Initiate and read SD lamp system.
- Clear all event flags remaining.
- Record scaler readings.

The effective duration of an SPS burst was measured to be around 1.2 seconds.

3.2. The Magic Box Trigger Electronics

The bulk of control of the trigger was performed by universal programmable logic units, produced by C.A.E.N. Viareggio, Italy. For brevity these were called magic boxes (hereafter MB). The MBs were CAMAC standard units which could handle ECL or NIM standard input / output signals. Each MB had eight or ten input latches, each of these received a High or Low signal as illustrated in Figure 3.3. There were six output latches on which was placed the result (High or Low) of a determined logic operation. The MBs could also receive a strobe input, which set a time window within which signals were processed. MBs could operate at rates between from 30Hz to 64Hz depending on details of how the signals are handled. The MBs contained an array of random access read / write memory, and serving electronics. The input signals were used to determine a memory address, and the contents of that address were placed on the output latches. The contents of the MB memory were set via CAMAC, and could be read back to check that the contents were intact. It was also possible to read the state of the input latches through CAMAC thus permitting easy monitoring at each stage of the trigger chain.

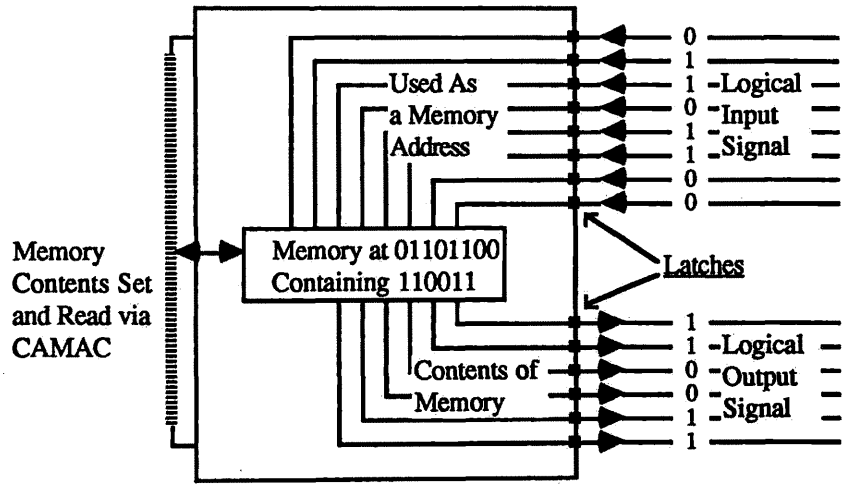

Figure 3.3. The Principle of Operation of the Magic Box Trigger Units

The contents of an MB memory could be determined by a computer programme written in any high level language such as FORTRAN. Such a programme only needed to be run once, and its results loaded into the MBs when needed. In NA1 any given trigger condition was determined by a set of such programmes, these programmes being loaded into the MBs when the trigger was selected. In this way parts of the trigger were re-configured without the need to change the physical electronics or wiring.

3.3. Overview Of The Trigger

There were two main parts of the trigger. The first, called the STROBE, indicated that an interaction had occurred in the apparatus. The second type of trigger, called FINAL, indicated that the interaction was probably of a type of interest, and should be written to computer tape. The STROBE was fanned out to all parts of the data acquisition to provide timing signals and logic gates. In the ADCs the strobe provided a start time, from which they began to integrate charge coming from parts of the apparatus. In the TDCs the STROBE provided a start time used to measure the drift times - the STOP was provided by a signal from the drift or delay wires of the drift chambers. The STROBE was passed to the fast logic units which made the FINAL trigger. Here it provided a time window within which to make a decision.

The FINAL trigger was composed of signals from many parts of the apparatus. The objective of the FINAL trigger was to indicate that the event was not electromagnetic and was open in other ways. In one spill of the SPS we expected approximately 30 useful events. The computer was capable of writing events at this rate, thus with the FINAL trigger filtering most-ly hadronic events were writen to tape and the data acquisition was not swamped with electromagnetic events.

3.4. The Strobe

The STROBE provided timing for higher level parts of the trigger, and components on the data acquisition. A number of different definitions of STROBE were used for various aspects of the data taking and setting up of the experiment.

3.4.1. CHARGE Definition of STROBE

The main STROBE used, called CHARGE, indicated that a photon had entered and that charge had left the target. A photon was defined using the tagging counters, the B1 and the BØØ scintillation counters. Charge leaving the target was defined using the TCØ scintillation counter. These were combined to give the STROBE defined as:

$$\text{CHARGE} = \text{BØØ} \wedge \text{TAGG} \wedge \neg\text{B1} \wedge \text{TCØ} \qquad (3.1)$$

The elements BØØ, TAGG , B1, TCØ were composed as follows (for each element the expected rate calculated on the basis of electro-magnetic interaction is quoted).

BØØ - Beam Line Trigger

BØØ was a scintillation counter located before the electron-photon converter. BØØ produces a signal indicating that an electron had entered the electron-photon converter. The signal was transmitted to the data acquisition by fast cable. This counter operated at around 1.4MHz per SPS spill.

TTn - An Electron in a Tagging Counter

The signals from the tagging calorimeters were split, part of the signal going to the ADC's to be recorded with the event data and part being used in the trigger. There were too many counters in the tagging system for them all to be easily used in the trigger. For this reason, the signals were grouped by a system of mixer units into 4 groups; TT1, TT2, TT3 and TT4. The counters were grouped as shown in Table 3.1, and the signals were then passed to a logic unit, to be combined with the POS signal, to give the final TAGG logic signal.

Trigger Name	Counters Used	Photon Energy Range / Gev	Relative Flux†
TT1	1 -> 4	70 -> 104	61.7%
TT2	5 -> 12	105 -> 144	23.3%
TT3	13 -> 27	145 -> 160	6.5%
TT4	3 lead glass blocks	161 -> 175	8.5%

Table 3.1. Tagging Counter Trigger Grouping

† Calculated using the EGS Monte Carlo programme [FORD87].

POS - Positron Veto

POS was a scintillation counter hodoscope located to the left of the electron-photon converter, after the sweeping magnet. If an electron, entering the converter, produced an additional electron / positron pair, the positron would be directed into POS by the sweeping magnet. Around 1.5% of electrons entering the converter were calculated to produced e^+e^- pairs which would be detected by the POS counter using the EGS programme [FORD87].

TAGG - Signal in Tagging Counters

The signals POS, TT1,TT2,TT3 and TT4 were combined to give a final trigger element called TAGG. TAGG indicated that there had been a response from the tagging system consistent with a photon having been produced there. The signals from these components were timed together, and fed into a magic box. This magic box produced a positive signal, for the trigger, when the condition:

$$TAGG = \neg POS \wedge (TT1 \vee TT2 \vee TT3 \vee TT4) \qquad (3.2)$$

was met. That is, a signal in the tagging calorimeters, and no positron signal. Equation (2.1) may be used to estimate the proportion of photons produced within the energy acceptance of the tagging system. A TAGG signal was expected for 8.7% of the BØØ rate.

TCØ - Charged Particles Exiting Target

TCØ was a disk scintillation counter located after the target (outside the cryostat). Its pulse height provided a measure of the number of charged particles leaving the target and could resolve charge multiplicities of up to six particles clearly.

The TCØ signal was used in different ways in the STROBE, in the composition of ¬B1 and in the FINAL triggers. The electronics chain for TCØ is shown in Figure 3.4. The STROBE contribution was a level indicating interaction in the target. For the final trigger, the signal from TCØ was passed through a series of discriminators to distinguish 0 2 4 6 8+ particles. The discriminator signals were fed into a magic box. The magic box could then be set to give a positive signal depending on the number of particles required from the target. Normal running conditions required two or more particles exiting the target.

The target presented approximately 0.3rl of material giving 24% of incoming particles interacting in the target, the primary kind of interaction being electromagnetic.

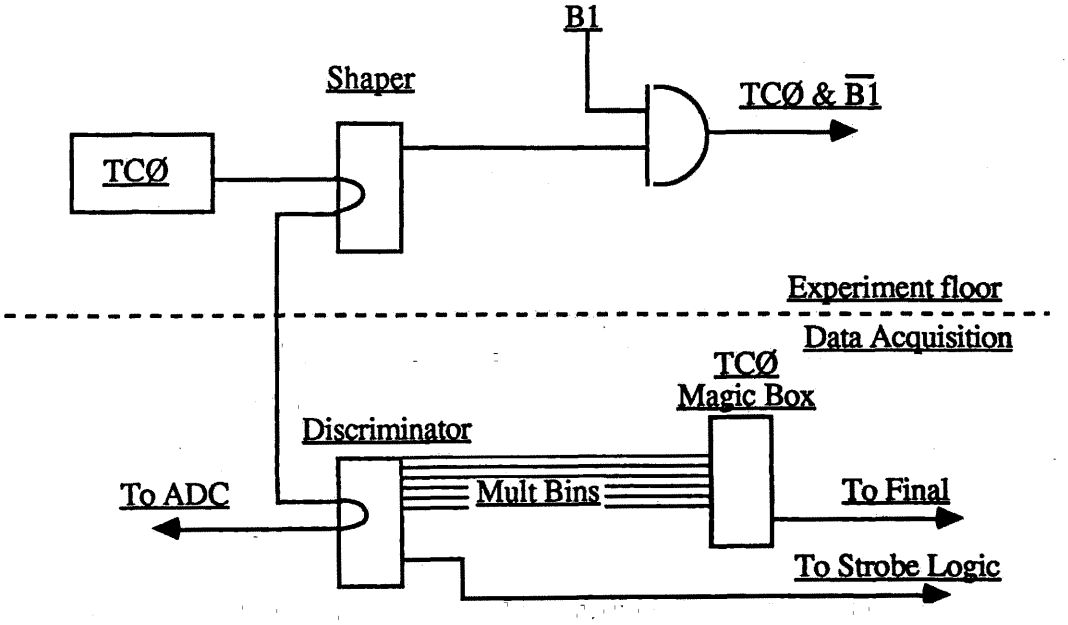

Figure 3.4. The Construction of the TCØ ∧ ¬B1 Trigger Element

¬B1 - Photon entering target

B1 was a scintillation counter located after the collimator. A signal in B1 indicated that the beam electron had not interacted in the converter, thus a null signal in B1 indicated that a photon entered the target. A null signal from the scintillation counter, taken on its own, was not meaningful. A coincidence of B1 and TCØ was composed close to the apparatus, and sent to the data acquisition to be used in the trigger logic. The TCØ

signal here was just a pulse height above a threshold and should not be confused with the TCØ signal described below. Thus when ¬B1 is referred to, the signal was:

$$\text{TCØ (above threshold)} \wedge \neg B1 \qquad (3.3)$$

The tagging system was not involved in this trigger element, thus the expected rate for ¬B1 covers photons produced over the full energy range. Again considering equation (2.1) and using a low energy cut off of 1Gev for the integral 52% of all incoming electrons should have produced a bremsstrahlung photon. Of these 24% would interact in the target electromagnetically. Thus we expected the rate for ¬B1 to be 12% of the BØØ rate.

3.4.2.Strobe Paralysis

The STROBE signal was combined with elements internal to the data acquisition to produce the paralysed strobe (PAR.STROBE). It was PAR.STROBE which was used to trigger the DAQ logic and the computer system. A PAR.STROBE was produced when there was a strobe, and the data acquisition was ready to handle another signal. In this way beam photons were not counted while an event was being processed. The effective beam flux was thus given by the PAR.STROBE rate. The conditions for PAR.STROBE were:

- a STROBE had occurred, and there was:
- a delay of around 28nsec had occurred before the last strobe.
- a RMH had been set by the FPDA computer.
- a set from the free trigger MB.

RMH - PDP generated gate

Once the computer FPDA had completed the reading and recording of an event, it set a flag on CAMAC to remove the paralysed strobe inhibit. This flag, called RMH, allowed the strobe to continue the trigger chain.

3.4.3. CHARGE Strobe Rates

The rates from each element of the trigger were counted on a set of scalers so that the trigger electronics may be quickly checked. Table 3.2 shows an example of the rates recorded for each of the CHARGE strobe elements. The expected rates, summarised from the above calculations, compare well with those recorded with the exception of the TCØ rates. This may be due to bad timing of the TCØ signal to the trigger scalers. The

total number of photons signaled by TAGG is given by the sum of TTn and the Lead Glass Tagging less the e^+ count. Thus 8.7% of all electrons give a photon between 70Gev and 170Gev. For reference, the number of FINAL event triggers (those recorded on tape) has been included.

Trigger Element	Rate	Percent of BØØ	Expected Rate of BØØ
BØØ / Burst	$1.3 \cdot 10^6$ / 10^6 BØØ	100%	
TTn	$8.3 \cdot 10^4$	8.3%	8.0%
Lead Glass Tagging	$2.1 \cdot 10^4$	2.1%	1.0%
e^+ Counter	$1.7 \cdot 10^4$	1.7%	1.5%
TCØ - Level	$1.2 \cdot 10^5$	12.2%	24%
¬B1	$1.1 \cdot 10^5$	11.0%	12%
¬B1 ∧ TAGG	$1.7 \cdot 10^4$	1.7%	2.0%
STROBE	$1.6 \cdot 10^4$	1.6%	1.7%
Par. Strobe	$1.5 \cdot 10^4$	1.5%	1.6%
FINAL events	~14		

Table 3.2. Strobe Element Rates

3.4.4. Other Strobe Triggers

A number of other kinds of strobe were defined for use with calibration runs and monitoring the data structure. These strobes were not used for data taking.

PULS - Artificially Generated Trigger

A timing unit existed which generated a pulsed signal. This trigger could be selected by changing the programme in the DAQTRGG magic box. Events could be read using PULS for testing trigger elements with no bias.

MUON - MIP trigger of SD1 Calibration

A halo of muons was produced from the decay of neutral pions from the initial targets of the SPS. These particles were highly relativistic and heavy. They thus pass through most material as minimum ionising particles, and can be used to help calibrate the

shower detectors. A simple trigger was built to collect events in which muons passed through SD1, and was set when there was no beam on H4. The trigger required one count in the front shower, one count in SD1 and a signal from SD2.

STROBE.TCØ

For runs intended to test the tagging counters the inclusion of TAGG would have provided a bias. For runs made to test parts of the apparatus, a looser strobe was used called STROBE.TCØ which was defined as:

$$TC\emptyset \wedge B1 \qquad (3.4)$$

This trigger was not used for the data taking runs.

3.5. Second Level Trigger

The rates estimated for STROBE above were calculated on the basis of total electromagnetic interactions. Clearly these dominated the event rate at the STROBE level. The second level trigger FINAL made use of a number of elements of the FRAMM spectrometer for the selection of hadronic events.

- The front shower detector and surrounding anti-counters.
- SD1 - the shower detector in stack 2
- SD2 - lead glass blocks in stack 3
- SD5 - the back stop lead glass
- The Multi wire proportional chamber located after Verginella drift chamber.

The shower detectors were used to detect the presence of hadrons or photons to indicate that a hadronic interaction had occurred. The multiwire proportional chamber was used to measure the opening angle of the event (DMAX).
The basic definition of FINAL was:

$$HADRON_{>1} \wedge GAMMA_{>1} \wedge \neg FA \wedge TC\emptyset \wedge DMAX \wedge \neg SD5 \qquad (3.5)$$

Each of these elements was composed in Magic Box logic from signals derived from the apparatus through discriminator and pattern units. The signals from the final signals of: HADRONS, PHOTONS, the FA, TCØ, DMAX and SD5 were all passed to the FINAL magic box. The programme in this magic box could be changed to select different combinations of these elements. Some runs were, for example, taken with SD5 out of the trigger to test the effect it had on the overall quality of the data. The definitions of each of these elements is discussed below.

DMAX - Event Minimum Opening Angle

The e^+e^- pairs from photo-production have zero opening angle. Hadronic events in general produce charged tracks with wide opening angles. A key feature of the trigger was a component making a decision on the overall opening angles of the event. DMAX was constructed from two multiwire proportional chambers located 70cm from the target (Figure 2.5) which had a wire spacing of 2mm. The signals from these chambers were passed through an electronics chain which generated two digital numbers. These numbers corresponded to a wire number in x and in y, such that that wire was the furthest from the zero axis to have a signal. These two numbers were passed to the DMAX MB, where the larger of the two numbers was selected as DMAX, and a

positive flag was set if this value was greater than a given threshold. These thresholds could be chosen as shown in Table 3.3. The acceptances for rho and omega have been calculated in a simulation program.

DMAX Setting	Opening Angle	Acceptance for Rho	Acceptance for Omega
4 mm	5.7mrad	48 %	57 %
8 mm	11.4mrad	25 %	42 %
30 mm	42.8mrad	0.05 %	0.5 %

Table 3.3. DMAX Acceptances

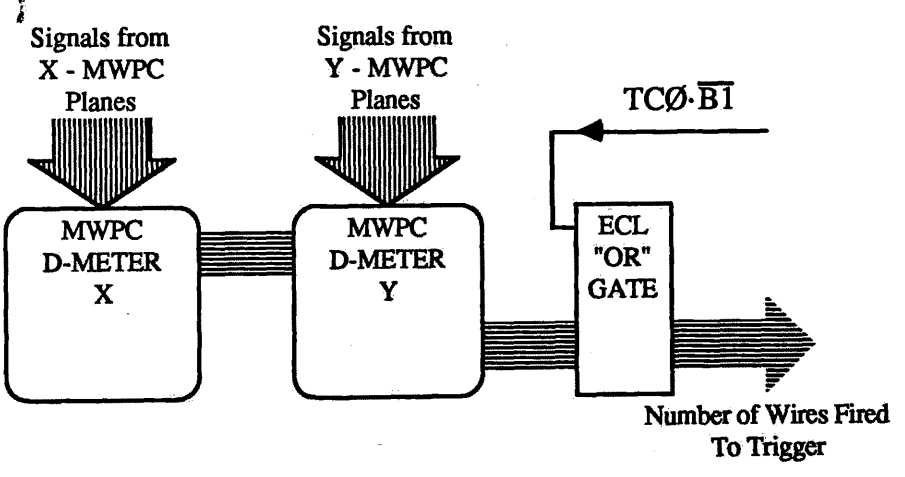

Figure 3.5. The Construction of the DMAX Trigger Element

The acceptance for e^+e^- production was expected to be close to zero. Electromagnetic events still pass this trigger requirement due to the number of such reactions which produce more than two charged particles, multiple scattering, and inefficiencies in the MWPC's. A DMAX setting of 4mm was used for normal running conditions. This corresponds to the minimum value measurable by the MWPC's.

FA & SA - Nuclear Breakup Veto

The photon interactions of interest to the experiment were produced through coherent processes (Section 1.3). To reduce the amount of data originating from hard, inelastic photon interactions giving rise to nuclear breakup in the target a veto was made on neutrons and wide angle protons.

SD5 - Beam Electron Veto

SD5 was composed of four blocks of lead glass plus a front lead glass block constructed very much like SD2 and SD4. It was located at the very end of the apparatus, in such a way as to detect all particles passing through the hole in SD2 (Figure 2.1). SD5 could be used in the reconstruction of events, and its signals were recorded, in the same way as those of SD2 and SD4. However its main role was in vetoing electromagnetic events and events in which a second, noninteracting photon was produced by double bremsstrahlung in the converter. SD5 veto was set with a threshold of 5Gev. The probability of double bremsstrahlung was estimated to be ~16%.

TCØ - Multiplicity Leaving the Target

Part of the TCØ signal was passed through a series of discriminators, each set with a different threshold. The output from these units were passed to the TCØ magic box, giving levels for: > 1, > 2, > 3, > 4 particles. The logic of this magic box could be altered for different running conditions. The output indicated that the multiplicity in TCØ was above or equal to a given value. Under normal running conditions, a multiplicity of greater than two charged particles leaving the target was required.

Hadrons and Gammas in the Shower Detectors

The signals from the front lead glass (FLG) were obtained as follows:

- The signal was passed through a delay unit so that signals from all parts of the apparatus arrived at their destination in time.
- The signal was then passed through a splitter unit from which a signal was passed to the data acquisition.
- Part of the signal was then amplified and passed to a chain of shaper units.
- The shaper units produce a signal which conforms with ECL standard, for the logic units. The shaper units also have thresholds set. If the signal is above a low threshold, a positive signal was sent from the first shaper unit
- If the signal was above a high threshold a signal was sent from the second shaper unit.

The signals from the back lead glass blocks (BLG) were also split, and part of the signal was passed through a mixer unit. These combined signals corresponded to each front lead glass. The signals from the mixers were then passed through an amplifier/shaper chain as described above for the front lead glass. The back signal was only passed through a low threshold.

The signals from SD1 were handled in a similar way to those from SD2. The front part of SD1 was taken to correspond to the front lead glass, the back part of SD1 corresponding to the back lead glass units. There were too many strips of scintillator in SD1 to allow each to be conveniently handled by the logic units. The signals were combined in regions corresponding to the width of the FLG (in SD2 and SD4).

By tuning the high and low thresholds of the SDs in test beams, a decision could be made by the logic units as to whether hadron like or electromagnetic shower had occurred in the shower detector. Hadrons were not expected to produce a large shower in the front part of the lead glass; electromagnetic showers started early, and produced a large shower. All genuine showers were expected to produce a signal in the back shower detector. With the definitions:

$$BACK_{LOW} = \text{Back signal above threshold} \quad (3.6)$$

$$FRONT_{LOW} = \text{Front signal above lower threshold} \quad (3.7)$$

$$FRONT_{HIGH} = \text{Front signal above higher threshold} \quad (3.8)$$

Thus hadronic (HAD) and electromagnetic (EM) showers were defined for each region of SD1 and SD2 in terms of equations 3.6, 3.9 and 3.8:

$$HAD = FRONT_{LOW} \wedge \neg FRONT_{HIGH} \wedge BACK_{LOW} \quad (3.9)$$

$$EM = FRONT_{HIGH} \wedge BACK_{LOW} \quad (3.10)$$

The objective in counting EM showers was to trigger on photons originating from neutral pion decay. For this reason shower detector signals were only used for elements out of the central region of the shower detectors defined by the plane of the magnets. This avoided counting electrons.

T counters - Charge Entering the SD's

The T counters were strips of scintillator located before SD2 and SD4 (Figure 2.1). They matched the front lead glass blocks, *i.e.* one T counter per front lead glass. In principle, an electromagnetic signal in the SD's (EM), in coincidence with a T signal should have indicated an electron entering the SD's. The absence of a T signal thus indicating a photon. However, it was noted that there was a finite possibility of an electron being back scattered from a photon entering the front lead glass. Thus a photon could give a T signal, and look like an electron vetoing good hadronic events. For this reason the T counters were only used to define charged hadrons, and were normally absent from the gamma signal.

First Level Hadrons and Gammas

Signals $FRONT_{LOW}$, $FRONT_{HIGH}$, and $BACK_{LOW}$ from each group of detectors were passed to a group of magic boxes which produced a signal indicating that either a hadron is detected, a photon is detected, or neither. With the use of the T counters with HAD and EM, equations 3.9 and 3.10, hadrons and gammas were defined as:

$$HADRON = T \wedge HAD \tag{3.11}$$

$$GAMMA_T = \neg T \wedge EM \tag{3.12a}$$

$$GAMMA = EM \tag{3.12b}$$

The definition of GAMMA (3.12b) without the use of the T counters in anti-coincidence allows electrons to be misinterpreted as photons. Thus although definition 3.12b prevented many events with neutral pions in them from being vetoed as electromagnetic, it also allowed a large number of electromagnetic events into the final data. Data samples were taken both with photons defined with 3.12a and 3.12b.

Second and Third Level Hadrons and Gammas

The numbers of GAMMA and HADRON signals from each region of the shower detector were added together in two layers of magic boxes to give a total count for the final trigger. In this context the MBs were used to add numbers, the input signals being binary digits.

3.5.1. Rates for FINAL

No estimates were made for the expected rates for each element of the FINAL trigger. In Table 3.4 are shown examples of recorded rates for these elements corresponding to those given in Table 3.2.

Trigger Element	Rate for 10^6 Par.Strobes	Percent per Par.Strobe
Front Anti	$5.1 \cdot 10^4$	5.083
Surr. Anti	$1.4 \cdot 10^2$	0.014
DMAX	$6.0 \cdot 10^2$	0.060
Hadrons SD1	$1.1 \cdot 10^3$	0.109
Photons SD1	$3.2 \cdot 10^3$	0.323
Hadrons SD2	$3.6 \cdot 10^3$	0.359
Photons SD2	$6.0 \cdot 10^3$	0.600
Final	$9.0 \cdot 10^2$	0.090

Table 3.4. FINAL Trigger Elements Rates

A study with a simulation programme of the apparatus would have to be made to understand whether these rates were compatible with the physics processes at hand. However the primary objective of the trigger as a whole and FINAL in particular was to bring the rates down to levels with which the data read out can cope, without the loss of interesting events. It should be noted that without such a study, no estimate of the effects of the trigger on the experiment's acceptance can be made and thus any estimate of the yield or cross section for a given photon interaction channel will have large uncertainties.

3.6. Trigger Management Signals

DAQTRIGG - Data Acquisition Has An Event

This trigger element was constructed with a MB unit. The inputs to DAQTRIGG were; LAMP, PULS, TAGG and MUON. The setting of this MB and the DAQMODE MB determined which of these signals were used, and thus the final trigger strobe which initiated the data acquisition. DAQTRIGG gave a positive signal for one of many kinds of trigger.

DAQMODE - Final Trigger Control

DAQMODE produced the final event interrupt. The inputs to this logic were:

- FINAL
- from DAQTRIGG
- SOB and EOB from SPS.
- inhibit from FPDA.

DAQMODE then informed FPDA of a SOB, EOB or event. It was important to have this information controlled by an MB to avoid conflicting signals being sent to the computers *e.g.* an EOB arriving while an event was being read.

Chapter Four

Data Processing and Reconstruction

This Chapter contains a description of the processes through which the raw data was passed to prepare it for physics analysis. This covers the whole area from decoding the digitizations from electronic units, to the interpretation of the responses of the detectors in terms of elementary particles. A number of these stages are of little interest, for example ADC decoding. I have concentrated on those stages which have a material effect on the use of the data in the final analysis. Some emphasis is given to the handling and interpretation of the target data since this used some new techniques.

4.1. Data Processing

The stages through which the raw data was passed to prepare it for physics analysis are illustrated in Figure 4.1. Each of these steps involved passing the raw or processed data through a suit of computer programmes. The programme which reconstructed the data to give particle momenta and energies and which interpreted the responses of the target and Čerenkov required up to 2s per event. With $6.3 \cdot 10^6$ events written during the whole data taking, processing all these events would have required more computer time than was available if no further selection had been made of the data. For this reason the data was passed through a fast and simple programme, the soft trigger, to remove as many uninteresting events as possible with a minimal loss of useful data.

Data accepted by the soft trigger were passed through the full calibration and reconstruction programmes. The results of this processing were then summarised giving data summary tapes (DSTs) containing; the particle four momenta, the Čerenkov and shower detector responses, the target data, the photon beam energy and some general event parameters. During the production of the DSTs some further data selection was made against electromagnetic events. This summarised data was then used for physics analysis.

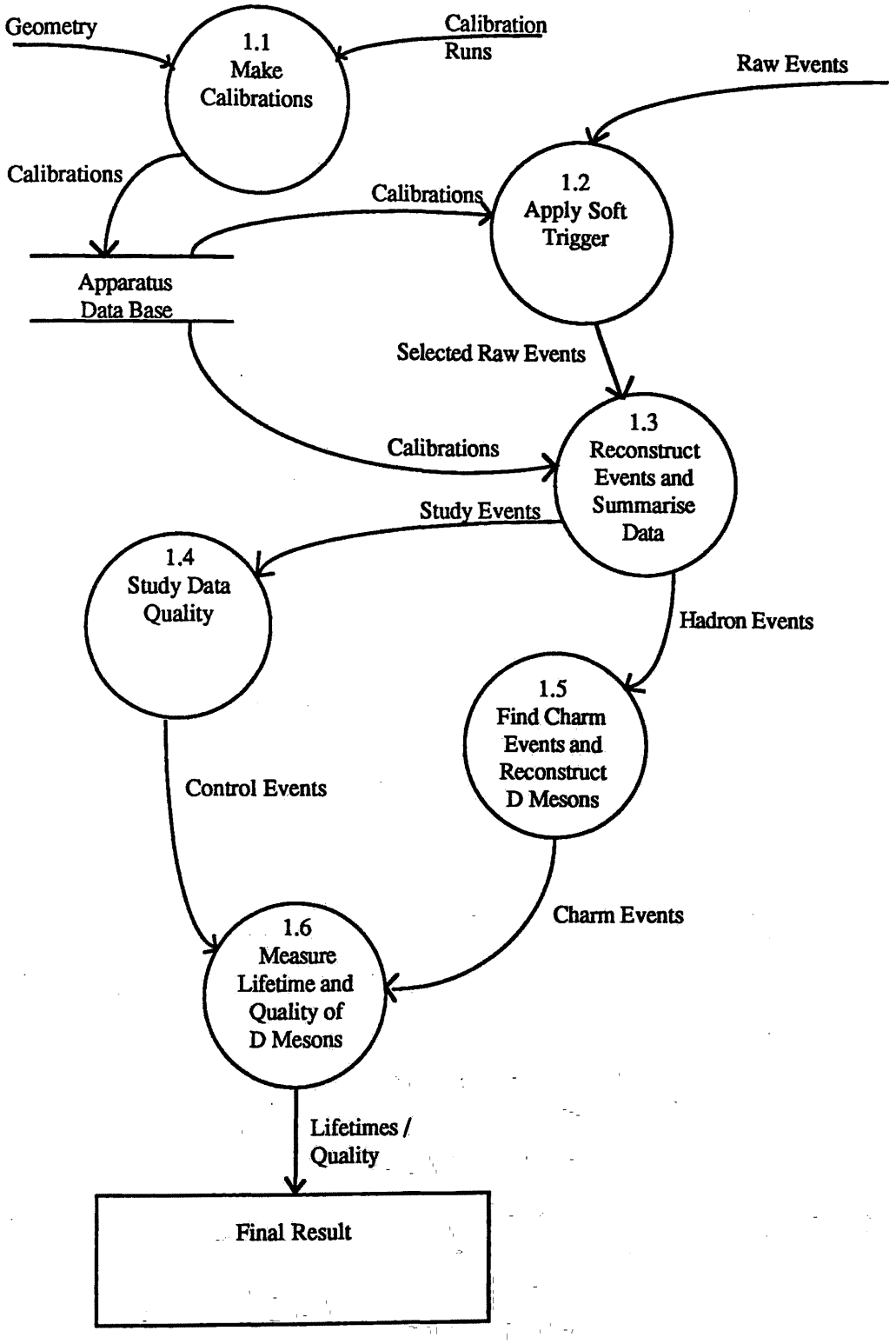

Figure 4.1. Off Line Production and Analysis Data Flow

4.2. The Soft Trigger

The soft trigger was used on the raw data to filter out those electromagnetic events which could be distinguished purely by the response of the shower detectors and T hodoscopes without the need for charge tracking. The steps in the soft trigger are illustrated in Figure 4.2. The definition of hadrons, photons or electrons followed those used in the trigger (Section 3.5). The main differences between the event filtering made on line and that made by the soft trigger was in the precision of the calibrations of the shower detectors and the intricacy in the acceptance / rejection criteria used. These criteria were set from the results of the scanning of a selection of events. The coded selection criteria allowed different kinds of events to be distinguished.

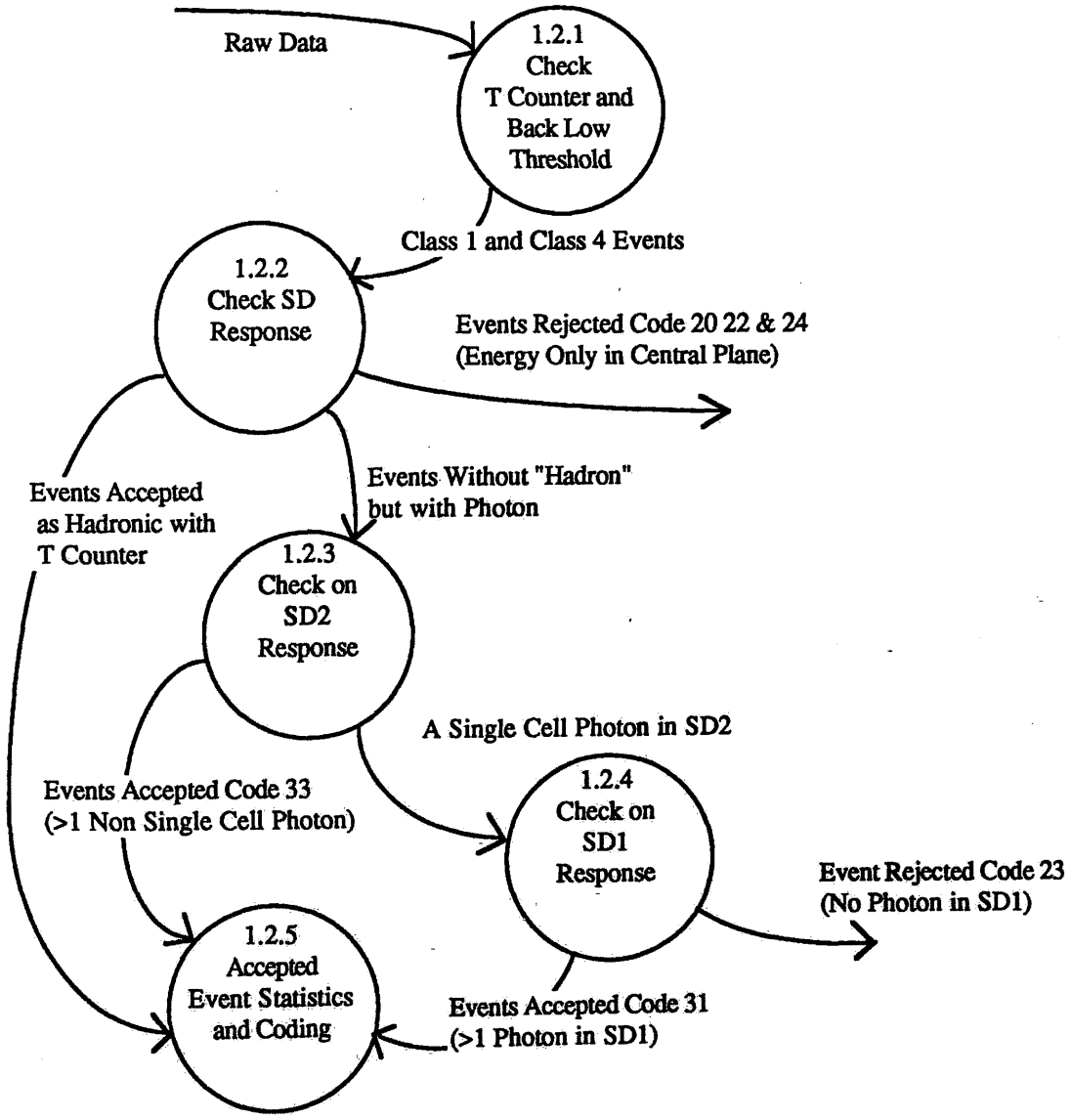

Figure 4.2. Soft Trigger Data Flow

CODE MEANING

1 All events exclusive of code 4 events.

4 These events contained at least one signal with; T counter fired, signals in back and front lead glass. These events were distinguished since they were often found to be hadronic events during the tuning of the soft trigger.

Rejected:

20 Events in which no energy had been deposited out of the central plane of shower detectors.

22 Events with energy deposited out of the central plane, but for which this energy may be attributed to "leakage" from the central plane.

23 Events which had energy deposited out of the central plane in SD2 but with all the energy contained in one lead glass block. These events were only rejected if there were no photons found in SD1. Thus this cut served to reject photons produced from bremsstrahlung of electrons. If there had been another photon then these may have been produced from π^0 decay.

24 Events from class 4 but rejected as for class 22 above.

Accepted:

30 Events with at least one hadron like signal.

31 Events with a "single cell" photon as in code 23 above, but for which an extra photon was found in SD1.

33 Events with at least one photon none of which are "single cell" photons.

34 Hadronic events as for code 30, from class 4 events.

The effects of these selection criteria were assessed for a number of samples of data. These events were fully reconstructed and further analysed by eye. In these events:

- There was a rejection rate of 75%.
- Of the accepted events, 57% were thought to be hadronic (classes 1 and 4).
- For class 4 data only, 90% of accepted events were hadronic.
- 5% of rejected events were hadronic.

The failure rate of 5% of the soft trigger, coresponding to a loss of 21% of hadronic events, was considered acceptable.

4.3. Tagging Resolution

The tagging shower detectors were calibrated with beams of electron of energies 100Gev, 50Gev and 25Gev. Figure 4.3 shows the plot of the spread in energy reconstructed in the tagging shower detectors (δE) over total beam energy against the inverse of the root of the beam energy. From this it has been found that:

$$\frac{\delta E}{E} = 1.3\,\% + \frac{21\,\%}{\sqrt{E}}$$

The position measurements from the drift chambers were favoured for accuracy. However they were not as efficient as the SDs which were used to verify electrons above noise in the chambers, and in cases where the drift chambers were not operating efficiently. The effective efficiencies of the SDs are given in Table 4.1.

Number of "electron" signals	Occurrences
0	2.9%
1	94.7%
2	2.0%

Table 4.1. The Tagging Efficiency

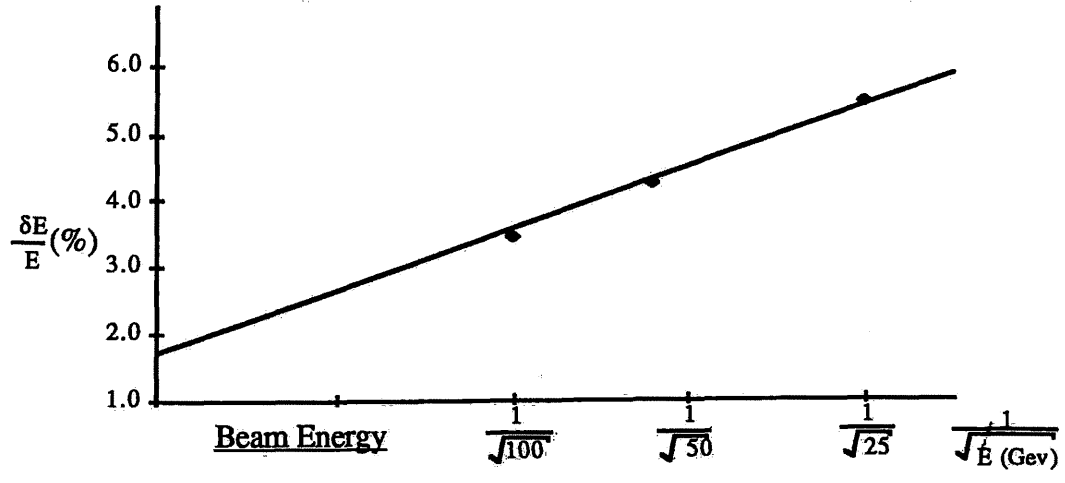

Figure 4.3. Tagging Calorimetric Resolution

4.4. Particle Reconstruction

The FRAMM spectrometer could determine the energy, momentum and charge sign of charged particles using a combination to tracking chambers, magnets and shower detectors. The energy and direction of photons originating from the beam, beam interactions or neutral particle decay was determined with the shower detectors. Figure 4.4 illustrates the data flow for particle reconstruction.

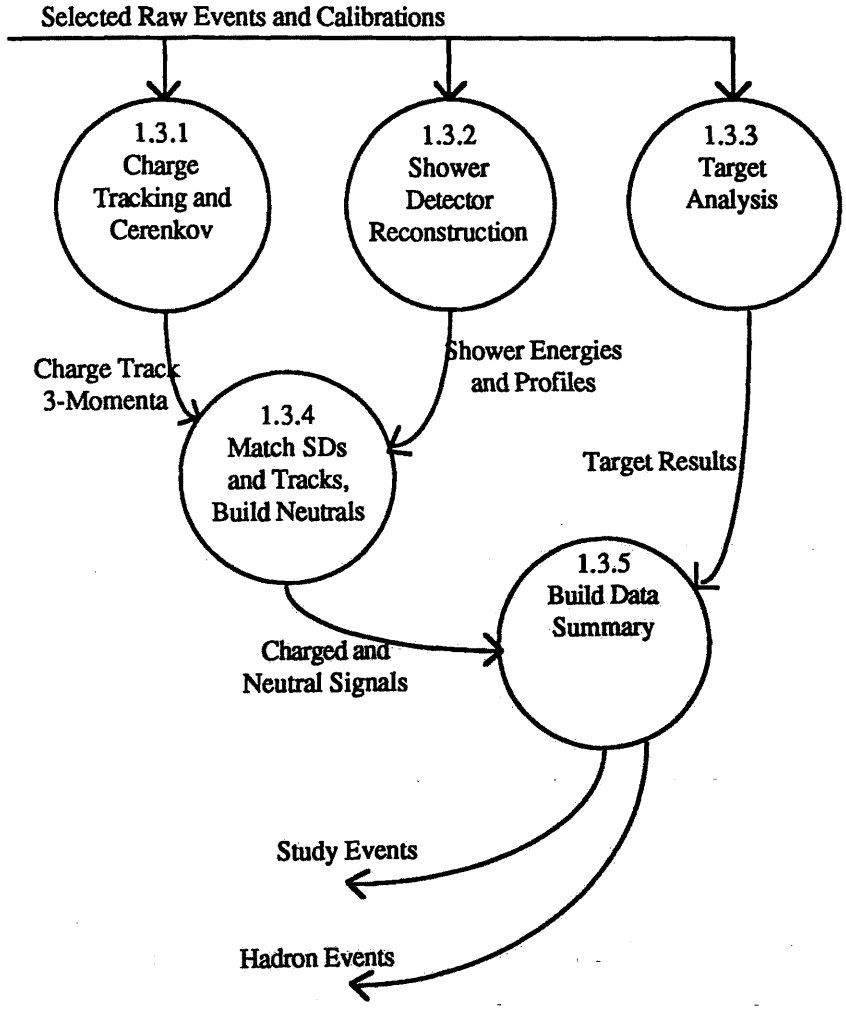

Figure 4.4. Reconstruction Data Flow

4.4.1. Calorimetry

The shower response of the calorimetry served to determine the energy of photons entering the shower detectors and to distinguish hadrons from electrons. To determine the energy of photons and electrons the response of both the FLG and BLG in the lead glass shower detectors, or the back and front parts of SD1, were calibrated and combined to give total deposited energy. For charged tracks the energy deposited in the front, back and whole calorimeter is related to the momentum of the incoming particle to distinguish the shower development of hadrons and electrons.

The total energy deposited in an element of the lead glass shower detectors was related to the total pulse height response (Ph_{SD}) by the equation:

$$E_{SD} = A \cdot Ph_{SD} + B \qquad (4.1)$$

The values of A and B were determined from calibration data for each shower detector and the total pulse height was given by the equation:

$$Ph_{SD} = \alpha \cdot Ph_{BLG} + \beta \cdot Ph_{FLG} \qquad (4.2)$$

where Ph_{BLG} and Ph_{FLG} are the pulse height responses of the back and front lead glass "equalized" to compensate for fluctuations between elements in each shower detector and drifts in the responses of the electronics.

It was found that the best energy resolution was achieved with a choice of α and β such that $\alpha = 1$ and β was a function of Ph_{BLG} of the form:

$$\beta = C \cdot Ln(D \cdot Ph_{BLG}) \qquad (4.3)$$

The values of C and D were determined using tagged photon beams with maximum energies of 50Gev and 100Gev. The photons entered the centre of nonets of lead glass blocks which had been moved in line with the beam. Plots of β against Ph_{BLG} are shown in Figure 4.5. By fitting (4.3) to these plots the values of C and D were obtained.

Detector	Value of C	Value of D
SD2	0.012	0.055
SD4	0.006	0.051

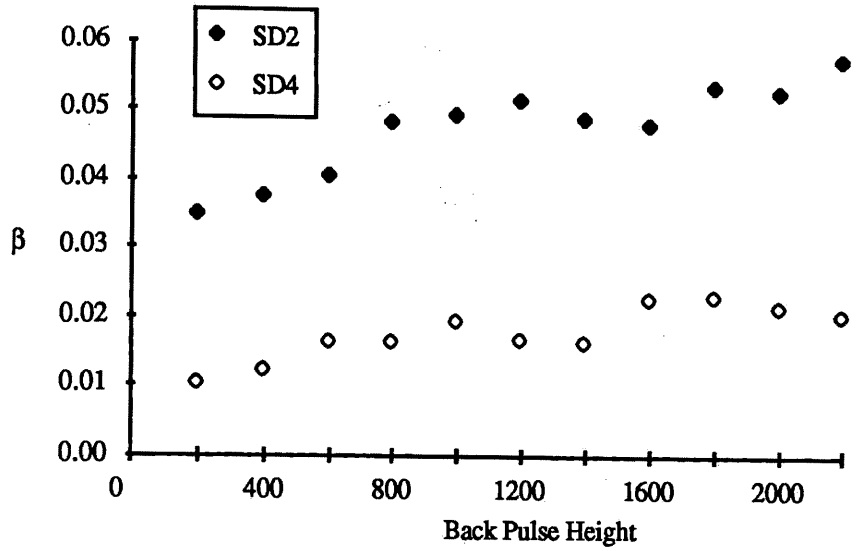

Figure 4.5. Back Lead Glass Pulse Height .v. β

The Ph_{SD} values calculated from (4.2) are shown in Figure 4.6 plotted against the tagged photon energy. The parameters for (4.1) could be determined from these plots with a linear fit giving the values:

Detector	Value of A	Value of B
SD2	0.48	0.037
SD4	0.097	2.94

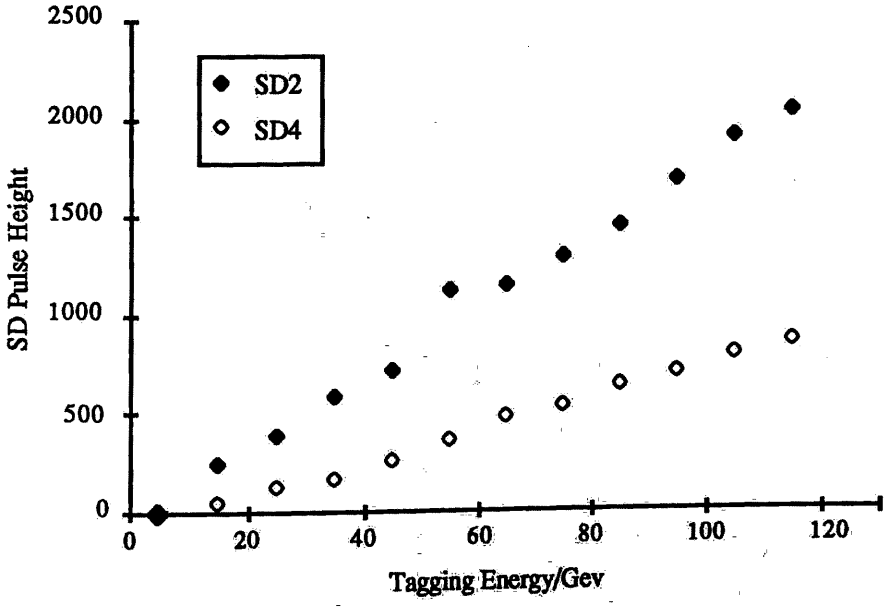

Figure 4.6. Tagging Energy .v. Lead Glass Pulse Height

In the SD1 the back and front parts were of the same construction and no energy dependent relation between the pulse heights and energy was used.

The physics basis for the above treatment is not clear however this method was found to give the best energy resolution. Note also that the above constants are only examples and that in practice detector and run dependence was considered. The final energy resolution was found from the above calibration data to be:

$$\frac{\delta E}{E} \approx \frac{20}{\sqrt{E}} \%$$

for the Lead Glass detectors and

$$\frac{\delta E}{E} \approx \frac{40}{\sqrt{E}} \%$$

for the SD1 Lead Scintillation detector. These values represent the best resolution available when a shower was totally contained within a nonet of lead glass blocks or totally within the SD1 scintillator fingers. Some loss of energy and thus degradation of resolution was found for showers occurring close to the edges of the detectors, principally close to the inner holes.

The position of a shower in the transverse planes of SD2 and SD4 could be determined with a precision of:

$$\Delta x = 2\text{mm}$$

by taking the barry-centre of the pulse heights in a nonet of detectors with the lead glass block with the greatest pulse height at the centre and the seven surrounding lead glass blocks. A similar precision was achieved for SD1 by fitting for the barry centre with each scintillation finger used in a shower and integrating in the PAD chamber coordinates.

4.4.2. Charged Track Spectroscopy

Charged tracks were reconstructed in a number of stages:

1) The drift times and delay line times on each wire were converted to space coordinates (hits).
2) In each stack, straight line tracks (rettas) were fitted to groups of hits. The rettas were constrained to point back to the target in the y-plane (no magnetic field). Some degree of hit sharing was allowed in order to minimise the losses.

3) Rettas in each stack were matched with an overall space fit giving the track parameters and a χ^2 used to select between ambiguities. As in step 2 several combinations of space tracks using a single retta was allowed.
4) An attempt to use hits not used by any retta was made with the space tracks to improve their precision and efficiency.

The vertex drift chamber was treated in much the same way as the other stacks although its retta fitting was more complicated and its contribution to the final χ^2 was much smaller given its better spacial resolution. This procedure allowed a number of incompatible solutions at each stage. The combinatorial method lessened the losses due to poor resolution and inefficiencies, however it allowed tracks to be fabricated and this was always considered during physics analysis.

For a pair of retta matched on either side of a magnet making an angle θ with each other, a momentum P may be found with:

$$P \approx 0.299 \cdot q \cdot B \cdot L \cdot \frac{1}{\theta} \qquad (4.4)$$

where, B is the magnetic field, L the length of the magnet and q the charge of the electron. From this the errors on the momentum can be related to those of σ_θ by:

$$\frac{\sigma_\theta}{\theta} \approx \frac{\sigma_p}{P} \qquad (4.5)$$

The distance between two stacks was approximately 1m and the sense wire resolution was $\overset{\circ}{\lambda}$2mm giving a value for σ_θ of ~0.2mr. Considering two retta which both use six hits a more exact value for σ_θ was 0.18mr. For an angle θ of 20mr this gave a value of ≈0.5% for (4.5). This was the best resolution for a track passing through two stacks and one magnet. The higher spatial resolution of Verginella was offset in these calculations by the larger distance between it and the chambers in stack 2.

For less ideal cases where retta do not have a full complement of hits and considering other statistical fluctuations, a final momentum resolution is expected of:

$$\frac{\sigma_p}{P} \approx 1\%$$

4.5. Particle Identification in FRAMM

The FRAMM spectrometer was used to detect the particles produced by the interaction of the tagged photon beam in the target. The directly detectable particles were;

- Charged Particles: The momenta of all charged particles were measured by tracking them through the magnetic spectrometer. The identification of such a track as a particular kind of particle used the Čerenkov counters and shower counters to distinguish hadronic matter from electrons.
  - Charged Pions: The most commonly produced hadronic matter. Such tracks were in general identified as pions by the null hypothesis that a track not identified as any other kind of hadron, was a pion.
  - Charged Kaons: Produced from strange or charmed interactions, their identification was important for finding charmed particles. The main tool for their identification was the Čerenkov counters.
  - Protons: Few of these were detected in FRAMM since they mostly originate from nuclear interactions of the photon in the target and most of this kind of interaction was vetoed in the trigger. For some momentum ranges the Čerenkov counters could distinguish protons.
  - Electrons: Pair produced from the electromagnetic interaction of the beam photons, electrons constitute the bulk of the background tracks. Their identification depended primarily on the use of the shower counters, with some contribution from the Čerenkov counters.
  - Other long lived charged particles such as heavy leptons were not identified in FRAMM.

- Neutral Particles: The only long lived neutral particle directly detectable in FRAMM was the photon. Other long lived neutrals such as the K_L^0 could not be identified. Neutral particles decaying in or shortly after the target were detected by reconstruction from their decay products.
  - Neutral Pion: This was one of the most important neutral particles originating from a number of vector meson decays.
  - The Eta: The η^0 particle was treated exactly as the π^0 except for its difference in mass.
  - Neutral Kaon: The K_S^0 could have been detected from its two pion decay channel. However this only applies for such particles decaying within one or two τ_S lifetimes leaving a small acceptance in FRAMM.

Other neutral particles were reconstructed as part of the physics analysis and did not concern the basic reconstruction of the data.

4.5.1. Photon Detection

Photons were primarily defined as showers for which no charged track match had been made and which were not involved in π^0 reconstruction. Photons which had converted into e^+e^- pairs were reconstructed by considering the gamma invariant mass γ_m and opening angle γ_θ of oppositely charged pairs of tracks both of which had been identified as electrons. To be considered as a candidate gamma the following cuts were applied:

$$\gamma_m < 0.07 \text{ Gev}$$
$$\gamma_\theta < 0.005 \text{ mr}$$

In addition, if several such candidate photons were found only the candidate with the lowest value of γ_m was used. This cut was applied since, for the physics of interest, most photons not originating from π^0 or η^0 decay, were expected to originate from secondary bremsstrahlung of the beam electrons.

4.5.2. Neutral Pion Reconstruction

To reconstruct π^0 particles pairs of photons were combined and assuming that they both originated from the target and an invariant mass was formed. These masses are shown in Figure 4.7(a-e) for photons detected in different combinations of shower detectors. No plot is shown for combinations for which both photons enter SD4 since the rate for this is low. All π^0 candidate mass combination are shown in Figure 4.7f.

The expected width of the reconstructed π^0 mass distribution is related to the energy and spatial resolution of the shower detectors used to measure the photon energy by:

$$\frac{\sigma_m^2}{M^2} \approx \frac{\sigma_E^2}{E_1^2} + \frac{\sigma_E^2}{E_2^2} + \frac{\sigma_\theta^2}{\theta^2} \qquad (4.6)$$

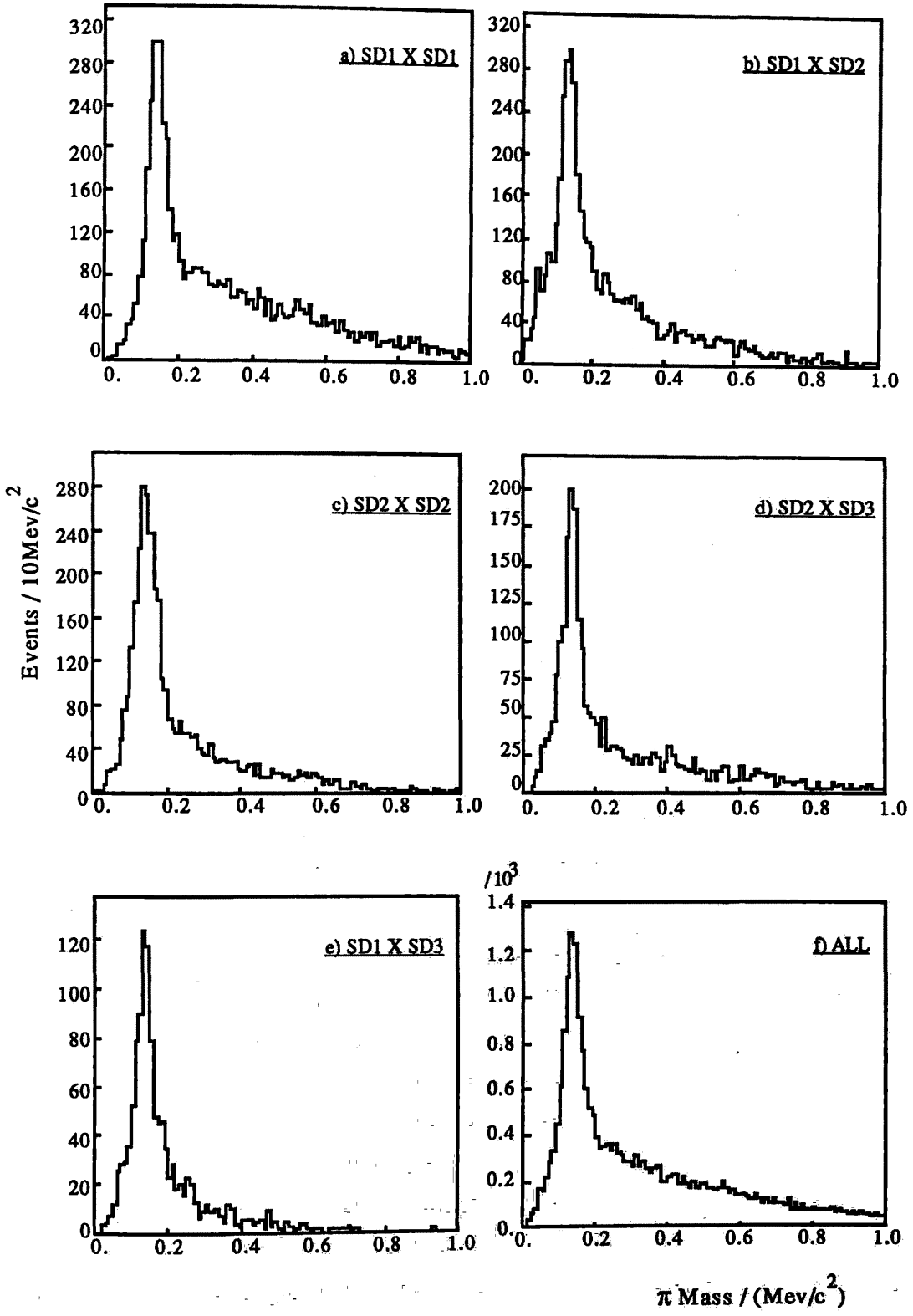

Figure 4.7. Neutral Pion Mass Plots

With the resolutions given in Section 4.3 the dominant affect on the mass resolution was from σ_E. For average energy photons of 20Gev a best value of σ_m of approximately 27Mev/c^2 was expected for π^0s. The full width at half maximum (FWHM) of the π^0 peak in Figure 4.7f is 60Mev/c^2 corresponding to σ_m = 25Mev/c^2. This value is compatible with expectations.

4.5.3. Hadron / Electron Discrimination

The use of shower detectors to make hadron / electron discrimination depended on them being made of a material with very different radiation and absorption lengths [FABJAN85], and their ability to measure the resultant difference in shower development for hadrons and electrons. The ratio of radiation length to interaction length is ~30 and ~13 for the lead glass shower detectors.

The segmentation, along the direction of shower development, of the FRAMM calorimeters was not fine enough to fully reconstruct the shower profile. To discriminate between hadrons and electrons the quantities:

E_{front} = Energy deposited in the front lead glass

and

E_{total} = Total energy deposited in the shower detector

were compared. In ideal conditions these parameters contained sufficient information to achieve the desired discrimination. Note that in the case of SD2 and SD4 E_{front} was undefined, however the technique still worked with E_{ph}, the front pulse height.

To illustrate this technique for hadron / electron discrimination some data from the NA7 experiment [AMENDOLIA86/2] was used. This experiment used the FRAMM spectrometer to study electron / pion scattering. For the main sample of their data the reconstructed kinematics of an event could distinguish the electron from the pion and this sample can be used to understand the responses of the show detectors. In Figure 4.8 E_{front} / E_{total} is plotted against E_{total} / $E_{particle}$ for well identified pions (4.8a) and electrons (4.8b). To avoid swamping Figure 4.7b the events at or close to (0,0) have been removed, these constitute $\frac{1}{3}$ of the total data sample. The particles in these plots had momenta greater than 100Gev/c. Electrons are seen to deposit almost all their energy, clustering around E_{total} / $E_{particle}$ = 1. Electrons also always start to shower in the FLG, E_{front} / E_{total} never being zero. In contrast, hadrons seldom deposit more than $\frac{1}{4}$ of their total energy in the shower detector and only around 1% deposit

more than 1Gev in the FLG. Under these conditions electron / hadron discrimination was made to better than 3%.

In the NA1 experiment, the average track momentum was below 40Gev/c and at these momenta the cross section for pions was larger than in the NA7 case since the pion hadronic cross section falls logarithmically with energy [BARNS70]. In Figures 4.9 The E_{front} / E_{total} versus $E_{total} / E_{particle}$ plot is shown for an set of NA1 data, having passed through the soft trigger, in SD2. The data has been divided into plots depending on the track angle measured at the target, the plots are in bins of 1mr. The electron and hadron regions may be seen in clear parallel to the NA7 plot (Figure 4.8) for the small angle plots (4.9a-c). A substantial amount of events away from either of these regions may also be seen. These data are due principally to pions which have interacted in the FLG and deposited a substantial part of their energy.

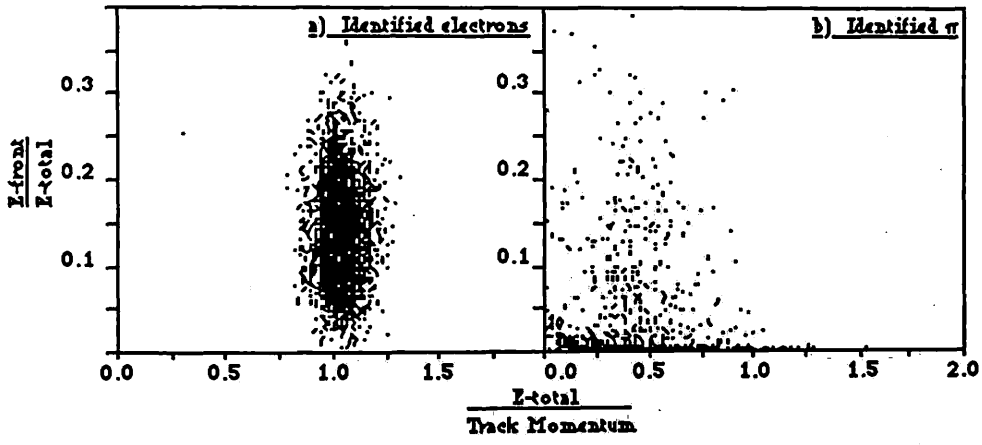

Figure 4.8. NA7 Pion / Electron Plot

Tracks with wide angles were less likely to be electrons, and the effect of pions interacting early in the SDs may be seen in the wide angle plots (Figurs 4.9g-j). In these plots the region where electrons may be found is populated uniformly with the surrounding regions. It is also interesting to note that the pion region, parallel to Figure 4.8b, becomes better populated at wide angles.

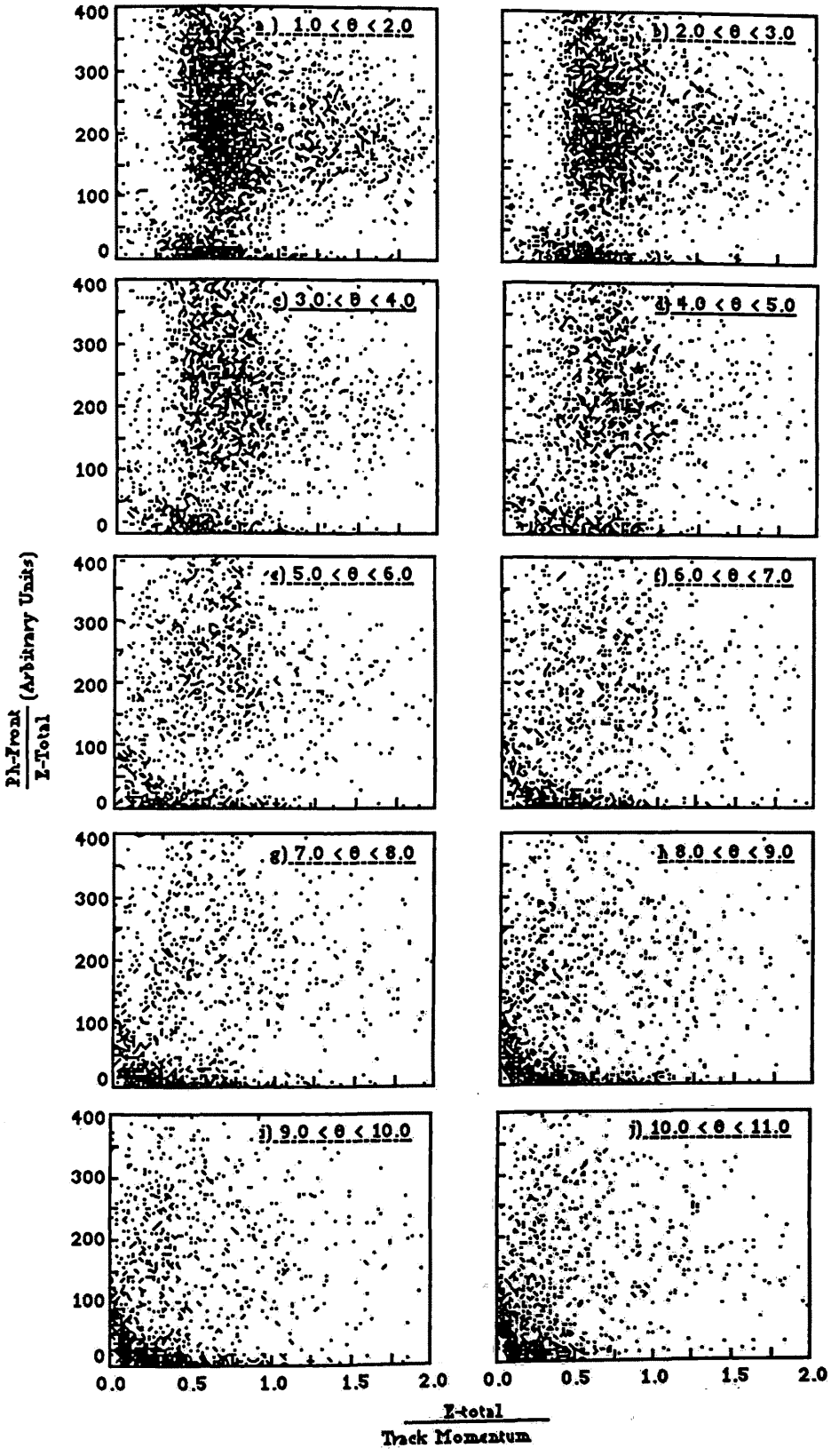

Figure 4.9. NA1 Pion / Electron Plot

4.5.4. Particle Identification with the Čerenkov Counters

The kaon candidate in a charm event was one of the key factors in D decay detection. No calculation of the working efficiency of the Čerenkov counters has been made, their efficiencies decreased in practice from those found in the test beam due to the Čerenkov counters not being able to make a decision in the following situations:

- Particles having momentum out of the dynamic range.
- More than one particle being in a given cell.
- A track crossing more than one cell.
- The photon detection electronics of a given cell not operating.

An estimate of this efficiency can be found from a selected set of well reconstructed events. These events contained at least one kaon candidate defined by the Čerenkovs, and four charged tracks. In this sample the following statistics were found:

Kaons Found:	1	2	3
Percent of events:	88%	11%	1%

Table 4.2. The Čerenkov Efficiency

Some idea of the actual performance of the Čerenkov counters may be derived from these statistics. Since kaons are pair produced in photon interactions there should always have been two kaons identified in any given event. In the events with more than two kaons, at least one kaon must have been a false identification by the Čerenkovs. This implies that less than 1% of all kaon identifications by the Čerenkovs were mistaken. In the events with just one kaon found the Čerenkov was seen to be 87% inefficient given that 1% of these particles were not true kaon candidates.

4.5.5. The Omega

As a check on the quality of the data the ω meson, produced readily with a photon beam through the VDM mechanism, was reconstructed. The invariant mass plot for ω candidates is shown in Figure 4.10. The FWHM of the mass peak in this plot is $\approx$100Mev/c^2, corresponding to $\sigma_\omega \approx$ 42Mev/c^2. This width is consistent with the expected width of the ω given the additional resolution of the calorimeter.

The mass resolution for reconstructed particles is in general a function of the measured mass. The ω is light and for heavier particles the resolution of the spectrometer will be more important.

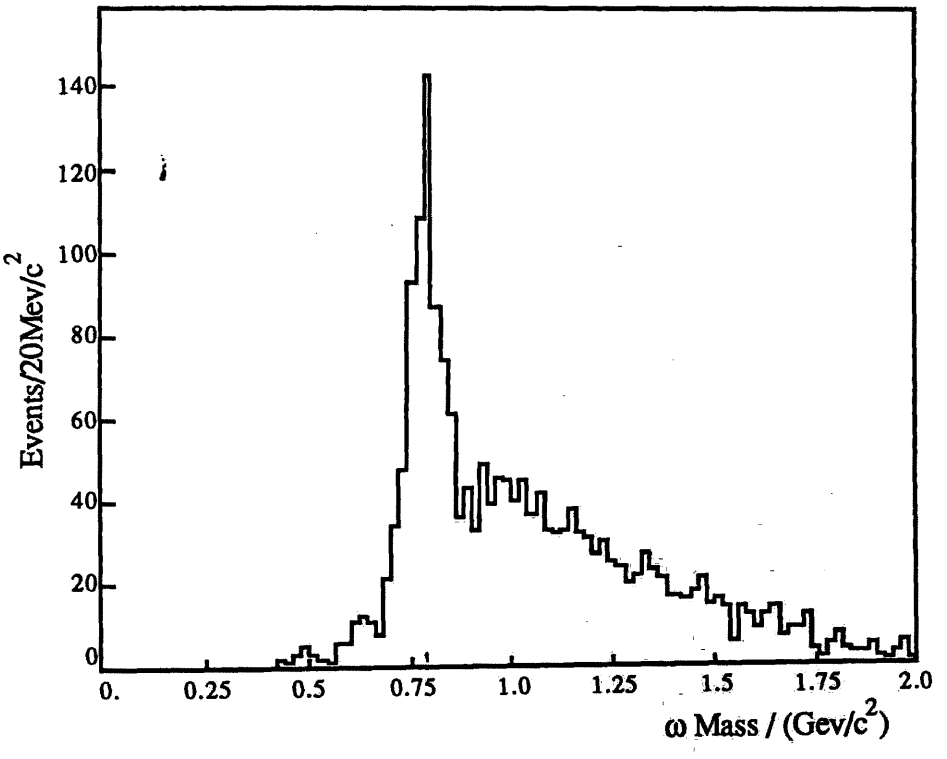

Figure 4.10. The ω Mass Plot

4.6. The Target

The NA1 target measured the number of minimum ionising particles (MIP) passing through it. Measurements of MIP were made by each pad of the germanium or strip of the silicon. The silicon strips were combined to give the overall response per plane. The relation between target strips, the MIP response and physics event is illustrated in Figure 4.11.

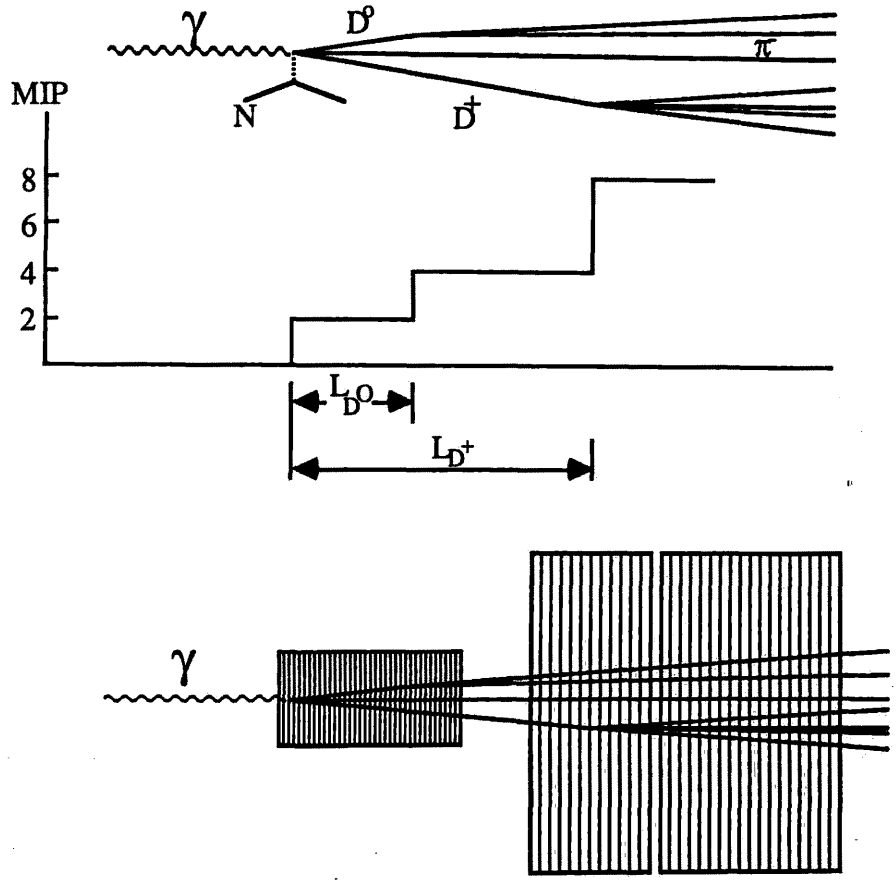

Figure 4.11. An Illustration of a Target Event

Pattern recognition in the target proceeded in a number of steps:

1) The ADC pulse heights were calibrated to compensate for differences in response of the electronics of each channel and for all channels across time. All responses of the target then being normalised to MIP pulse heights.
2) The number of particles crossing each strip was estimated.
3) Candidated points where changes in MIP, corresponding to production, decay or δ-ray generation points were found.
4) A final selection of interaction points was made and the distances between them calculated.

4.6.1. Calibration of the Target

Although there were fluctuations in the number of ADC channels recorded for different channels for a given number of MIP, the ADC count could be related to MIP by calibrating against the ADC pedestals (0 MIP response - Ph_0) and the 2 MIP count (Ph_2). Figure 4.12 shows the "raw" pulse height response for a germanium strip. The 0 and 2 particle response can be clearly seen.

For each target strip the values of Ph_0 and Ph_2 values were found. The positions of the higher MIP (Ph_n) peaks were then related to these positions with a linear fit:

$$Ph_n = Ph_0 + n \cdot (Ph_2 - Ph_0) \qquad (n = 4, 6 \text{ and } 8) \qquad (4.7)$$

This relation was then inverted, given the measured quantities Ph_0 and Ph_2, to give the MIP equivalent pulse height for each channel from the recorded ADC count. The calibration programme thus calculated a slope and intercept for each channel (the inverse of equation 4.7) and made a note of dead strips.

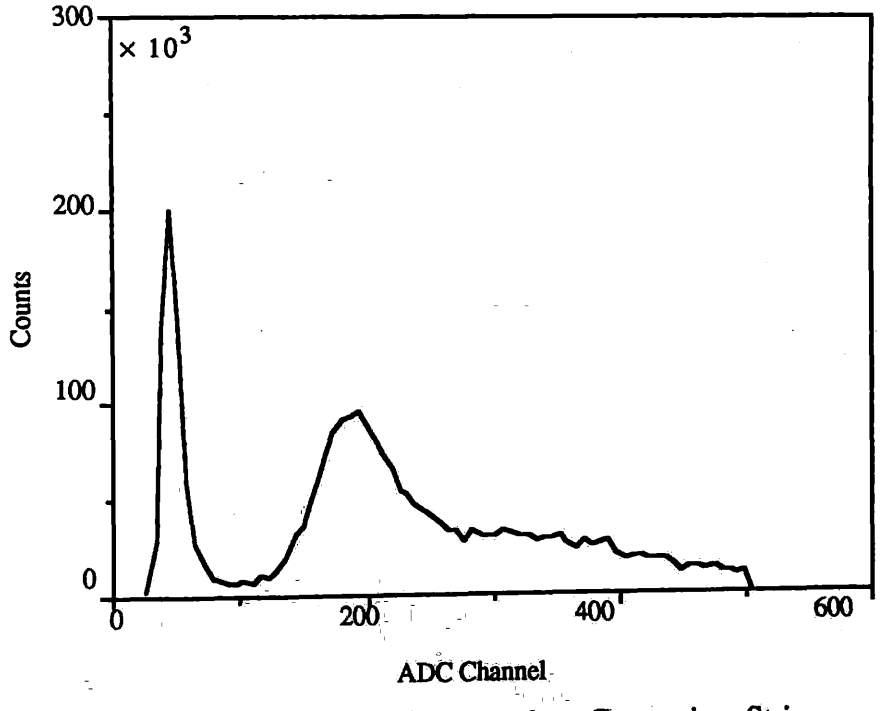

Figure 4.12. ADC Channel Counts for a Germanium Strip

4.6.2. The Relation of Pulse Height to MIP

The response of solid state detectors to ionising particles was fitted with an approximate Landau-Vavilov [KÖLBIG83, VAVILOV57] equation of the form:

$$L^{\alpha}_{\bar{x}\,\sigma} = A^{\alpha}_{\sigma}\, e^{-\alpha(\lambda + e^{-\lambda})} \tag{4.8}$$

where λ has the form:

$$\lambda = \frac{x - \bar{x}}{\sqrt{\alpha}\,.\,\sigma} \tag{4.9}$$

The variables $\bar{x}$ and σ are the mean and standard deviation of the target pulse height distributions (as for example in Figure 4.13.) for a given number of MIP. The variable α is a paramaterization of the target response and may have a value between $\frac{1}{4}$ and 4. A^{α}_{σ} gives the normalisation of the distribution.

The equation 4.8 was fitted to samples of the data and the constants of A^{α}_{σ} and α were found. This paramaterization was used to define cuts on the $\bar{x}$ and σ of the data to define the actual number of charged particles passing through strips of the target. This was done for groups of 3 strips in both the germanium and silicon. The use of these cuts is described in the next section.

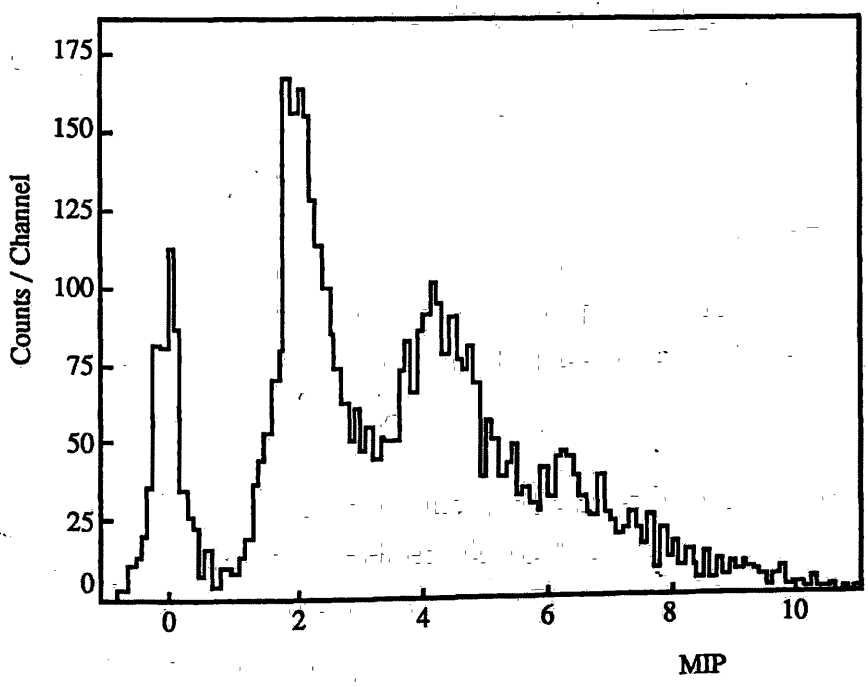

Figure 4.13. Calibrated Pulse Height for a Germanium Strip

4.6.3. Location of Decay Points

A method of finding production and decay points in the target was developed which could be applied by computer programme. In this way events with decays were selected quickly allowing fast selection of the events of interest. The use of such a programme also removed any human bias in the determination of decay lengths in the target. The primary problem in developing such a programme was to allow it to cope with fluctuations in the target responses which may hide or simulate decay points. An example of a target event with two steps and a δ-ray is shown in Figure 4.14. The MIP equivalent pulse heights shown are plotted in the centre of each strip. The line just below 6mm is located in the centre of the gap between the silicon and germanium targets.

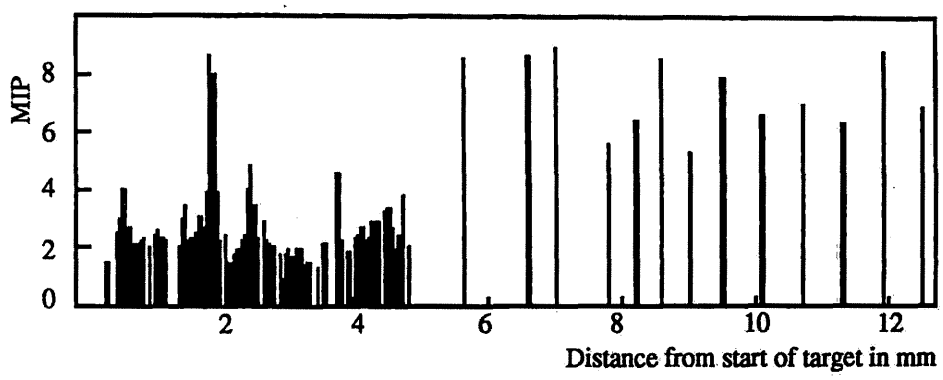

Figure 4.14. A Real Target Event with a δ-Ray

The target pattern recognition programme progressed along the following steps after calibration of the target:

i) If there was any signal in all of strips 2, 3 and 4 the event was rejected as having charge entering the target. Strip 1 was not considered due to end effects. This rejected events in which the initial interaction occurred outside the target.

ii) For each target strip "i" the mean and variance of the calibrated pulse heights P_i of that strip and one either side was formed:

$$P_i^m = \frac{1}{N} (P_{i-1} + P_i + P_{i+1})$$

$$P_i^\sigma = \sigma (P_{i-1}, P_i, P_{i+1})$$

Where N is the number of non-zero values of P. If both P_{i-1} and P_{i+1} are zero, P_i^m and P_i^σ were considered to be undefined.

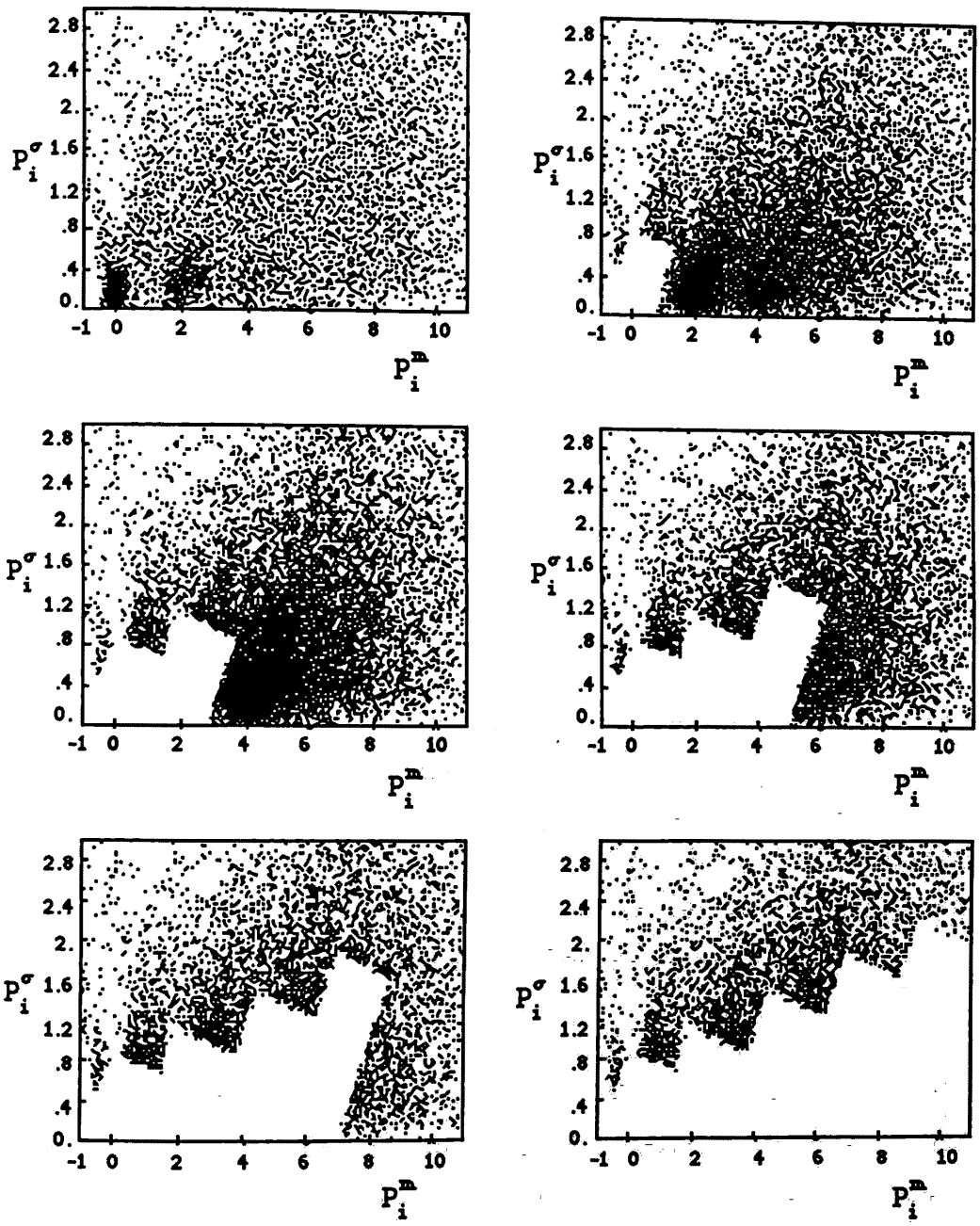

Figure 4.15. Mean .v. Variance of Target Pulse Heights

iii) A normalised value P_i^n was assigned to each strip "i" corresponding to the number of MIP in that strip. The values of P_i^n were taken to be an even integer and was set with the following cuts:

0- $P_i^\sigma < \frac{1}{1.7} . P_i^m + 0.9$ and $P_i^\sigma < -\frac{1}{7} \cdot P_i^m + 0.9$

2- $P_i^\sigma < P_i^m - 0.7$ and $P_i^\sigma < -\frac{1}{7} \cdot P_i^m + 1.4$

4- $P_i^\sigma < P_i^m - 2.85$ and $P_i^\sigma < -\frac{1}{7} \cdot P_i^m + 2.2$

6- $P_i^\sigma < P_i^m - 5.0$ and $P_i^\sigma < -\frac{1}{7} \cdot P_i^m + 2.8$

8- $P_i^\sigma < P_i^m - 7.0$ and $P_i^\sigma < -\frac{1}{7} \cdot P_i^m + 3.5$

If P_i^m or P_i^σ were undefined or they failed all of the above cuts then P_i^n was undefined. The regions defined with the above cuts are shown in Figure 4.15 on a plot of P_i^m against P_i^σ. The above parameters were set with respect to the distributions of pulse heights in the targets for each number of MIP.

iv) An attempt was made to find a strip number "i_j" corresponding to each possible MIP value (j = 2, 4, 6 or 8). This was done by locating the *last* strip in the target for which $P_i^n = j$. If no such strip existed for a given value of "j", then no jump to that multiplicity was considered to have occurred. In practice the analysis programme worked back from the last strip of the target recording drops in the value of P_i^n and ignoring rises in this quantity. In this way "spikes" from δ-rays or noisy strips did not deceive the programme. They may, however, lead to a miss-location of true decay points.

At this point a number of strips had been located corresponding to changes in multiplicity in the target. The region between two such strips, *i.e.* "i_a" and "i_b", corresponded to a level or step across which "b" charged particles were travelling. Those "b" particles having originated from a decay or production prior to which there were "a" charged particles.

v) The average pulse height P_l^m of all strips between each change in multiplicity was calculated for each such level "l" between two strips "i_a" and "i_b". The values of P_l^m were expected to correspond to the number of charged particles traversing that region "a". A given level "l" was rejected if:

a) $P_l^m - a > 2$

b) $P_l^m - P_{l+1}^m < 0.7 \wedge ((P_{l+1}^m < a_{l+1}) \vee (a < P_l^m \leq a + 2))$

Levels rejected by these tests were 'merged' with the next higher level. This served to remove false jumps defined as a result of holes and random fluctuations in pulse height.

The methodology described above, and the cuts used were developed to yield a sample of events with well defined target configurations. The efficiency was taken to be a secondary problem and some loss was tolerated.

In Table 4.2 are shown the statistics for finding jumps to given levels of MIP. The data used here has had no other selection applied to it other than the target analysis programme. A requirement for at least two jumps was made.

Jump To:	2	4	6	8
Step N^0				
1	91%	7%	2%	—
2	—	38%	5%	57%
3	—	—	10%	30%

Table 4.3. Target "Jump" Statistics: All Data

4.6.4. Losses Due to Target Pattern Recognition

To estimate the losses through bad pattern recognition 100 target event pictures were scanned by eye. These had been *rejected* by the target analysis programme. For the most part the rejected events had no obvious structure or if some decay could be seen the start or end points were not clear and could not be measured. An example of a rejected event is given in Figure 4.16.

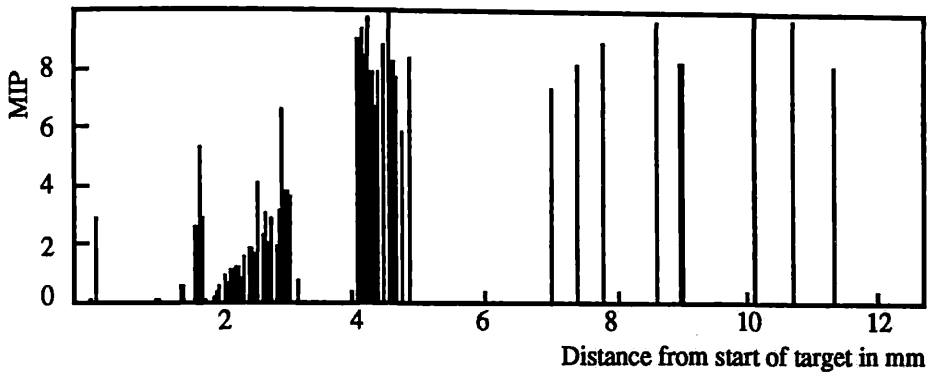

Figure 4.16. An Example of a Bad Target Event

In this event sample of rejected events, 11% appeared to have one or two clear changes in pulse height. All these events had been rejected by the target analysis programme due to charge entering the target (step i above). Rejection of events on these grounds does not bias the data since it does not depend on the actual configuration of decays in the target.

4.6.5. The Efficiency of the Target Analysis

To determine the effectiveness of the above technique the target pictures of a sample of 300 events were scanned. These events had been found to contain at least two changes in MIP and were selected to contain high mass particle combinations of kaons and pions, but with no special relation to the D mass combinations (Section 5.2). This was done to deplete the electromagnetic event content of the sample. The results of this analysis is given in Table 4.4.

	Target Programme:	2 Jumps Found	3 Jumps Found
Eye Scan			
2 - Jumps Seen:		41%	25%
3 - Jumps Seen:		2%	20%
Bad events:		7%	5%

Table 4.4. Results of Eye Scan of Target Events

These events spanned all the runs in the 1983 data sample. No great fluctuation was seen between the quality of events in the different runs. In the events where the target analysis programme appeared to invent a 3rd jump, the final jump normally occurred within about 3 or 4 strips of the end of the silicon target. The difficulty with identifying jumps in the region sets a limit for the effective length of the target (see Section 6.2.1).

No attempt was made to check the accuracy with which the jumps are identified in this data. No large divergence between the location of jumps found by the programme and that estimated by eye was noticed. A judgment by eye is suseptible to bias and, unlike the target programmes analysis, there is no guarantee that this bias remains constant. Thus in all cases unless the event was rejected completely, the measurements made by the target programme were accepted.

In the 12% of events which were considered to be bad the target showed large overflows in pulse height (flashes) and strips with no signal at all. The strips with no holes had misled the target analysis programme.

4.6.6. The Target Simulation Programme

To understand the performance and characteristics of the target and target analysis programme a computer programme was constructed to simulate a number of characteristics of the target. This programme produced data in the same format as the true target data so that the results of this programme could be passed through the target analysis programme. A number of "physical" features were built into the target simulation so as to give a good reflection of the real data.

All variables which had some random distribution in the experiment were generated with the appropriate random distributions. Thus over a large number of simulation "events", the integral affect should mirror that of the true data. The use of random variables is expected to give a result which converges with those achieved by scanning

across all values of each variable with a reduction in the number of events which need to be generated. This is the Monte Carlo technique [JAMES80]. I would like to acknowledge here the work done in implementing this programme by Jeremy Carter at Royal Holloway & Bedford New College.

Dynamics of The Particles

No dynamics of D decay or production were used apart from the selection of decay channel. In order to build in production and decay matrix elements (and nuclear interactions) would require the use of a QCD Monte Carlo programme. These are very time consuming and for the study done would not have yielded very much extra information. For simplicity in calculating the kinematics of D production the photon was considered to pass through an intermediate vector resonance (about the mass of the Ψ'') with zero lifetime in the process: $\gamma \rightarrow \Psi'' \rightarrow D\bar{D}$. The only error this induced was in the transverse momentum of the D decay products which, if large, could cause these particles to leave the target through the sides rather than the end.

The D mesons could be produced directly or via a D^* state as appropriate. The decay channels of the D could be chosen at random with respect to the known branching ratios or fixed decay modes could be used. For most cases the former was used.

Kinematics of Charm Production, Decay & Nuclear Recoil.

The production and decay of the Ψ'' and decay of the D mesons was simulated using random phase space methods [JAMES68]. Photon energies were generated with an exponential distribution to reflect the bremsstrahlung character of the true photon beam. The interaction point of the photon was calculated using the photon attenuation length λ of $\approx 20 g/cm^2$ with an exponential decay normalised so that all photons interact in the target.

To conserve momentum some momentum transfer (t) is needed to the target. The kinetic energy transferred is given by [BELLINI82]:

$$T = \frac{|t|}{2M_{nucleus}} \qquad (4.10)$$

with

$$\sqrt{|t|} = P_{inc} \cdot \theta + \frac{(m^2 - m_{inc}^2)}{2E_{inc}} \qquad (4.11)$$

P_{inc} and m_{inc} are the momentum and mass (zero for a photon) of the incoming particle, θ the angle of the out going particle and m the mass of the resonance.

For coherent processes, θ is close to zero and the momentum transfer was calculated with the approximation to 4.11 of:

$$\sqrt{|t|} = \frac{m^2}{2E_{inc}} \qquad (4.12)$$

With this approximation the energy of the recoil can be calculated with the energy lost in ionization of around $\frac{1}{2}T$. Only some tens of Kev are available for ionization and the response is expected to be between 0.1 and 0.6 MIP equivalent. Thus we do not expect to see any nuclear recoil.

Calculations of decay and production kinematics were done in the centre of mass or lab frame as appropriate. All final results were in the lab frame.

Secondary Interactions

The secondary processes of most interest in understanding the performance of the target were δ-ray production and photon (from π^0 decay) conversion. Both of these can cause spikes or fluctuations in pulse height in the target.

During the process for conversion from the number of charged particles in a strip to MIP equivalent pulse height, a test was made for δ-rays in each strip. A delta ray was distinguished from other energized electrons by cuts on the energy lost in a given strip E_{los}:

For Germanium; $E_{los} > 0.148$Gev

For Silicon; $E_{los} > 0.137$Gev

If the energy lost passed these cuts, then the kinematics and energy release of the electron were calculated and added to the ionization energy of the other particles.

The decay probability of a π^0 produced through the channel $D^0 \rightarrow K^-\pi^+\pi^0$ was considered and the probability for photon conversion to e^-e^+ was also calculated. The ionization from electrons from converted photons was added to the overall ionization of each strip through which they passed and added to ionization from other sources.

Ionization Response

The energy release for each strip in the target was calculated to give the MIP equivalent pulse height. The number of charged particles passing through each strip was known and the energy release calculated using a function derived from equation 4.8. The full derivation of this parameterization is outside the scope of this thesis. The parameters

used depended on the number of charged particles and the material. The parameters used for germanium and silicon are shown in Table 4.5.

	$\bar{x}$	σ	α
Silicon			
2 Mip	2.0	0.487	2.19
4 Mip	4.0	0.650	1.00
6 Mip	6.0	1.427	1.61
8 Mip	8.0	1.447	3.07
Germanium			
2 Mip	2.0	0.237	2.28
4 Mip	4.0	0.395	7.90
6 Mip	6.0	0.725	21.1
8 Mip	8.0	1.020	5.60

Table 4.5. Parameters Used to Generate Pulse Height for MIP

In addition to the contributions to the calculated pulse height from; decay product particles, δ-rays and electrons from converted photons, a random noise contribution was added in corresponding to an average of 0.5MIP with a spread of 0.05.

Figure 4.17. shows a target event produced by the simulation programme.

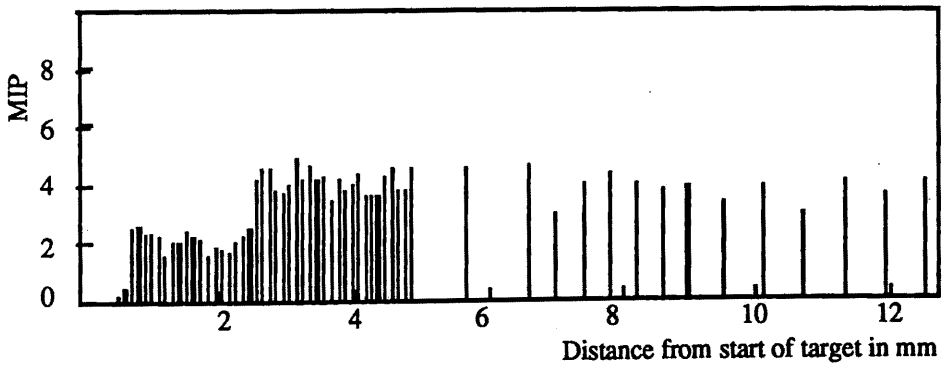

Figure 4.17. An Illustration of a Simulated Target Event

4.6.7. Target Efficencies from the Simulation Programme

By passing the results of the simulation programme through the standard target analysis programme a comparison with produced and found jumps and jump lengths may be made. A plot of the ratio of the efficiency for finding jumps of differing lengths is shown in Figure 4.18. The number of events with a given decay length is divided by the number of events found with that decay length. Efficiencies above 1 were possible since the target analysis programme may have "invented" jumps. The plot starts from a miminum number of jumps in a strip of 3. This is due to the fact that strips are grouped into triplets as part of the jump finding methodology described in Section 4.6.3.

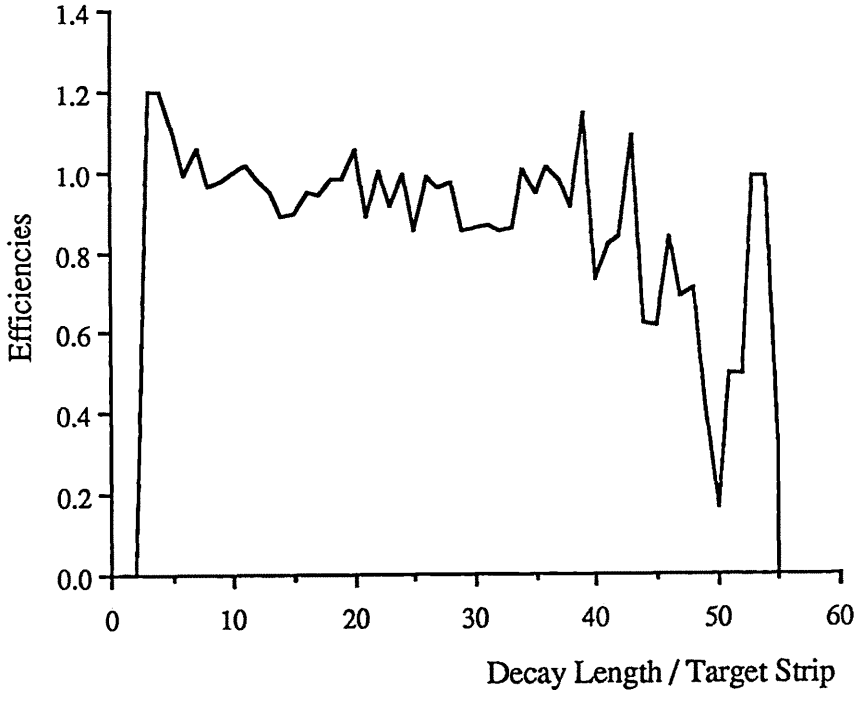

Figure 4.18. Efficiency for Finding Target Decays

The fluctuations toward the high decay lengths were due to the lack of statistics in this region.

4.7. Final DST Selections

A final selection was made from the full, produced data sets to discard events which were badly reconstructed. The data on the DSTs were required to pass the following selection criteria:

- Total number of charged tracks ≥ 2
- Number of clusters in the tagging calorimetor = 1
- The ratio of reconstructed energy to photon energy E_{rap} must fall within the limits $0.2 \leq E_{rap} \leq 1.5$
- Total spectrometor energy $\geq$ 35Gev

Due to the rejected events being badly reconstructed, no estimate of the loss of hadronic events could be made. The statistics for the data analysis chain are summarised in table 4.6.

Period	Raw Events	After Soft Trigger	After Production	On DST
5A	$600 \cdot 10^3$	$200 \cdot 10^3$	$200 \cdot 10^3$	$40 \cdot 10^3$
5B	$225 \cdot 10^3$	$60 \cdot 10^3$	Not produced since no target.	
5C	$930 \cdot 10^3$	$430 \cdot 10^3$	$430 \cdot 10^3$	$110 \cdot 10^3$

Table 4.6. Data Statistics for 1983 Running Period

Chapter Five

D Meson Reconstruction

The method of identifying events as containing D^0 mesons is discussed in this chapter. The work presented here is entirely my own and constitutes only one of a number of approaches used to find charm events. A final sample of D^0 mesons and a Dalitz plot for the three body decay mode are presented. No attempt has been made to reconstruct other charmed particles.

5.1. The Charm Decay Modes Searched

The events containing charm were identified by reconstructing the masses of the D mesons from their decay products detected in the FRAMM spectrometer. The presence of particles from more than one D decay or particles produced with the $D\bar{D}$ pair gave rise to the need to form a number of mass combinations in each event. Most of these combinations were of an arbitrary set of particles and these formed a combinatorial background. A final choice of a D decay candidate was made among the mass combinations in each event. Selecting kinds of charm events to be searched for was done with a view to reducing the problems of combinatorial backgrounds and maximisation of the available statistics. Additional selections were made on the target configuration and against general event characteristics to reduce background from non charm events.

5.1.1. The D^* Decay

A set of D^0 events was selected by searching for the cascade decays:

$$\begin{array}{l} D^{*+} \rightarrow D^0 \pi^+ \\ \qquad \hookrightarrow K^- + n\pi \end{array} \qquad (1)$$

and the conjugate decay:

$$\begin{array}{l} D^{*-} \rightarrow \bar{D}^0 \pi^- \\ \qquad \hookrightarrow K^+ + n\pi \end{array} \qquad (2)$$

The discussions below are in terms of the particle decays (1), everything said goes *mutantis mutandis* for the conjugate particle decay channels (2).

The events with the process $D^{*+} \rightarrow D^0 + \pi^+$ were constrained not only by the two invariant masses, but by the particular kinematics of the radiated π^+ originating from the strong decay of the D^*. The radiated pion only had 0.14Gev of energy available to it due to the difference in mass between the D^{*+} and its ground state. Thus the requirement of good invariant masses for the D^{*+} or D^0 and a slow π^+ is highly constraining. For preliminary selections of events the mass difference (ΔM) of 145.5Mev/c^2 between the D^0 and the D^* was used as a selection cut which was independent of any mass shift due to systematic behaviour of the apparatus. The selection of a mass combination by a combination of a cut on ΔM and either the D mass or the radiated pion momentum were equivalent.

5.1.2. The D^0 Decay Channels

The three D^0 decay channels most suited to the characteristics of the FRAMM spectrometer were;

D Decay Channel:

1) $K^+\pi^-$: Branching ratio = 5.4%.
   - Good efficiency due to low multiplicity.
   - Constrained by phase space. Combinations of two particles to give high mass final states was suppressed for background.
   - Constrained if 1 out of 2 of the decay particles was truly identified as a Kaon.
   - Some combinatorial backgrounds from high multiplicity events and hard hadronic processes.

2) $K^+\pi^-\pi^0$: Branching ratio = 17.3%.
   - Some loss of efficiency due to poor π^0 detection.
   - Possible incompatibility of resolution with channels 1) and 3) due to presence of a neutral particle.
   - Highly constrained decay products since identification of the π^0 is unambiguous.

3) $K^+\pi^-\pi^+\pi^-$: Branching ratio = 10.9%
   - Poor efficiency due to high multiplicity.
   - High combinatorial background which was accentuated if the Kaon is not identified.

The final efficiencies for detection of each of these channels in FRAMM has not been calculated. Some reflection of the above branching ratios was expected in the statistics of the final D data sample, given the above points.

5.1.3. The Combinatorial Technique

To identify charm events by reconstructing the decay products of the charm mesons, sets of detected $\pi^{\pm}$, $K^{\pm}$ and π^0 particles were used to form an invariant mass close to that of the D^0. In each event a number of mass combinations were formed. Charged tracks not identified as pions or kaons may have been used as both in different mass combinations. For each event, a Preferred D candidate was selected for use in a final event selection.

The use of this technique to identify the charmed particles in an event, and to eliminate background events had complications in situations where detected particles formed masses close to that of the D^0 even though no such particle was present. Other complications arose even in charm events since several combinations of particles may be formed, only one of which was that of the D^0 decay products. This effect was accentuated due to a number of causes:

- Charged tracks were used both as candidates for $\pi^{\pm}$ and $K^{\pm}$ due to inefficiencies in the Čerenkov.
- Charged particle candidates "invented" by the tracking programmes contributed to mass combinations.
- Poor hadron / electron separation from the shower detectors lead to the inclusion of electromagnetic events.

Such false invariant masses formed a combinatorial background and led to difficulty in understanding the event, and analysis techniques. For these reasons criteria were used for selecting combinations of particles and in general events to use for the charm search.

5.2. Data Reconstruction

A final selection of data was made following the selections on the data of the soft trigger and those made when writing the DSTs.

5.2.1 Target Filter

Only events which had decays found in the target could be used to measure lifetimes. Selection of events by the target analysis programmes also selected for charm events by their characteristic short decay times. A further advantage of the target selection was to eliminate events originating from hard hadronic interactions of the photon with the target nuclei. The analysis of the NA1 target was made by computer programme and was one of the faster parts of the analysis chain. Thus the target was used to filter events which may contain charm for the final analysis.

Use of the target as an event filter required an understanding of the topology expected by charm decay. The D^{*+} decays into a D^0 meson and a π^+ via strong interactions and with a rate very much faster than the weak charm decays. Within the constraints of the momentum of the particles in this experiment, and the resolution of the target, the decay of the D^{*+} state cannot be detected and could be considered as instantaneous. The production of a D^{*+} would be with an accompanying charge conjugate particle, either an oppositely charged D^* or D^+. This gave a requirement of an initial plateau of two minimum ionising particles (MIP) in the target. This was in common with D^+D^- production, e^+e^- production or the production of a number of vector meson channels, *e.g.* ρ decay.

In the cases where other charged particles were produced with the $D\bar{D}$ pairs, the requirement of 2 MIP would lead to a loss of up to 90% of charm events. Thus a softer requirement of two or four MIP was considered to be reasonable. The decay of the D^0 results in a total of four or six MIP in the target. The D^0 decay to 2 or 4 charged particles gave the requirement of a second step of four, six or eight MIP cleanly inside the target. The same configuration was given by decay of the conjugate D^+ or, if the first step was from non-charm interactions, a step may have beeen generated by pair production, nuclear interactions or the liberation of electrons in the target. Thus the topology of 2(4) to 4(6) or 6(8) MIP did not uniquely distinguish charm decays. However it was a necessary signal for a D^0 decays originating from D^* decay.

Passing the events from the final reconstruction packages and soft filter through the target programme requiring a step of two or four MIP followed by a step of four, six or eight MIP and any other step resulted in a final selection of 9478 events from periods 5A and 5C.

5.2.2. Selection for Hadronic Events

A final selection for hadronic and against electromagnetic events was made for decay channels 1) and 3) above. This selection was in complement to the online trigger and soft trigger. These selections were not applied to channel 2) since the presence of a π^0 was a good criteria for a hadronic event. The selection was based on the absence of electrons and presence of charged hadronic particles. The following definitions of electrons and hadrons were used:

A charged track, unidentified by the Čerenkov was taken to be an electron if:

- It was identified as electrons by the shower detectors and
- The track had a total angle from the beam axis less than:
  - 8mr for tracks stopping in SD 1
  - 6mr for tracks stopping in SD 2
  - 6mr for tracks stopping in SD 4

These angles, defined at the target, were derived from the fact that electrons which originate from electromagnetic interactions of the beam photon were produced with a small angle relative to the beam axis. The radiated pion of D^* decay was produced with low momentum and small angle. The above identifications for electrons lessened the possibility of this pion being misidentified as an electron leading to losses of D^* events.

A charged track was identified as a hadron if:

- The track was identified as a hadron by the shower detectors and its angle was greater than:
  - 3mr for tracks stopping in SD 1
  - 2mr for tracks stopping in SD 2
  - 2mr for tracks stopping in SD 4
- The track had no kind of signal in the shower detectors and its angle was greater than:
  - 8mr for tracks stopping in SD 1
  - 4mr for tracks stopping in SD 2
  - 4mr for tracks stopping in SD 4

The angle cuts used were set using plots like those shown in Figure 4.9. considering each shower detector separately.

Events were only accepted if; no electron candidates were found and one or more hadron candidates were found. The rates for counting electron and hadron candidates are shown in Table 5.1. These do not represent an absolute reduction in data since some of the events rejected by these selections were used for the $D^0 \rightarrow K^+\pi^-\pi^0$ decay channel.

	Hadrons								
	0	1	2	3	4	5	6	7	8
Electrons									
0	5.5	11.9	12.1	6.8	3.5	0.9	0.12	0.01	0.02
1	11.0	13.3	7.1	2.3	0.6	0.2	0.03	0.01	
2	10.1	6.6	2.2	0.6	0.12	0.04	0.02		
3	2.9	1.5	0.3	0.12	0.03	0.01			
4	0.4	0.1	0.02						
5	0.01	0.01							

Table 5.1. Hadron / Electron Selection Statistics

The events accepted by these selections constituted 35% of the data which had passed the target selection (3380 events).

5.3. Expected Yield

A calculation of the number of charm events expected was useful to gauge the performance of the reconstruction routines. However such a calculation involved a number of uncertainties:

- No calculation of the acceptance for charm events in FRAMM has been made
- No direct measure of the photon flux exists since the basic trigger required an interacting photon.
- There is uncertainty in the photon charm cross section for coherent production. This factor is accentuated by the new MARK III D decay branching ratios.
- There is uncertainty in the dependence of the cross section on the atomic number.

To derive the total photon flux during the running time in question the number of events written to tape was related back to the number of events written per photon through the trigger elements.

- There were a total of $1.53 \cdot 10^6$ events written to tape which were usable for analysis (*i.e.* not calibration data).
- With $9.9 \cdot 10^2$ events written to tape for 10^6 paralysed strobes (Table 3.4), the number of events on tape corresponds to $1.6 \cdot 10^9$ paralysed strobes.
- Approximately 8.7% of electrons on the converter produced photons between 70Gev and 175Gev and 1.6% of these electrons produced a paralysed strobe signal. This gives 5.4 photons for each paralysed strobe.
- Thus for each event on tape there were $5.5 \cdot 10^3$ photons.
- The number of events on tape gives a total photon flux of: $N_\gamma = 8 \cdot 10^9$

For a charm event to have contributed to a lifetime measurement the production will have occurred in the germanium target. This gave the number of nucleons in the target (Table 2.1) as $N_A = 1.6 \cdot 10^{24}$. This number was re-scaled with an A dependence. The $A^{2/3}$ dependence was used as an approximation for coherent production. Since only these kinds of events were useful for measuring lifetimes this was reasonable. This gave the effective number of "interaction centres" in the target as; $N_N = 3.8 \cdot 10^{23}$.

The uncertainties in the charm cross section is large compared with the expected variation with energy (Section 1.3) The error in taking a constant cross section should

be small in comparison with the other uncertainties involved in this calculation. Thus the total charm cross section on a proton was taken to be $\sigma_c = 500nb$.

Combining these numbers gave a total yield for charm particles of $N_c \approx 1.5 \cdot 10^4$ events. Of these charm events the predominant channel was to D mesons. Assuming little difference between D^0, D^- and D^+ production, about $\frac{1}{3}$ the charm events should have given neutral D mesons (including D^*). With little information about the relative production rates of D^0/D^* production another factor of 0.5 may be used for D^* production. The D^* decay to D^0 has a branching ratio of 49±8% which gave another factor of a half for the channels in question.

The combination of factors for D^0 and D^* production brought the charm cross section σ_c to the cross section for D^* production $\sigma(\gamma P \rightarrow D^*)$, of ≈ 80nb. This is comparable with the measured value by E516 [NASH83] for this process.

Finally considering the branching ratios for the three channels of D^0 decay considered here (33% of total) approximately 420 D^* events was estimated for the available D^0 yield. This number was considered as only a guideline giving the order of magnitude of events to be found.

5.4. Neutral D Reconstruction

5.4.1. Particle Identification for Charm

Particle identification for the decay channels of interest depended heavily on selecting the K^- candidate. This would reduce the problems of combinatorials in truly reconstructing the decay and in eliminating false events. The Čerenkov counters had most problems for high multiplicity events since they were not able to make an identification if more than one track passes through a cell. This effect was accentuated for decay channel 3) since it has a high multiplicity. The following particle definitions were used:

- All tracks identified as π,K,P or e^- by the Čerenkovs were taken as such.
- A charged track unidentified by the Čerenkovs was at least a π candidate.
- If no Kaons had been identified, all unidentified tracks were in addition taken as Kaon candidates.
- If one or more K^- had been identified with no K^+, all and only +ve unidentified tracks were used both as Kaon and pion candidates.
- Conversely, if one or more K^+ had been identified with no K^-, all and only -ve unidentified tracks were used both as Kaon and pion candidates.

In this way some attempt was made to reduce the overall number of possible combinations of tracks which were used to reconstruct D^0 particles, while compensating as far as possible for inefficiencies in the Čerenkovs.

With the above particle definitions all combinations of particles which could have decayed via the channels 1), 2) or 3) from a D^0 were formed. If there was a remaining π^+ candidate which may be added to legally make up a D^* the invariant mass of this was calculated. All combinations were made with the requirement:

$$1.50\text{Gev}/c^2 < \text{Mass } D^0 < 2.10\text{Gev}/c^2$$
$$1.70\text{Gev}/c^2 < \text{Mass } D^* < 2.30\text{Gev}/c^2$$
$$\text{Mass difference } < 0.170.\text{Gev}/c^2$$

Events with one or more such candidate and in addition two particles not used in the mass combination were accepted.

5.4.2. Event selection

The Figures 5.1a-f show the invariant mass distributions of all the D^0 and D^* candidates for the channels 1), 2) and 3) after the above selections. At this stage a number of candidate combinations for each event were allowed. The statistics for multiple combinations in these channels are given in Table 5.2:

Number of Combinations:	Occurrences for each channel: $K^-\pi^+$	$K^-\pi^+\pi^0$	$K^-\pi^+\pi^-\pi^+$
1	78	95	43
2	24	35	33
3	7	16	15
4	2	14	6
5	2	5	13
6	0	2	15
7	1	1	5
8 and above:	1	7	41
Total:	179	496	1082
N° of D^0:	87	282	564
N° of $\bar{D}^0$:	92	214	518
Mean‡ N° of Combinations:	1.6 ± 1.4	2.2 ± 3.3	5.8 ± 6.5

‡Quoted here is the mean and σ of the number of combinations. These combinations do not follow a normal distribution and these statistics do not strictly apply. They are shown to give some feel for the combinatorial problem.

Table 5.2. Total Combinatorial Statistics

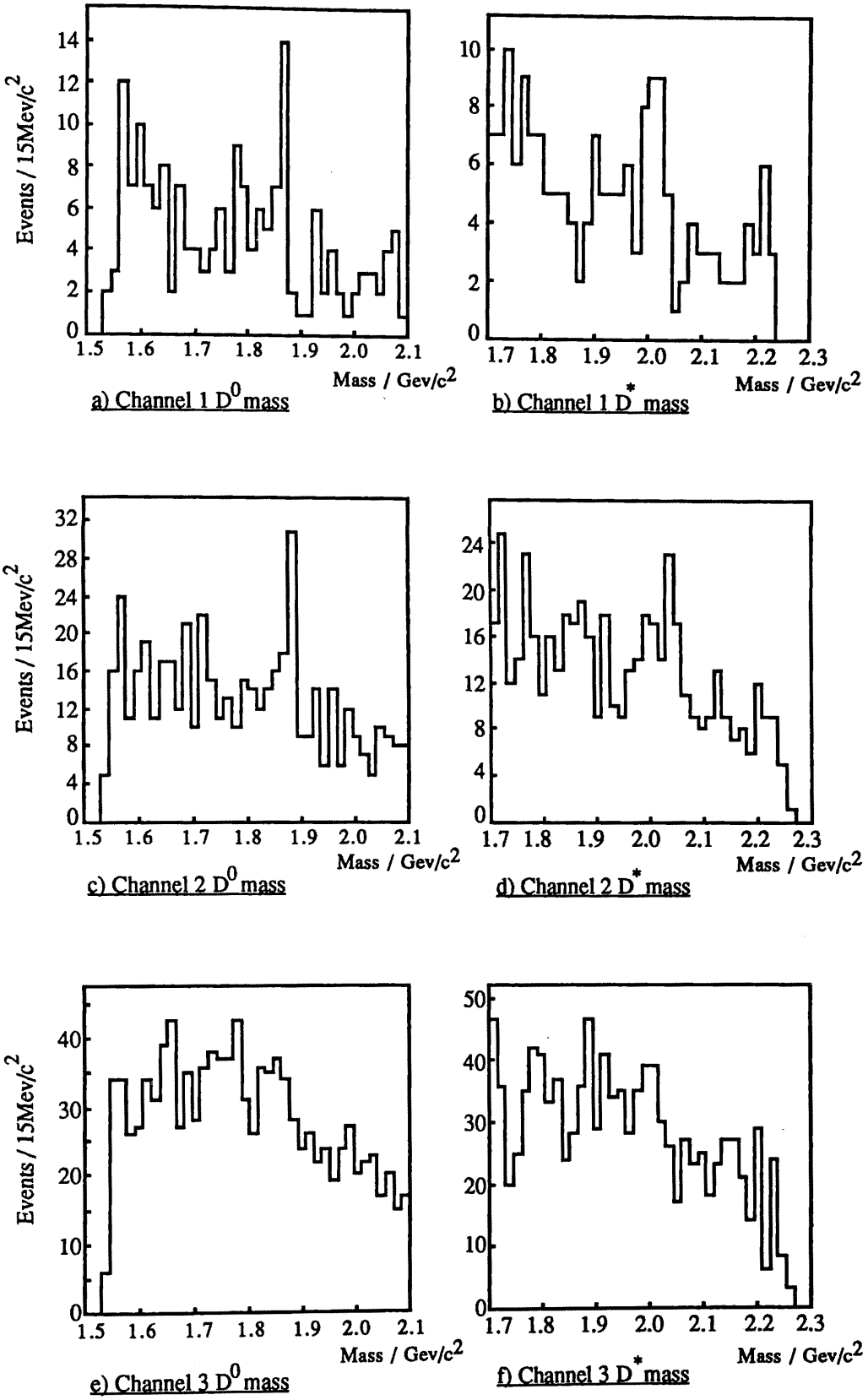

Figure 5.1. All Combinations of D^0 and D^* Mass Plots

A reasonable signal was seen for both channels 1) and 2). The mass peak for channel 2 was high by 20Mev/c^2. This mass shift was not seen in channel 1 and was attributed to the presence of the π^0. In all selections which were mass dependent this shift was compensated for.

There was little evidence for events in either the D^0 or D^* mass plots for the three pion decay of channel 3). Any evidence for charm here was lost in the combinatorial background and the mass plot reflects the statistics given in Table 5.2.

For each event and each channel separately the invariant mass combination closest to the D mass peak was chosen as the candidate D. This leaves the statistics in Table 5.3. The mass plots for the events left are shown in Figures 5.2.

Channel:	$K^-\pi^+$	$K^-\pi^+\pi^0$	$K^-\pi^+\pi^-\pi^+$
No of D^0:	53	93	92
No of $\bar{D}^0$:	56	92	81
Total:	109	185	173

Table 5.3. Single Decay Candidate Statistics

Of these 467 combinations there were 388 unique events with 38 events containing candidates from two of the channels and one event with a candidate from each channel. In 17 of these events one candidate was conjugate to the other, *i.e.* D and $\bar{D}$. It was tempting to take the 18 $D\bar{D}$ events as completely reconstructed. Since the number of events with conjugate channels was comparable to the number of events with candidates of the same conjugation it was unjustified to treat them differently.

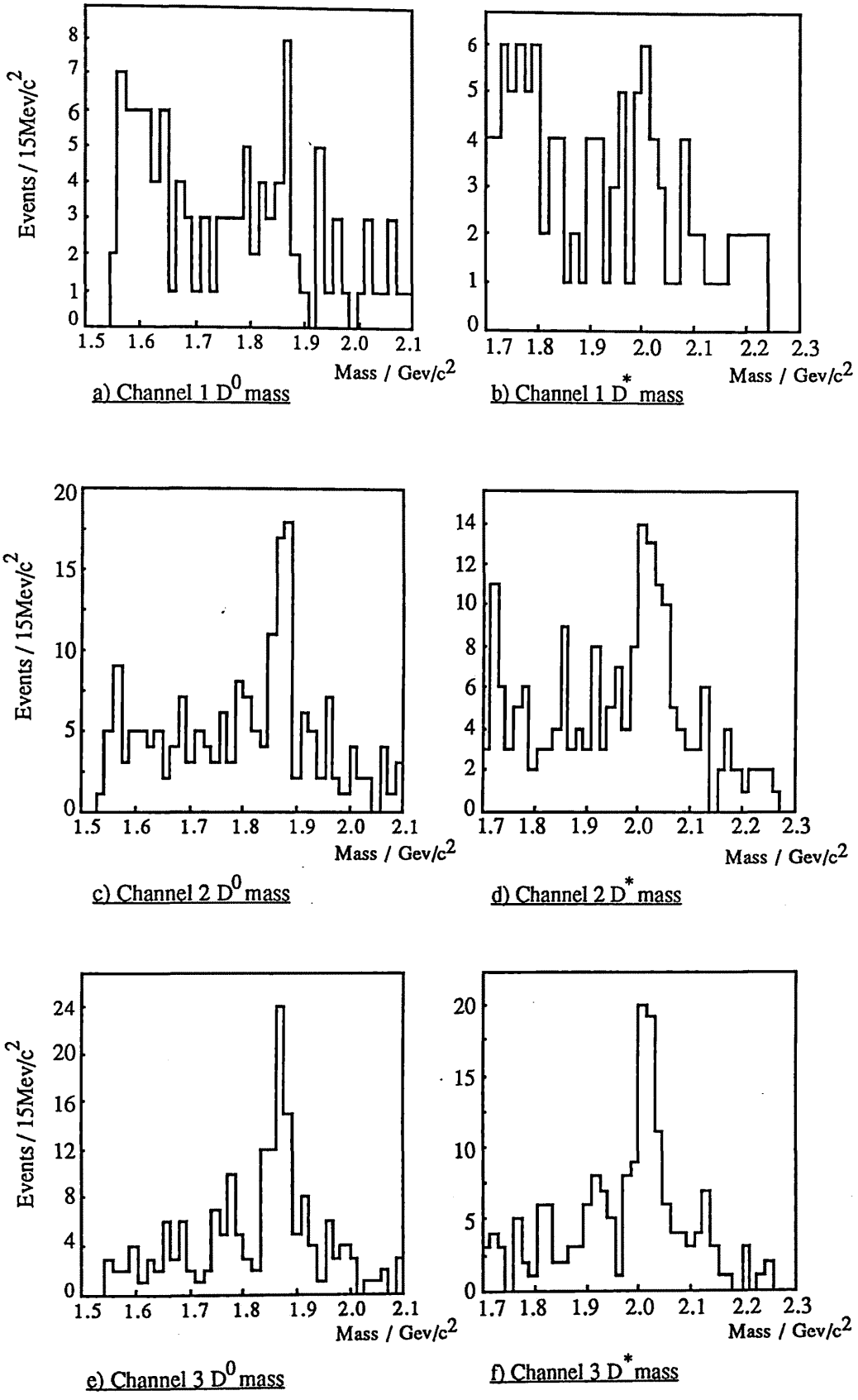

Figure 5.2. D Mass Plots with Best Candidate for Each Event

One candidate from each of the 39 events containing two or three candidates was accepted by selecting the decay channel for which the invariant mass of the D^0 was closest to the mass peak of its channel. The statistics remaining are given in Table 5.3.

Channel:	$K^-\pi^+$	$K^-\pi^+\pi^0$	$K^-\pi^+\pi^-\pi^+$
No of D^0:	42	91	86
No of $\bar{D}^0$:	46	85	77
Total:	88	176	163

Table 5.4. Best Candidate Per Event Statistics

The invariant mass distributions for each of these channels is shown in Figures 5.3 for the individual decay modes and in Figures 5.4. for the combined statistics. The above statistics correlate with the known branching ratios of these channels as do the number of events under each of the D peaks.

The exact form of the background event distribution was not known. To estimate this background the D^* mass plot was considered - the D^0 mass was used for event selection and would have a more artificial distribution. The bin containing the D^* mass and 2 bins on either side were considered for the mass peak giveing 107 events. A flat background was assumed of 3 events per bin. Thus of the 107 events 15% could be background events.

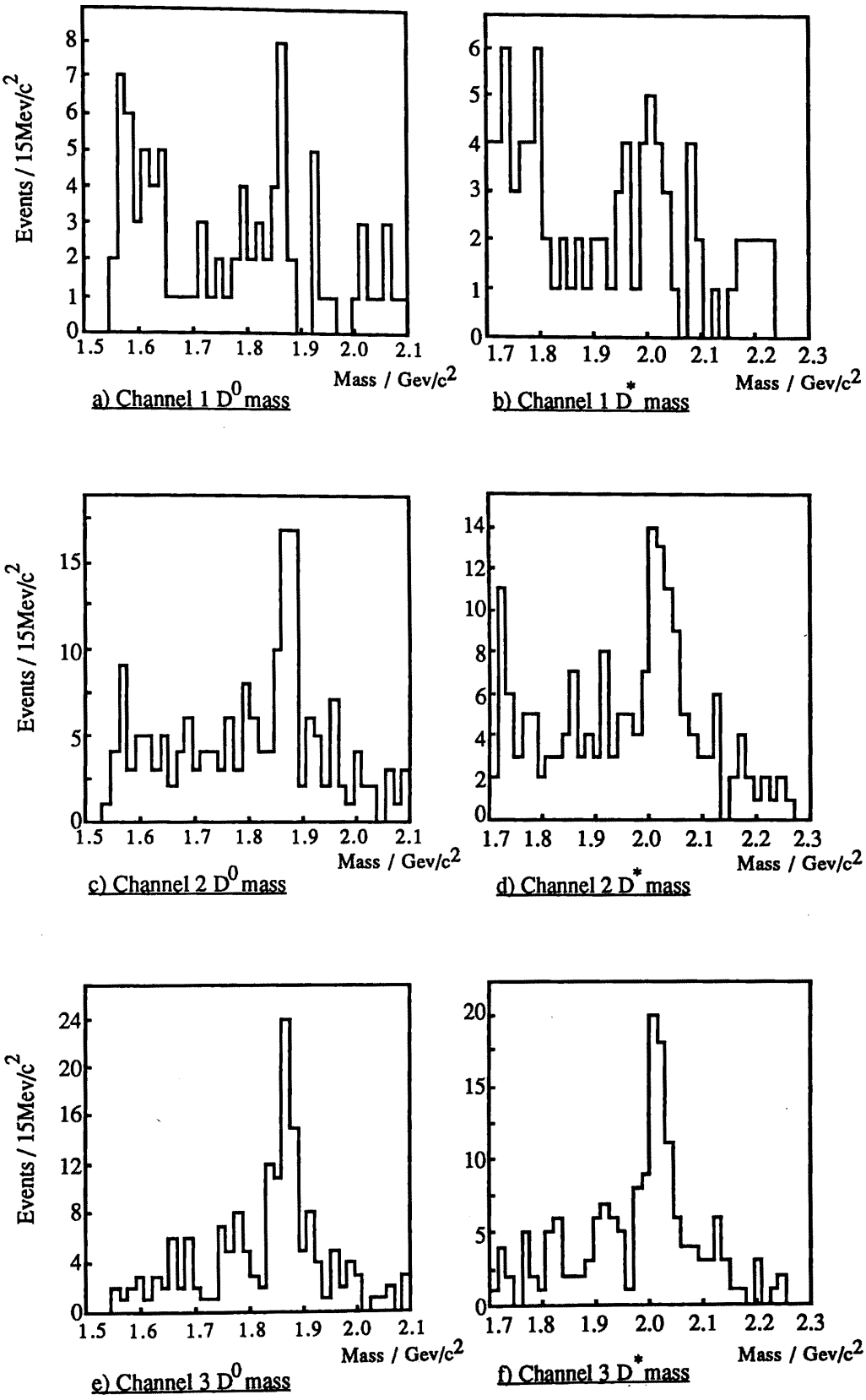

Figure 5.3. Final Mass Plots for Each D Decay Channel

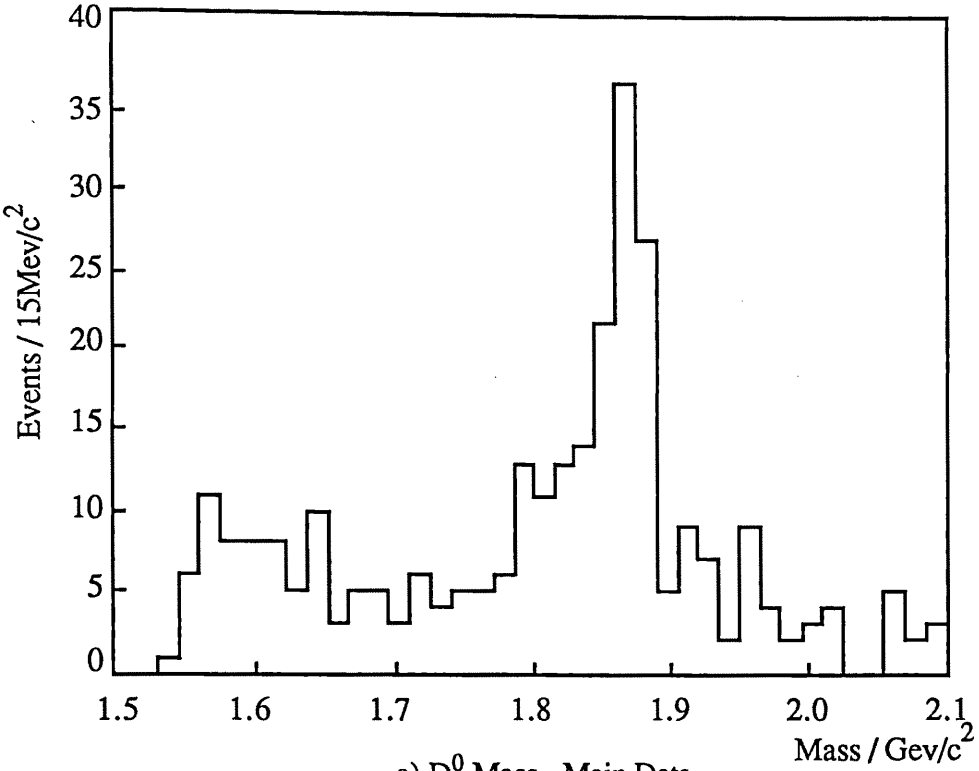

a) D^0 Mass - Main Data

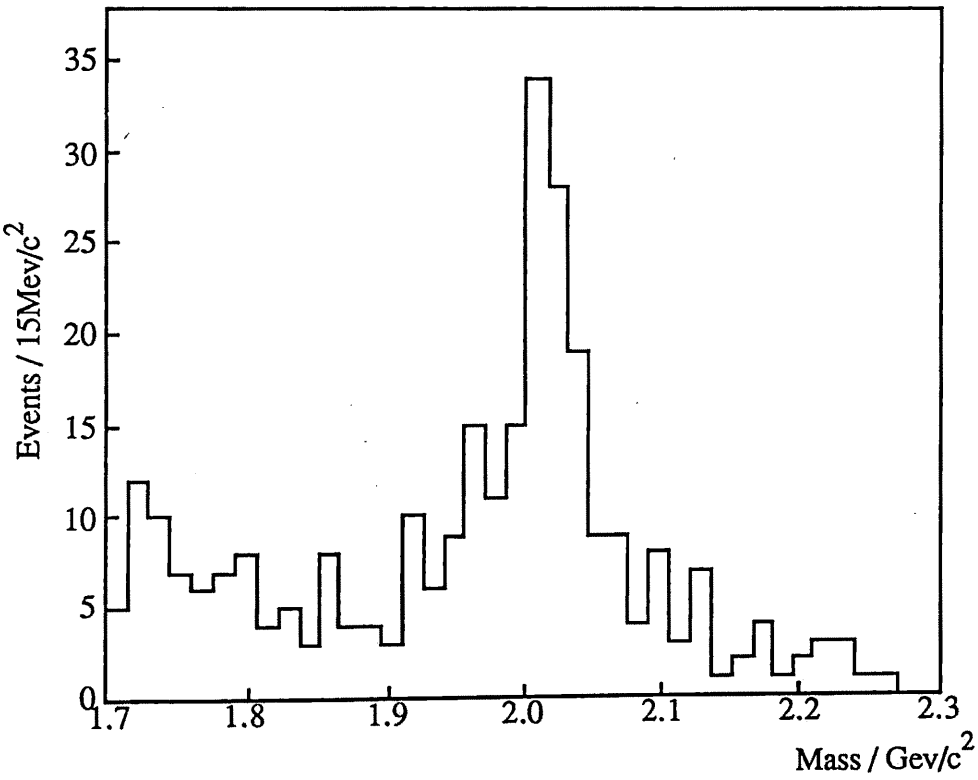

b) D^* Mass - Main Data

Figure 5.4. Final Mass Plots

5.5. Intermediate States

As noted in Section 1.1 there was a high probability for the final state pions and kaon in the $D^0 \rightarrow K^-\pi^+\pi^0$ decay channel to pass through intermediate resonant states (ρ and K^*). Evidence for these resonances is found from Datliz plots with the K and π invariant masses. In these plots the resonances were expected to show up as groupings of events close to the resonance invariant mass. In addition, for particle combinations arbitrarily selected (*i.e* . not through charm decay channels) phase space was expected to uniformaly populate an area of the plot bound by the total invariant mass of the particles. Nonuniform population of this area may be due both to nonuniform phase space acceptance of the spectrometer, and to the particles actually having originated from the decay of a charm particles.

Figure 5.5c shows the Dalitz plot with the invariant mass; $M^2(\pi^+\pi^0)$ and $M^2(K^-\pi^+)$, for the D^0 decays found. For contrast the same plot for particle combinations from non-charm events is shown in Figure 5.5a. The events in Figure 5.5a tend to populate the border of the D invariant mass region and some grouping around the $\rho^+(770)$ invariant mass is evident around $M^2(\pi^+\pi^0) = 0.6 Gev^2/c^4$.

The Dalitz plot for the masses; $M^2(\pi^+\pi^0)$ and $M^2(K^-\pi^0)$ for the D^0 events is shown in Figure 5.5d, with the non-charm mass combinations shown in Figure 5.5b. As above there is some de-population of the central region of the plot. There is little evidence for the $\rho^+(770)$ in this plot. The $K^*(892)$ is also not evident, however some enhancement around $M^2(K^-\pi^0) = 1.8 Gev^2/c^4$ may be seen, corresponding to the $K^*(1430)$.

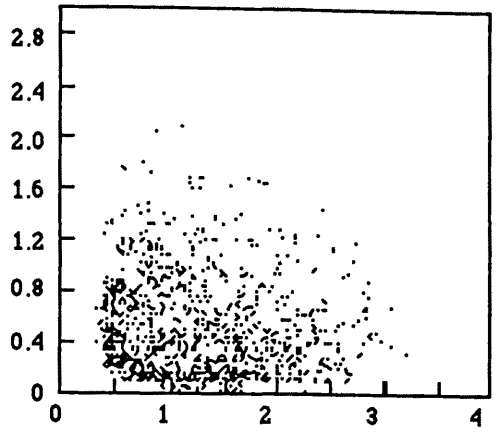

a) Background:
$M^2(\pi^{\pm}\pi^0)$ .v. $M^2(K^{\pm}\pi^{\pm})$

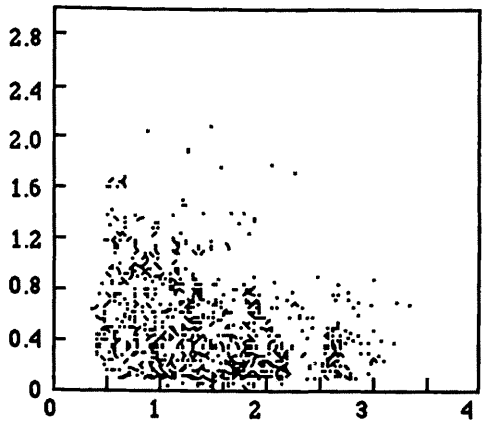

b) Background:
$M^2(\pi^{\pm}\pi^0)$ .v. $M^2(K^{\pm}\pi^0)$

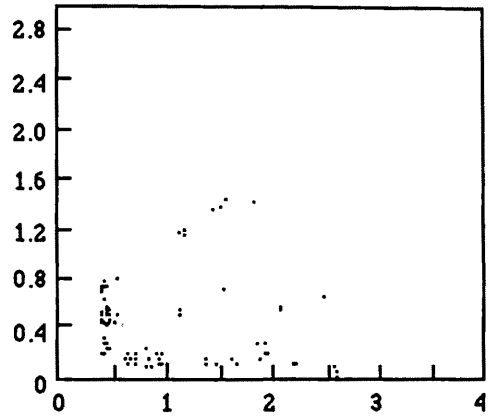

c) D^0 Events:
$M^2(\pi^{\pm}\pi^0)$ .v. $M^2(K^{\pm}\pi^{\pm})$

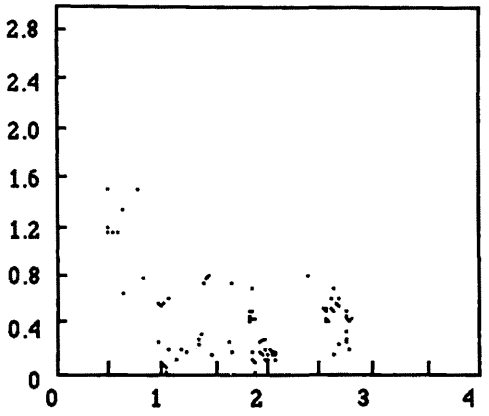

d) D^0 Events:
$M^2(\pi^{\pm}\pi^0)$ .v. $M^2(K^{\pm}\pi^0)$

Figure 5.5. Dalitz plot for D^0 decay

5.6. Control Data

To understand to what degree the data in the above samples had been "invented" by the analysis technique a control data sample was generated. This control sample used the fact that the charges of the D^*, the radiated pion and the kaon are correlated. The charge of the K must be opposite to that of the radiated pion. Decays with these signs the same are either un-physical or cabbibo suppressed given the conjugation of the D^*, *i.e* :

$$D^{*-} \rightarrow D^0 \pi^- \quad (3)$$
$$\hookrightarrow K^- + n\pi$$

and

$$D^{*+} \rightarrow \bar{D}^0 \pi^+ \quad (4)$$
$$\hookrightarrow K^+ + n\pi$$

Where the "$n\pi$" are chosen so as to keep the D neutral. Thus these decays are physical outside of the context of the quark model. There was no reason why combinations of particles compatible with the processes (3) and (4), could not be manufactured by the analysis programmes.

Combinations have been produced for decays with $n\pi = \pi^+$ and $\pi^+\pi^0$. The three charge pion decay channels were disregarded since the natural combinatorial problem illustrated above would permit the allowed D decay channels into the sample. Figure 5.6 shows the D^0 and D^* invariant mass plots for 251 events from the above hypothetical decays. These events are labeled "All" and the statistics for this sample are:

Channel:	$K^-\pi^+$	$K^-\pi^+\pi^0$
No of D^0:	50	48
No of $\bar{D}^0$:	67	86
Total:	117	134

Table 5.5. Control Data Statistics

The events selected this far contained 117 events in common with the main data sample. The invariant mass plots for these events only are shown in Figure 5.6 labled "Only". In this sample of data there are 68 events from channel 1) and 72 from channel 2).

The mass plots centre around the masses of the D and D^*. This was to be expected since for each event the mass combination closest to the D mass was selected. These

plots should be compared with those for the allowed decay channel (Figure 5.4). A clear difference in distribution may be seen.

The number of events in this controll data for each channel were not observed to bare any relation to the expected decay branching ratios of those channels. This was seen to be true for the full data sample and for events selected close to the D^0 invariant mass. This is in contrast with the main data sample which show some relation to the measured branching ratios for each channel.

The relations between the number of events found and the branching ratios and the contrast between the invariant mass distribution of the control data and the main data samples gave some confidance that a sample of D^0 decay events had been found.

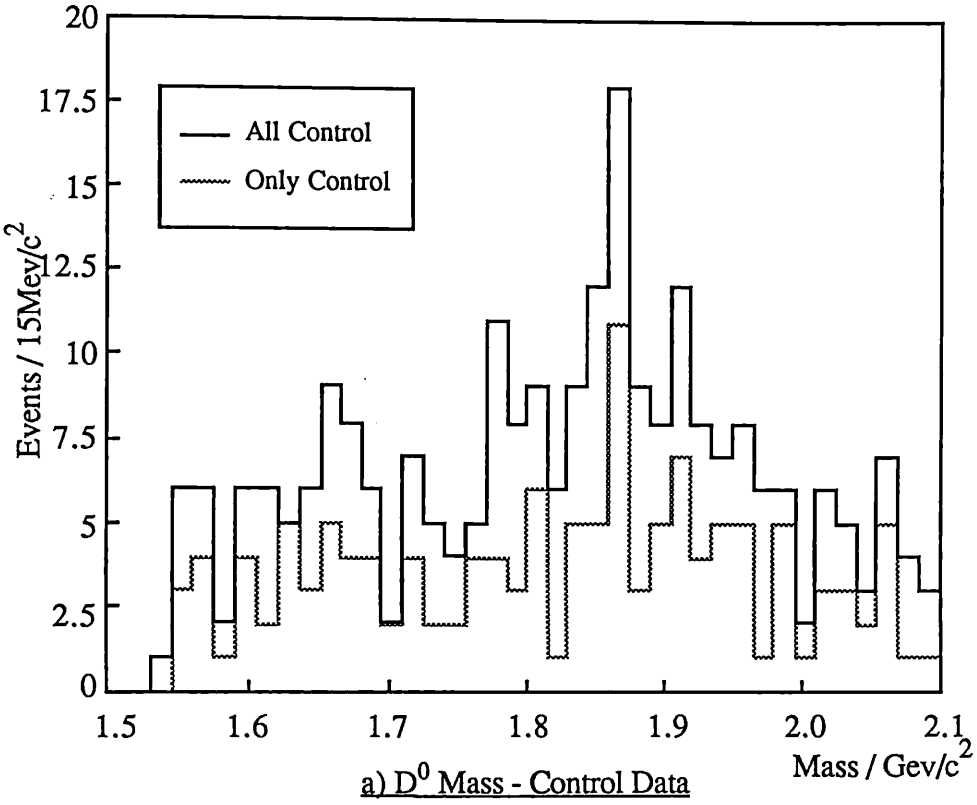

a) D^0 Mass - Control Data

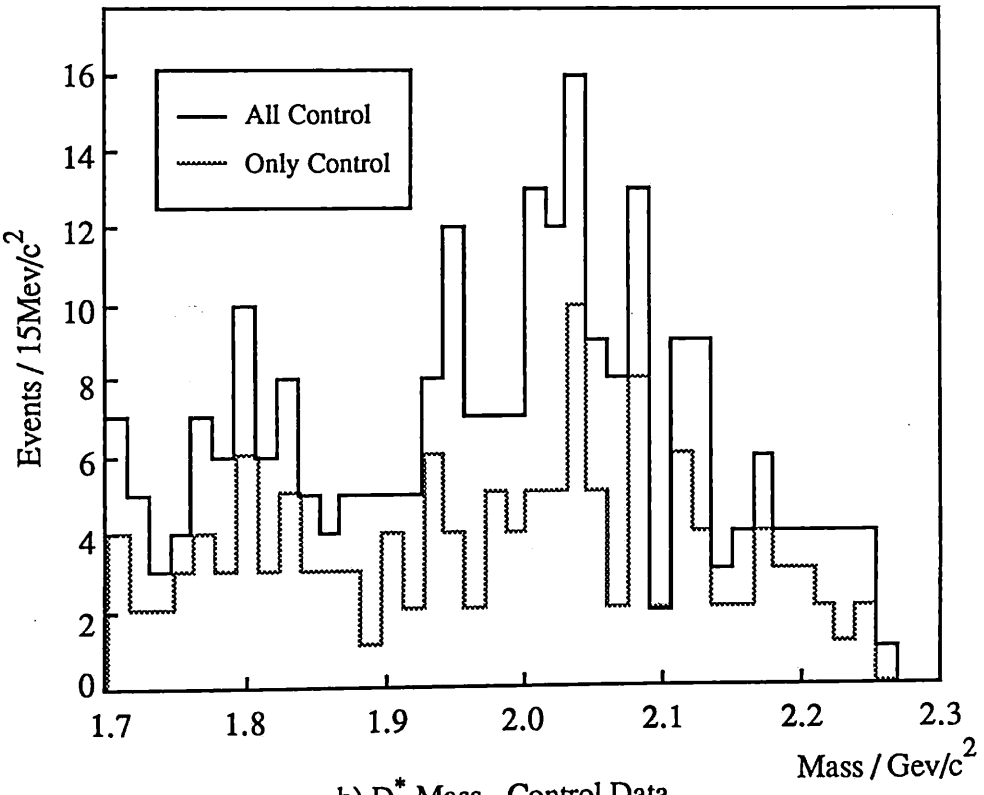

b) D^* Mass - Control Data

Figure 5.6. Control Data Mass Plots

Chapter Six

Lifetime Measurement

A number of techniques may be used to fit a set of data to a given distribution. The principal among these are:

- If an estimator for the distribution exists, this may be used directly.
- A χ^2 fit may be made. The data must be grouped into bins and a fit of the function made minimising the χ^2.
- The likelihood method may be used, if a probability density function exists.

In many situations these methods may be shown to be completely equivalent. If this is not the case it is necessary to choose the most appropriate fitting technique. The method used for calculating the lifetime of the events found determines how the errors on the measurements should be understood. It must be appropriate for the kind and quantity of data found and also yield a result which can be compared with existing measurements.

For exponential decays the estimator is the mean of the distribution $\bar{t}$ since $\bar{t} \equiv \tau$. If the distribution is unbiased in any way, this provides a good value for the proper decay time. In most experiments the distribution of decay times is not unbiased and it is not always obvious that a modified estimator may be found. This method has been used [ABE85] in situations where the bias of each measurement was known. However if the observed distribution is known not to cover the full range of the exponential distribution due to effects of resolution and sensitive lengths, the estimator may not be used.

In the χ^2 test an estimate for the lifetime τ is found by finding stationary values for the function:

$$\chi^2 = \left(\frac{P(t,\tau) - O(t)}{\sigma_t} \right)^2 \qquad (6.1)$$

Where $P(t;\tau)$ is the probability of observing $O(t)$ events at decay time t given a lifetime τ, and σ_t is the error on the value of $O(t)$. It is thus necessary to group the observations into binned intervals in order to have a value for $O(t)$. This loss of information may impair a measurement when the statistics are in any case small.

The likelihood method [EDWARDS, FRODESEN, KALBLEISHC/2] has become widely used by lifetime experiments. In the Likelihood fit each data is used individually thus not leading to the loss of information found in the χ^2 method.

6.1. Maximum -Likelihood Estimator

The use of the likelihood method requires maximization of the function L(x,y) with respect to y, where y parameterises the theory or hypothesis for the distribution of the set {x} of n measurements. L(x,y) is defined as:

$$L(x,y) = \prod_{i=1}^{i=n} P(x_i,y) \qquad (6.2)$$

Where $P(x_i,y)$ is the probability density function (P.D.F.) of an event i having the value x_i given the hypothesis y.

If $P(x_i,y)$ has a first and second derivative, the maxima of L(x,y) may be found by calculating the value of y for at which the score of L(x,y) is zero. The score of a likelihood function S(x,y) is defined as the first derivative of L(x,y) , L'(x,y) .

For computational reasons the natural log of L(x,y) is often used. This is called the support function l(x,y) = Ln(L(x,y)), and is defined by:

$$l(x,y) = \sum_{i=1}^{i=n} Ln(P(x_i,y)) \qquad (6.3)$$

The score s(x,y) is defined for the support function, if the natural log of the probability has a first derivative.

6.1.1. The Statistical Error

For a given estimate of the paramater y for data {x} a coverage probability CP is defined for interval [A,B] which is the probability that the true value of y falls between the limits A and B. In terms of the likelihood function, the probability that the parameter has the value A given the true parameter y, is given by:

$$P(A;x) = \frac{L(x,y)}{L(x,A)} \qquad (6.4)$$

Thus, given the function L(x,y), either the limits [A,B] may be calculated to give a fixed coverage probability (*e.g.* 95%) or these limits may be fixed and the coverage probability calculated.

For a normal distribution the limits [A,B] corresponding to P(A;x) = P(B;x) = 1.96 gives a 95% coverage probability. In this way the coverage probability may be related to the σ statistic of normal distributions. The 95% coverage probability corresponding to the two standard deviation limits. In the discussion below for each fit made using the likelihood function the limits A and B are quoted for this 95% interval.

6.1.2. The Exponential Decay

The probability for a particle with lifetime t to decay within a time ∂t is $\frac{1}{\tau}\partial t$ and for exponential decay lifetimes the probability that a particle will decay at time t_i is $e^{-t/\tau}$. Combining these gives the P.D.F. for a particle decaying at time t_i :

$$P(t_i,\tau) = \frac{1}{\tau} e^{-t/\tau} \qquad (6.5)$$

This formula depends on being able to measure the lifetimes of all particles for t_i arbitrarily close to zero. This is not in practice the case, and the lower bound must be set to some finite small value t_{min}. Similarly, lifetimes cannot be measured above a given finite time t_{max}. The values for t_{min} and t_{max} will, in practice, be event dependent and I have omitted the index. The P.D.F. $P(t_i,\tau)$ can redefine to be zero outside these limits giving the new P.D.F. :

$$P(t_i,\tau) = \frac{\frac{1}{\tau} e^{-t_i/\tau}}{\frac{1}{\tau}\int_{t=t_{min}}^{t=t_{max}} e^{-t/\tau}\,dt} \qquad (6.6)$$

Integrating this over t gives:

$$P(t_i,t) = \frac{\frac{1}{\tau} e^{-t_i/\tau}}{e^{-t_{min}/\tau} - e^{-t_{max}/\tau}} \qquad (6.7)$$

and the support function for n lifetime measurements is given by:

$$l(t_i,\tau) = \sum_{i=1}^{i=n} -\ln(\tau) - \frac{t_i}{\tau} - \ln\left(e^{-t_{min}/\tau} - e^{-t_{max}/\tau}\right) \qquad (6.8)$$

If the values of t_{min} and t_{max} were constant the score for $l(t_i,\tau)$ would be well defined in terms of t_i. t_{min} and t_{max} are defined as follows: Given that particle D_i is first detected at position x_i in the target, decays at position y_i and has a velocity V_i. The particle thus travels a distance ∂x_i. The resolution of the target, in terms of length is x_s and the target has a total length of x_L. Then:

$$t_{min} = (x_i - x_s) / V_i \tag{6.9}$$

$$t_{max} = (x_L - x_i) / V_i \tag{6.10}$$

These variables are different per event, and the support function is not easily solved analytically. To compute the support and likelihood values, and to find their minima, non-analytic computer techniques are used. The values of t_{min} and t_{max} are dictated primarily by the target analysis programme and the geometry of the target. The target analysis programme takes groups of three strips to establish a pulse height and smooth statistical and mechanical effects giving a minimum resolution of three strips for the part of the target in which a decay is found. The value of t_{min} is thus calculated using three strips for x_s. To establish a level the target analysis requires four or five strips giving the target as a whole a reduced length since the final decay must happen some distance before the end of the target for the decay products to be measurable. The value of t_{max} is calculated with x_L taken at six strips back from the end of the target.

6.1.3. Decay Time Precision

The error on a decay time measurement may be calculated from the normal relation between decay distance, velocity and decay time $t = L/V$, with L the decay length and V the velocity. From this relation the relation 6.11. may be formed:

$$\frac{\sigma_t^2}{t^2} = \frac{\sigma_L^2}{L^2} + \frac{\sigma_V^2}{V^2} \tag{6.11}$$

The error on the decay length is given by the resolution of the target. This may be taken as 3 times the pitch of the target, the factor of 3 arising from the target analysis programme needing to group triplets of target strips for pattern recognition. For a measurement of a decay distance at the start and end, totally within the germanium, σ_t is given by:

$$\sigma_L = \sqrt{2} \cdot 3 \cdot 50\mu m \tag{6.12}$$

For an example decay distance of 50 germanium target strips the contribution to (6.11) would be:

$$\frac{\sigma_L}{L} = 0.08 \qquad (6.13)$$

The contribution from the velocity or momentum component is harder to estimate due to the mixture of neutral and charged particles used to reconstruct the D mesons. For a simple decay configuration with n charged particles the total momentum resolution is given by:

$$\frac{\sigma_P}{P} = \sqrt{n} \cdot 0.01 \qquad (6.14)$$

Where the value of 0.01 is the 1% resolution for charge tracking. Using (6.13) and (6.14) an approximate value for (6.11) may be given of:

$$\frac{\sigma_t}{t} \approx 9\% \qquad (6.15)$$

6.1.4. A χ^2 Fit to the Data

As discussed above, to calculate the χ^2 of the P.D.F. of the exponential distribution to a sample of data the data must be grouped into time "bins". The probability distribution of a decay occurring within a bin of width Δt at time t is described by the poisson distribution with mean = variance = $\frac{1}{\tau}$ [KALBFLEISCH/1]. For a lifetime distribution the variance used in a χ^2 calculation (σ^2) may be approximated by the mean number of events in each bin only if the number of events is greater than four, under which condition the poisson distribution tends toward the normal distribution by the central limit theorem.

In the lifetime plots given below, the bin widths are of the same size unless they would contain less than 5 events. In this case the points are rebinned.

6.2. Lifetime Fit to Data

The D^0 events discussed in Chapter 5 were used with the likelihood fit to calculate the lifetime τ_D. A selection of these events was made by cutting on the D^0 mass peak. A selection was also made of events for those which could be used in a likelihood lifetime fit with respect to the values of t_{min} and t_{max}. For each event the proper decay time was calculated from the reconstructed momentum and a decay distance given by the length of the first decay seen in the target. This choice of which decay distance to use gave rise to some background measurements. The effect of this is discussed in later sections.

There were sufficient events in each of channels 1), 2) and 3) as shown in Table 5.3 to calculate a lifetime τ_D for each of the channels separately. This provided a cross check on the coherence of the data sample.

6.2.1. Final Data Selection

For the sample of events shown in Table 5.3 values of t_{min} and t_{max} were calculated using equations (6.9) and (6.10). t_{min} is calculated with a proper distance of three strips from the first decay point and t_{max} was calculated using the proper distance from the first decay point to five target strips from the end of the target. These values of t_{min} and t_{max} were dictated by the characteristics of the target analysis programmes. The lengths used to calculate these parameters represent the limits on the acceptance of the target, the effect of the acceptance of the target is discussed below.

Events were then rejected for which the values of t_i, t_{min} and t_{max} were not compatible. This gives the following statistics for the 291 events in the total data sample:

Channel:	$K^-\pi^+$	$K^-\pi^+\pi^0$	$K^-\pi^+\pi^-\pi^+$
No of D^0:	32	72	20
No of $\bar{D}^0$:	41	71	45
Total:	73	143	45

Table 6.1. Final Event Statistics With t_{min} Cut

Taking into consideration the small mass shift of decay channel 2) a cut of $\pm 0.03 Gev/c^2$ is made about the D^0 mass for each decay channel. This left 100 events in the total D^0 data sample:

Channel:	$K^-\pi^+$	$K^-\pi^+\pi^0$	$K^-\pi^+\pi^-\pi^+$
No of D^0:	5	20	15
No of $\bar{D}^0$:	9	20	31
Total:	14	40	46

Table 6.2. Final Lifetime Event Statistics

6.2.2. Lifetime Fit

The lifetimes of the D^0 events of Table 6.2 were measured using the likelihood fit of equation (6.8). Making the fit for each of the final D^0 data decay channels separately gives the following lifetimes τ_D:

$K^-\pi^+$ Channel Only:	$\tau_D = (3.1\ ^{+2.1}_{-0.9}) \cdot 10^{-13}$
$K^-\pi^+\pi^0$ Channel Only:	$\tau_D = (3.8\ ^{+0.9}_{-0.6}) \cdot 10^{-13}$
$K^-\pi^+\pi^-\pi^+$ Channel Only:	$\tau_D = (3.5\ ^{+0.8}_{-0.6}) \cdot 10^{-13}$

These lifetimes are comparable with each other given the statistical errors. The events used may be merged and an overall lifetime fitted.

All Events:	$\tau_D = (3.6\ ^{+0.5}_{-0.4}) \cdot 10^{-13}$

The distribution of proper decay times for these 100 events is shown in Figure 6.1.

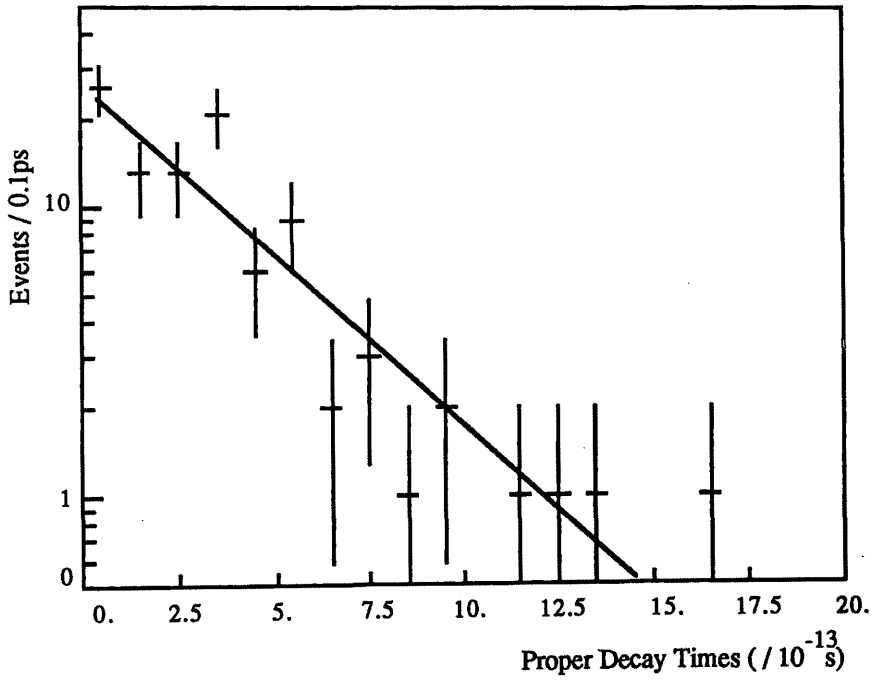

Figure 6.1. Proper Decay Times of the Final Data Sample

The final eight bins of Figure 6.1. contain less than five entries each. To calculate the goodness of the likelihood fit to this data by use of the χ^2 it was necessary to rebin these points. The rebinned plot of the proper decay times is shown in Figure 6.2.

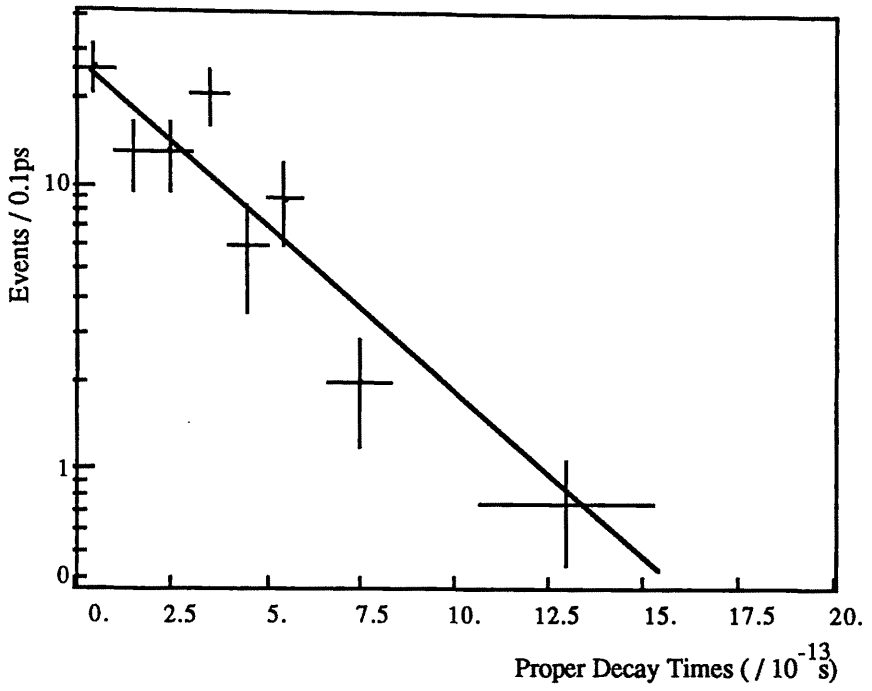

Figure 6.2. Re-Binned Proper Decay Times of the Final Data Sample

The χ^2 for the above fitted lifetime was calculated as 15.2 for the plot in Figure 6.2. There are eight points in this plot leaving seven degrees of freedom for the fit. The confidence level for this value of χ^2 is 5%. This is compatible with the statistical error from the likelihood fit.

The exponential distribution has the property that it is *memoryless* [KALBFLRISCH/1]. That is, a constant value may be subtracted from each point without varying the actual exponential decay distribution *i.e.* the lifetime stays the same. For each event used in the likelihood fit a minimum decay time t_{min} was determined as representing the smallest possible decay time detectable. This value also represents an offset from the true start time for timing the particles proper decay time. Thus the proper quantity to plot is $t-t_{min}$ where t is the measured decay time. This quantity represents the recordable decay time of a given particle.

As discussed above t_{min} is event dependant. In Figure 6.3. the plot of $t-t_{min}$ is shown for the final data sample.

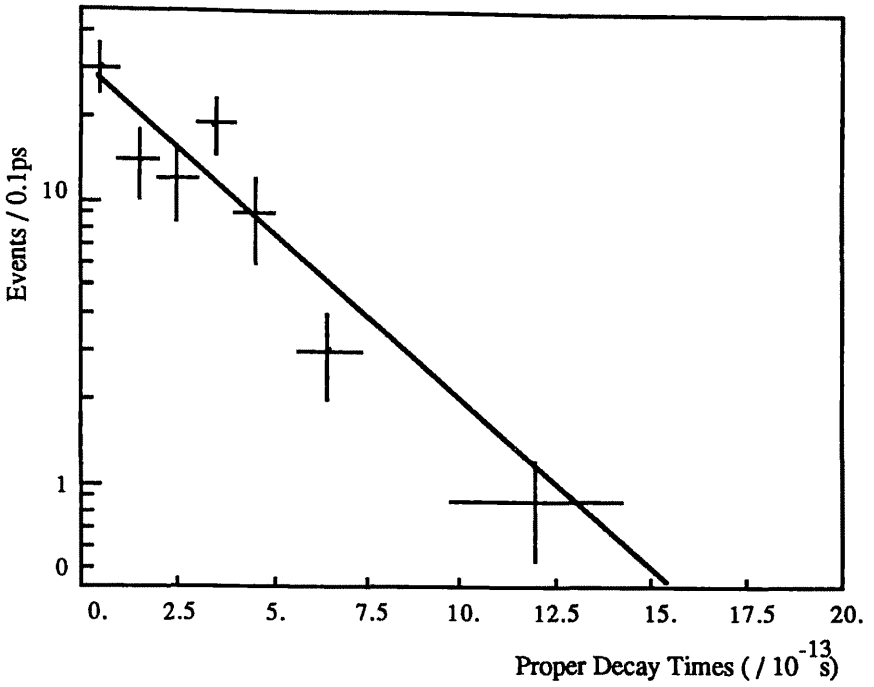

Figure 6.3. Plot of $t-t_{min}$ for The Final Data Sample

The χ^2 for the fitted decay time for Figure 6.3. is 13.1 for seven bins representing six degrees of freedom. This represents a confidence level of 4%.

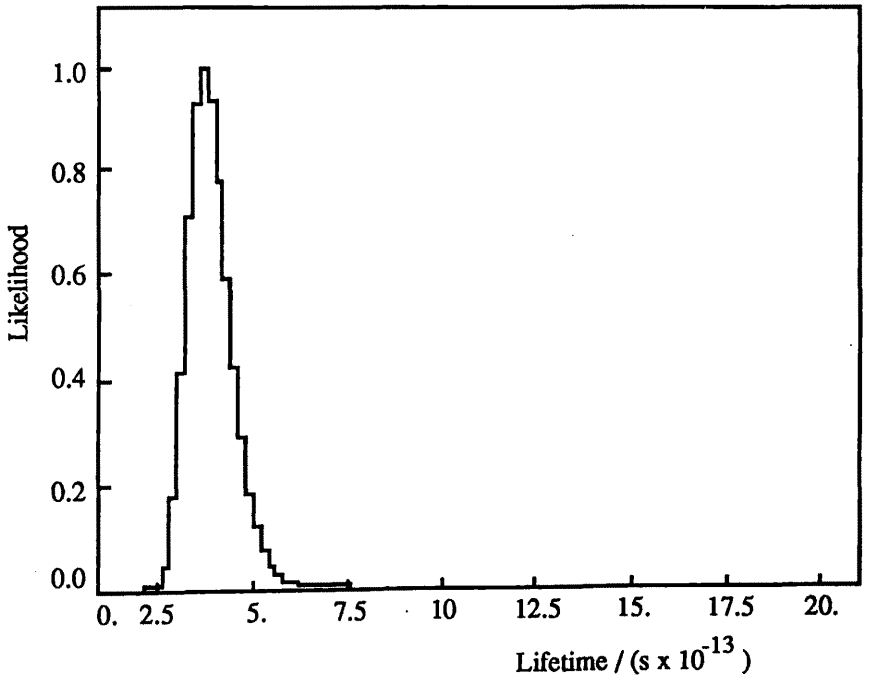

Figure 6.4. Likelihood Distribution for Final Data Sample

6.2.3. The Support for the Exponential Fit

The statistical error for the lifetime fit was derived from the coverage limits for the likelihood distribution. This distribution is shown in Figure 6.4. The distribution has been normalised to the maximum likelihood since the values of the likelihood calculated are only defined to an aribtrary constant.

The support distribution is often shown instead of the likelihood distribution. Being a Log function, it varies slower than the likelihood distribution and the coverage intervals may be gauged more easily. The support distribution corresponding to the likelihood distribution of Figure 6.4. is shown in Figure 6.5.

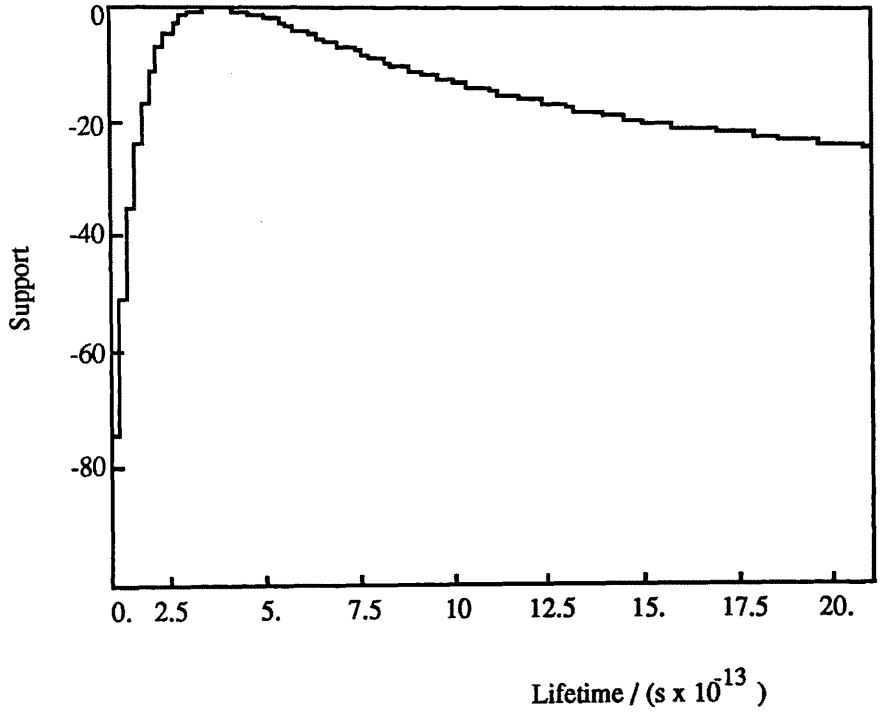

Figure 6.5. Support Distribution for Final Data Sample

6.3. Background Events

There are two main mechanisms by which some of the measurements in the final data sample above may not be of D^0 decays:

- Bad Target Events: Some of the target events may have been erroneously identified by the target analysis program.
- Background D^0 Events: There may have been mass combinations generated which were not of D^0 mesons.

In addition, the measurements used may be wrong either through misassociation found between decay particle and measured decay length, or by the kinematics of the reconstructed charm particle being badly measured.

6.3.1. Background Target Events

To this point the selection of the target analysis programmes have been taken as "true". As discussed in Section 4.6 around 10% of events passed by these programmes are likely to be badly analysed. The target distribution for the above 100 events were scanned with the same criteria used in Section 4.6 and events which were seen to be totally incompatible with the analysis programmes results were rejected. This gives a scanned data sample with 90 events left:

Channel:	$K^-\pi^+$	$K^-\pi^+\pi^0$	$K^-\pi^+\pi^-\pi^+$
No of D^0:	4	17	15
No of $\bar{D}^0$:	7	18	29
Total:	11	35	44

Table 6.3. Final Lifetime Event Statistics After Target Scan

The data of the events left in this and the un-scanned data samples are compatible with the known branching ratios. They are also internally consistent to the extent that there are the same number of D candidates as $\bar{D}$ candidates to within the statistical limits of the size of the data samples.

This data contained the 10 events rejected by an eye scan of the target. The events rejected by this scan comprise only one set of kinds of events badly interpreted by the target. Other kinds of bad target analysis may not be rejected by hand since this could

not be done without bias. To help in understanding the effect of bad target events the lifetime measured above may be compared with that of the 90 events remaining after eye scanning in Table 6.3. Applying the likelihood fit to these 90 events gives the lifetime:

Eye Scaned Data: $\tau_D = (3.7\ ^{+0.6}_{-0.5}) \cdot 10^{-13}$

The lifetimes for the individual decay channels showed only small variance from those quoted above. This result is not significantly different to that of the previous fit to the full 100 events. However, the data in this sample contains significantly less background. The proper decay times for this subgroup of data is shown in Figure 6.6.

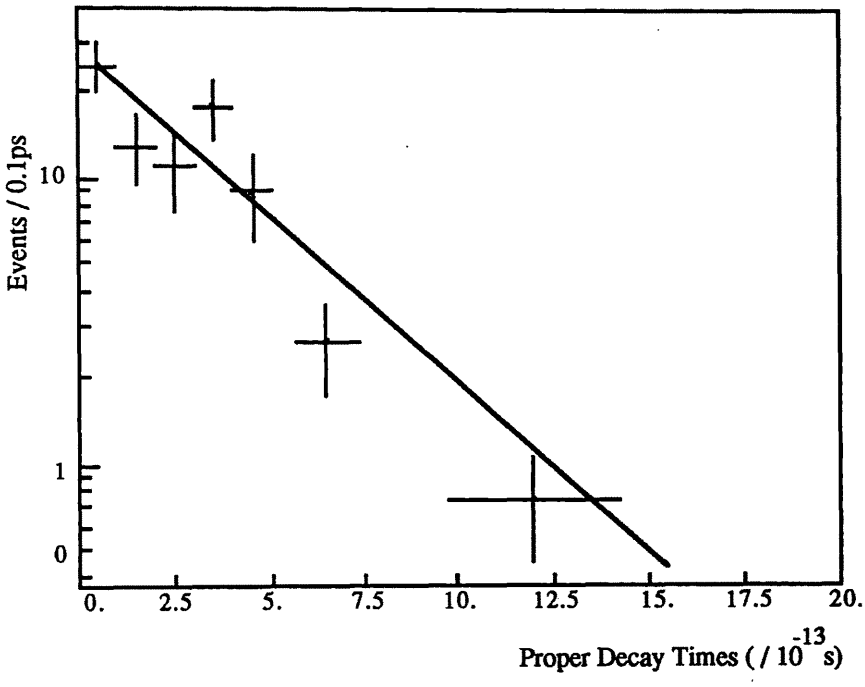

Figure 6.6. Final Proper Decay Time Distribution After Target Scan

The background selected by target scanning was only one possible kind of bad target analysis. The conclusion from the comparison of the lifetime fit from this set of data and from the full data sample is that this source of background has little effect on the lifetime distributions found.

6.3.2. Background D Events in the Selection

From the mass plot in Figure 5.5 a background of 14% of events was estimated. This would give 14 events under the mass peak which was cut around to give the final selection of data. The effect of this background was estimated by considering the events in Figure 5.5 which fall away from the mass peak itself. If all 291 events are used in a likelihood fit a lifetime of:

All Events $\tau_D = (4.4 ^{+0.4}_{-0.4}) \cdot 10^{-13}$

is found. This lifetime was not significantly different to that found in the above fits. The errors from the likelihood 95% confidence level were small and this was due to the high statistics used. The χ^2 for this fit was 55.5 for 11 degrees of freedom. This corresponded to a confidence limit of 0.001%. This is to be compared with the χ^2 confidence limit of 5% for the 100 events fit above.

Data was selected from the tails of the mass distribution and the lifetime found. The mass cuts used here were selected so that the number of events selected was compatible with the final data sample but did not contain events from within the D^0 mass peak. The fit statistics for the tails were:

- Low tail at (1.63 ± 0.1)Gev/c^2:
  - $\tau = (4.9^{+1.1}_{-0.8}) \cdot 10^{-13}$ for 81 Events.
  - $\chi^2 = 28.3$ for 7 degrees of freedom.

- high tail at (2.00 ± 0.1)Gev/c^2
  - $\tau = (5.4^{+1.4}_{-1.0}) \cdot 10^{-13}$ for 51 Events.
  - $\chi^2 = 11.4$ for 6 degrees of freedom.

These lifetimes are compatible with the measured lifetime for the events in the mass peak to within the statistical errors (2σ). The similarity between the lifetimes of the tails and the D mass peak may have been due to the presence of badlly reconstructed D^0 mesons in these regions.

6.3.3. Non-Charm Events: The Control Sample

There was a possibility that the above lifetimes were determined completely by the selection criteria of events and the finite length of the target. To help in understanding these effects for the lifetime measurement, the control sample introduced in Section 5.4. was used. Fitting a value for the lifetime of all 251 events in the control sample gave:

$$\text{All Control} \qquad \tau = (13.4 \, ^{+1.8}_{-1.5}) \cdot 10^{-13}$$

In spite of the increase in statistics of over a factor of 2 in this sample, both the statistical errors and measured lifetime are significantly higher than those of the main data sample. The final analysis made a selection of $\pm 0.03 Gev/c^2$ on the D^0 mass peak. Applying this same cut to the control data gave 46 events with a fitted lifetime of:

$$\text{Control with } \pm 0.03 Gev/c^2 \text{ cut:} \qquad \tau = (11.2^{+3.5}_{-2.3}) \cdot 10^{-13}$$

The statistical errors on this result indicated that almost any lifetime may have been assigned to this data sample. The number of events in this data sample was not the same as the statistics of the main data sample.

To make the number of events similar and thus make a truly comparable lifetime fit to the control data a mass width of $\pm 0.07 Gev/c^2$ was used. This gave 95 events with a fitted lifetime of:

$$\text{Control with } \pm 0.07 Gev/c^2 \text{ cut:} \qquad \tau = (11.6^{+3.6}_{-1.9}) \cdot 10^{-13}$$

The control sample contained 117 events in common with the main data sample. These events have been included in the events used in the above fits. A sample of 90 events may be selected which have no overlap with the main data sample with a mass cut of $\pm 0.17 Gev/c^2$ around the D^0 mass. Fitting the lifetime for these events gave a value of:

$$\text{Exclusive Controll Data:} \qquad \tau = (16.95^{+5.1}_{-3.3}) \cdot 10^{-13}$$

The decay time distribution for this sample of data is shown in Figure 6.6. For comparison with the main data sample the support distribution for this lifetime fit is shown in Figure 6.7. and the likelihood and support plots are shown in Figures 6.8. and 6.9. each of which have the distributions for the main data sample superimposed.

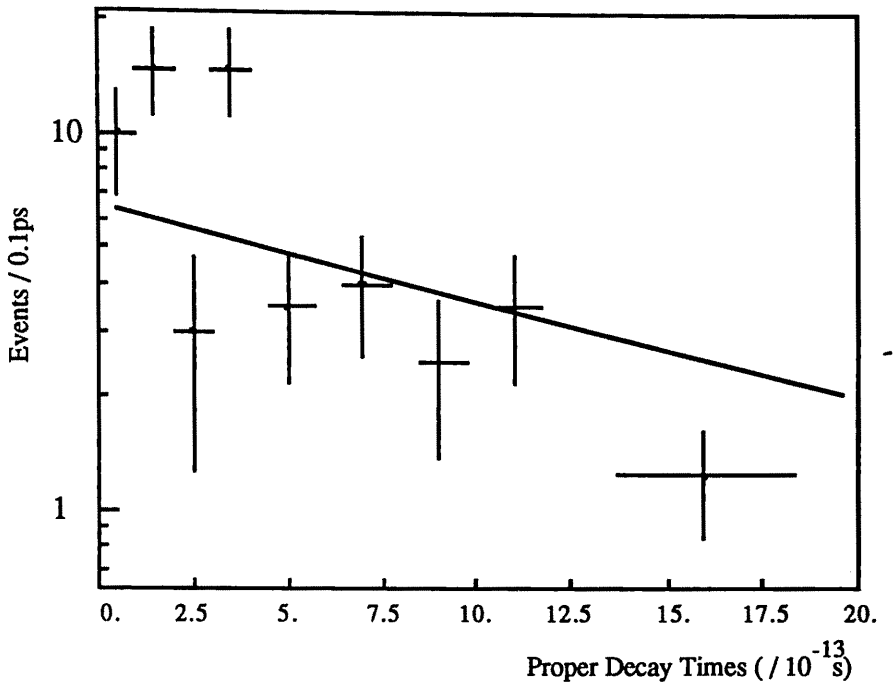

Figure 6.7. Proper Decay Times for Control Data

The poor fit as judged by eye in Figure 6.7. reflects the fact that the data does not follow an exponential distribution. This distorts the fit with respect to the simple exponential P.D.F. (6.5) and further with respect to the normalisatoin used in (6.7).

For lifetimes the control data sample was incompatible with the main data sample and this indicated that the lifetime measured for the D^0 events was not a fabrication of the analysis technique used.

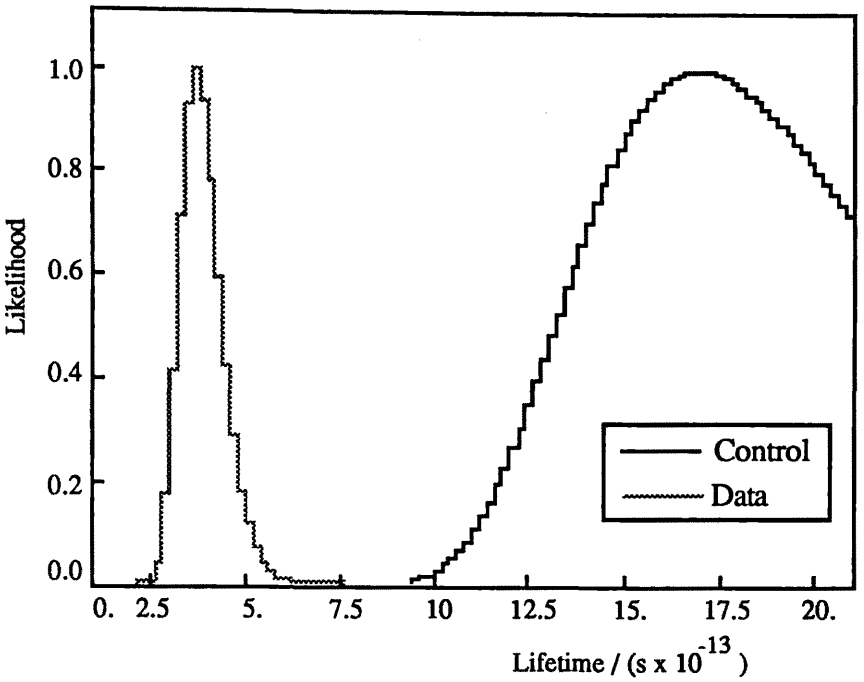

Figure 6.8. Likelihood Distribution for Control Data

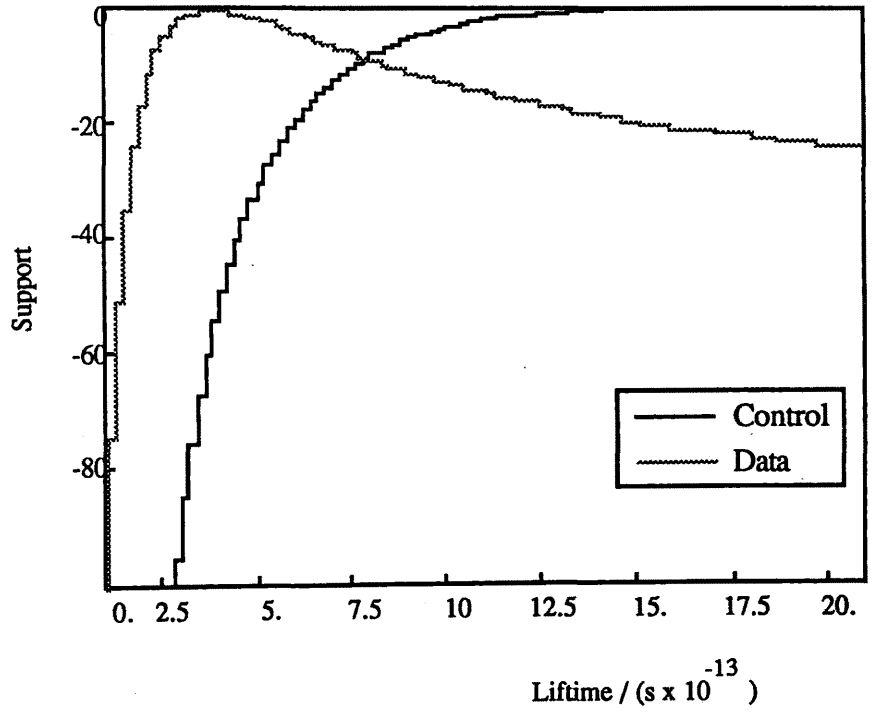

Figure 6.9. Support Distribution for Control Data

6.4. Misassociation of Decay and Reconstructed Particle

In the analysis discussed above the possibility existed that the decay observed and measured in the target was not the decay of the reconstructed D^0 used to provide the Lorenz boost factor. The three most likely ways in which this may have occured were:

1) Production of D^{*-} and D^{*+} giving rise to a $D^0\bar{D}^0$ pair:
   - Total Branching ratio given an identified D^* = 32%

2) Production of D^{*-} and a D^{*+} decaying to a D^0 and a D^-:
   - Total Branching ratio given an identified D^* = 18%
   - Proportion in which the $\bar{D}^-$ decayed first = 5.4%

3) Production of D^{*-} and a D^+:
   - Total Branching ratio given an identified D^* = 50%
   - Proportion in which the D^+ decayed first = 15%

The total branching ratios for these processes were calculated from the known branching ratios of the D^* decays and the assumption that the probability of producing a D^*D^* pair equals that of producing a D^*D^+ combination.

The calculation of the proportion in which the charged D decayed first in cases 2) and 3) was based on a probability of ~0.3 for a particle with lifetime of $9.2 \cdot 10^{-13}$s decaying before one of $4.3 \cdot 10^{-13}$s (the world average D^0 lifetime). This was calculated with a small Monte Carlo programme. For the value of τ_D measured above the probability of the charged D mesons decaying before the D^0 would be ~0.25.

Some effort has been made in understanding case 1 above. Although all three cases constitute a source of error in the lifetime measurement, only case 1 is strictly correlated with the lifetime being fitted.

6.4.1. Case 1: Two Neutral D Mesons

To study this in detail the proper decay times of a number of Monte Carlo events were calculated using, as for the data, the first decay in the target, and the momenta from both the particle which gave rise to that decay, and the particle produced in association. As for the true data no distinction is made between the true and false pairings and just t_1 from the first particle and t_2 from the second particle is used. A graph of each of t_1 plotted against t_2 is shown in Figure 6.10. The points in this graph show no regular deviation from the line $t_1 = t_2$ although the spread of the points gets broader as t_1 (or t_2) increase.

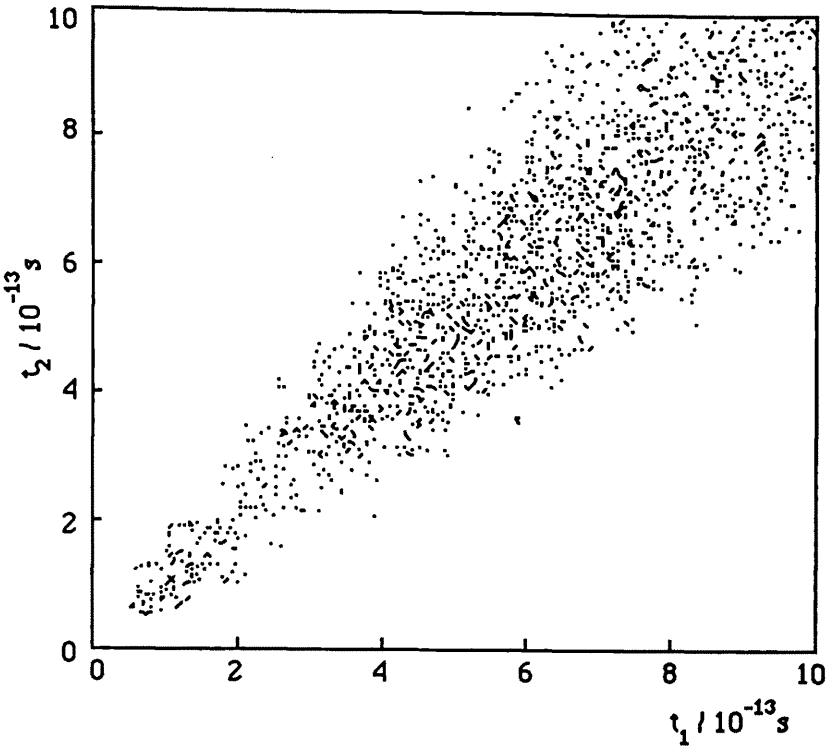

Figure 6.10 Monte Carlo Plot of True and Misassociated Decay Times

To understand the above effect, the widths of the points along sections perpendicular to the line $t_1 = t_2$ were calculated. A graph of these widths σ_{t_a} against $t_a = \frac{1}{2}(t_1 + t_2)$ the average decay time, is shown in Figure 6.11.

The width may be seen to increase linearly with t_a. A linear regression was made on these points giving the fit:

$$\sigma_{t_a} = 0.05 \cdot t_a + 0.07 \qquad (6.16)$$

Neglecting the small offset, the approximate relation may be used:

$$\frac{\sigma_{t_a}}{t_a} = 0.05 \qquad (6.17)$$

This approximate linear dependence of the error produced by case 2) events may be compared to the form of the natural error of the decay time measurements (6.11). The contribution from this effect is of the same order as that given in (6.14).

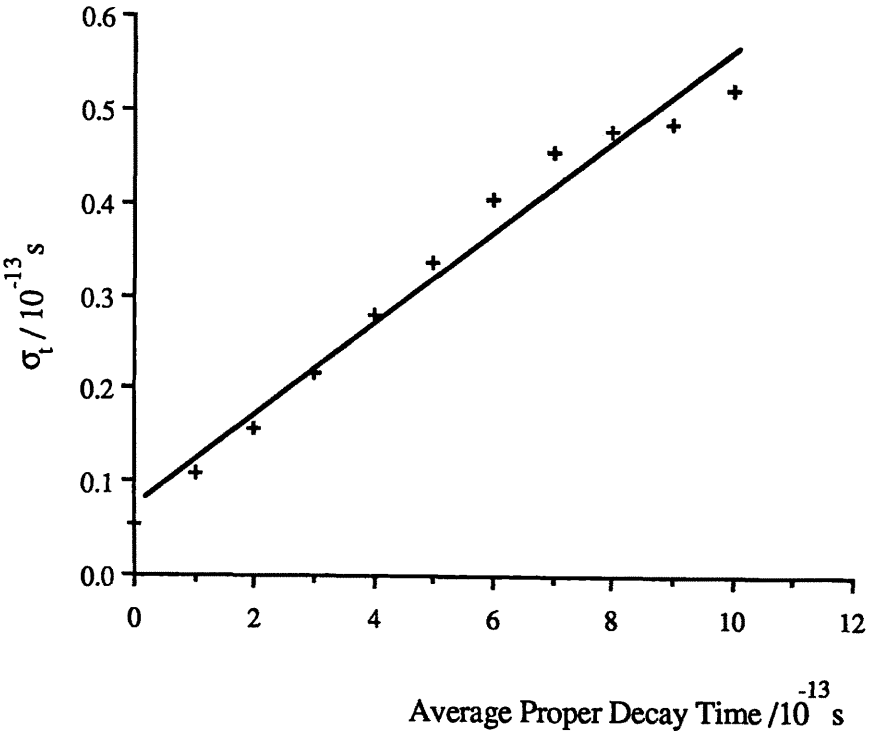

Figure 6.11. Monte Carlo Decay Times Errors

This result may be understood by studying the correlation between the momenta of the two produced D^*s and thus the measured D^0s. The momenta of the two produced D^0 particles each carry an average of 0.4 the photon energy. The spread of this fraction is small for $D^0\bar{D}^0$ production , approximatly 0.4Gev/c (FWHM) for $D^*\bar{D}^*$ production. Thus the momenta of each D^0 is closely correlated and choosing the wrong momenta adds an extra error (either larger or smaller) in addition to the momentum resolution of the spectrometer.

6.4.2. Cases 2 & 3: Mixed Neutral and Charged Decays

From the above discussions in 20.4% of events the charged D meson decayed before the D^0 giving rise to the possibility of measuring the lifetimes of the wrong particles. Of all D^- decay modes 33% give rise to a change in the total charge. Thus in 6.8% of the events used in the lifetime measurements the measured decay length was of a D^- or D^+ decay. This fraction is less than that estimated from the non charm or target background. It was thus felt justified to treat these case 2 and case 3 events as a contribution to background.

6.5. The Overall Effect of Target Resolution and Background

To study the overall effect of the target resolution and background events the target Monte Carlo was used to generate 200 events at a series of lifetimes. These events were passed through the target analysis programmes and a lifetime was fitted. A plot of the lifetimes fitted verse the lifetimes used is shown in Figure 6.12.

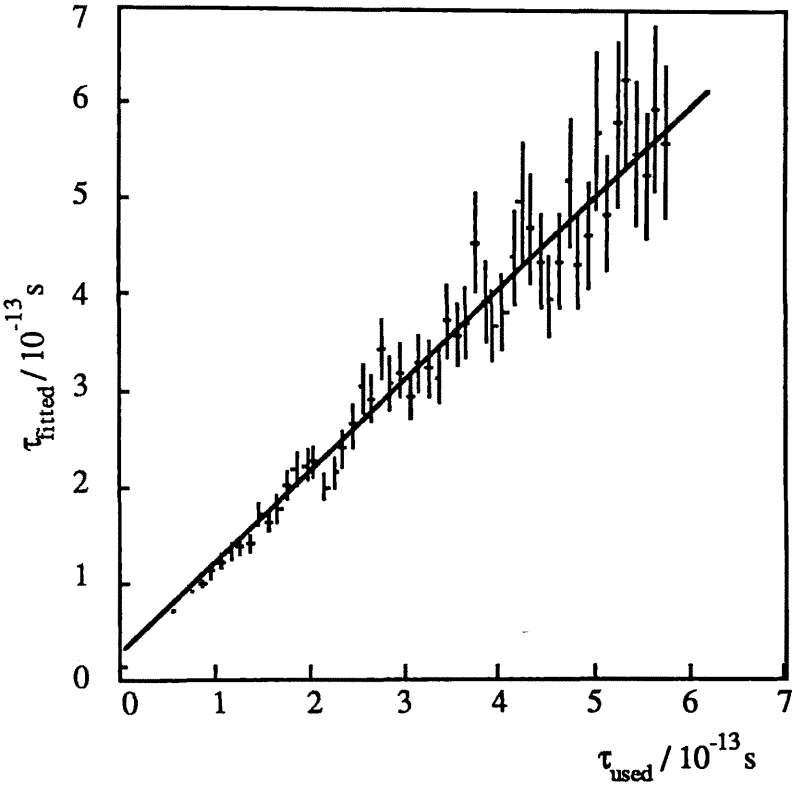

Figure 6.12. Monte Carlo Lifetime Scan

The events used in this study were constrained by the request that the points found by the target analysis programme fell to within 5 target strips of the true position of the decay. This constraint only affected the very short lifetimes. The branching ratios of all D states are used.

To use these results to estimate the effect on the measured lifetime a linear regression fit was made over the range $\tau = 2.5 \cdot 10^{-13}$ to $\tau = 5.5 \cdot 10^{-13}$. The result of this fit is given in Table 6.4. For the parameterisation: $\tau_{found} = a \cdot \tau_{used} + b$.

Parameter	Value	σ	Correlation
a	0.97	0.02	0.97
b	0.09	0.06	0.97

χ^2 for fit:	141.6
Degrees of Freedom:	30

Table 6.4. Fit Parameters For Monte Carlo Lifetime Scan

From this fit a corrected lifetime may be estimated. Using the result from the 90 events of the target scanned data sample with $\tau_D = 3.7$ as a value of τ_{found} gives a value for τ_{used} of 3.7. There is no offset. The error on this value may be calculated from the errors on the linear regression fit giving a value of $\sigma_\tau = \pm 0.2$.

Conclusions

A sample of 90 events containing decays of the D^0 meson has been found. This sample showed internal coherence as the number of events found for each of the decay channels searched was in agreement with published branching ratios for these channels. The possibility of constructing this result by dint of analysis technique used was seen to be small by the use of the kinematically similar control data channels. The number of decays found in the control data for different D decay channels did not match the expected branching ratios. The contrast of the invariant mass distributions of the control data and the main data samples lent extra confidence to the verity of the main data sample and analysis technique.

The measured lifetime of these events was within one standard deviation of most of the past measurements of this value. The lifetimes for each of the decay channels searched was also measured. These lifetimes were found to agree well within the statistical errors and this provided extra confidence in the coherence of the data sample used. The possibility of this lifetime being forced by any kinematic cuts made, either in the analysis or by the acceptance of the spectrometer, was seen to be small by comparing the lifetime of the main data sample with the lifetime measured for the control data sample. These lifetimes are summarised in Table 6.5.

Data Sample	Lifetime / 10^{-13}s	Number of Events
Final:	$3.7\ ^{+0.6}_{-0.5}$	90
$K^-\pi^+$ Only¶:	$3.1\ ^{+2.1}_{-0.9}$	14
$K^-\pi^+\pi^0$ Only¶:	$3.8\ ^{+0.9}_{-0.6}$	40
$K^-\pi^+\pi^-\pi^+$ Only¶:	$3.5\ ^{+0.8}_{-0.6}$	46
Control:	$16.95^{+5.1}_{-3.3}$	90

Table 6.5. Summary of Lifetimes
¶Before Target Visual Selection.

The control data shows that the lifetimes are not forced by either the analysis or overall construction of the experiment. The lifetimes of the events in the tails of the mass plot (Figure 5.4) are not significantly different from those in the main peak. This is not understood and may be due to not fully reconstructed events.

A number of sources of background contributions to the final measurements were considered. These backgrounds may have originated either; from non charm physics, from badly reconstructed target decay lengths or may be due to measuring the wrong decay length in the target. The contributions from the first and second of these was estimated to be small. The contribution to the error from the third of these sources was estimated to be of the same order as other backgrounds for the case when the measured decay was of charged D decay. The effect on the lifetime for the case of measuring the decay of a D^0 which was not the reconstructed particle was seen to have no overall effect on the measured lifetime but lessened the overall precision of the measured proper decay times.

There was no direct contribution to the statistical errors quoted for the final lifetime deriving from the precision of the proper decay time measurements. To understand the effect from the precision of the individual decay time measurements a target simulation programme was used. This study gave an additional error of 5% stemming primarily from the resolution and efficiency of the target and target analysis programmes. This error is quoted as a statistical error in addition to that derived from the lifetime fit techniques used.

Of the three D^0 decay channels considered, the four charge channel (3 above) is the weakest, with little sign of a signal above background in Figure 5.1. The only surety as to the usefulness of the events used from this channel is their coherence with the other channels both in comparison of branching ratios and lifetime.

Due to the preliminary nature of the analysis presented here a number of omissions have been made; no details of the kinematics of the D meson sample has been given, no production cross section is quoted, a number of additional checks on the data have not yet been made and some advanced fitting techniques have not been used. The systematic effects of the selection criteria used and the acceptance of the target and spectrometer has not yet been calculated. This may be estimated by consideration of the variation in lifetimes between individual decay channels since each of these depended on systematic effects in different ways. The total variation between these measurements represents a 20% effect and is thus of the same order as the statistical error quoted.

References

ABE84/1: K.Abe *et al* ., Phys. Rev., D30, 1984.

ABE84/2: K.Abe *et al* ., SLAC-PUB-3493, 1984.

ABE85: K.Abe *et al* ., SLAC-PUB-3722, 1985.

ADEVA81: B.Adeva *et al* ., Phys. Lett., 102B, 1981, P.265.

ADOMOVICH80: M.I.Adomovich *et al* ., Phys. Lett., 89B, 1980, P.427.

AFEK80: Y.Afek, C.Leroy & B.Margolis, Phys. Rev. D, Vol.22, 1980, P.93

AGUILAR83: M.Aguilar-Benitez *et al* ., Phys. Lett., 122B,1983, P.312

AGUILAR84: M.Aguilar-Benitez *et al* ., Rev. Mod. Phys., Vol.56, N^0 2, Part 2, 1984. "Review of Particle Properties"

AGUILAR86: M.Aguilar-Benitez *et al* ., Phys. Lett., 170B, 1986. "Review of Particle Properties"

AITCHISON: I.J.R.Aitchison & A.J.G.Hey, "Gauge Theories in Particle Physics"

ALBINI82: E.Albini *et al* ., Phys. Lett., 110B, 1982, P.339.

ALLASIA80: D.Allasia *et al* ., Nucl. Phys., B176, 1980, P.13

AMENDOLIA74: S.R.Amondolia *et al* ., CERN/SPSC/74-83.

AMENDOLIA79: S.R.Amondolia *et al* .,CERN/SPSC/79-112.

AMENDOLIA80/1: S.R.Amondolia *et al* ., N.I.M., 176, 1980, P.461

AMENDOLIA80/2: S.R.Amondolia *et al* ., Pisa 80-4, May 1980

AMENDOLIA80/3: S.R.Amondolia *et al* ., N.I.M. 206, 1980, P.367

AMENDOLIA80/4: S.R.Amondolia *et al* ., N.I.M. 176, 1980, P.449.

AMENDOLIA82: S.R.Amondolia *et al* ., PPESP/82/4 and CERN/SPSC/82-33.

References

AMENDOLIA83: S.R.Amondolia *et al* ., IEEE Transations on Nuclear Science, Vol. NS-30, N^0.1, 1983

AMENDOLIA84: S.R.Amondolia *et al* ., IEEE Transations on Nuclear Science, Vol. NS-31, N^0.2, 1984

AMENDOLIA86/1: S.R.Amondolia *et al* ., In: 23^{rd} International Conferance on High Energy Physics, Berkely 1986.

AMENDOLIA86/2: S.R.Amondolia *et al* ., Nuc. Phys. B, 277,1986.

ANJOS86: J.C.C. dos Anjos *et al* ., In: Proc. BERKELY conferance 1986

ARMENISE79: N.Armenise *et al* ., Phys. Lett., 86B , 1979, P.115

AUBERT74: J.J.Aubert *et al* ., Phys. Rev. Lett., D12, 1974, P.1884

AUGUSTIN74: J.E.Augustin *et al* ., Phys. Rev. Lett., 33, 1974, P.1406

BARNS70: A.V.Barns *et al* ., Phys. Rev. Lett., 37, 1970, P.76

BAUER78: T.H.Bauer *et al* ., Rev. Modern Phys., V.50, N°2. 1978

BADERTSCHER83: A.Badertscher *et al* ., Phys. Lett., 123B, 1983, P.471

BAILEY85: R.Bailey *et al* ., Zeit. Für Phys. C 28, 1985, P.357

BALLAGH80: H.C.Ballagh *et al* ., Phys. Lett., 89B,1980 , P.423

BALTRUSAITIS85: R.M.Baltrusaitis *et al* ., SLAC-PUB-3861, 1985.

BELLINI82: G.Bellini *et al* ., Phys. Rep., V.83, N^0.1, 1982, 1

BISWAL81: K.Biswal & S.P.Misra, Phys. Rev. D, Vol.24, 1981, P.106

CASO85: C.Caso & M.C.Touboul, CERN/EP 85-176, 1985

CLINE86: David B. Cline, Comments® on Nuclear and Particle Physics V.XVI. Number 3(1986)

CLOSE: F.Close, "An INtroduction to Quarks and Partons"

COWARD85: D.H.Coward, SLAC-PUB-3818, 1985

DAMERELL86 C.J.S.Damerell, RAL 86-077, 1986

References

DOBLE76: N.Doble, "Notes on Beam H4/E4 Used to Transport Electrons for the Production of a Photon Beam", SPS/EA/Note 76/16

EDWARDS: A.W.F. Edwards, "LIKELIHOOD"

ELLIS75: J.Ellis, M.K.Gaillard & D.V.Nanopoulos, Nucl. Phys. B100, 1975, P.313-328

FABJAN85: C.W.Fabjan, CERN-EP/85-54

FONTANNAZ81: M.Fontannaz, B.Pire & D.Schiff, Z.Phys C. 11, 1981, P.211

FORD78: R.L.Ford & W.R.Nelson, SLAC-210 June 1978

FRODESEN: A.G.Frodesen, O.Skjeggestad & H. Tøfte, "Probability and Statistics in Particle Physics"

FUCHI81: H.Fuchi et al, Nuovo Cim., 31,1981, P.199

GILCHRESE86: Gilchrese, International Conferance of HEP, Berkely, 1986

GAILLARD75: M.K.Gaillard, B.W.Lee & J.L.Rosner, Rev. of Modern Physics V.47, No2, April 1975

GEORGI76: H.Georgi, A.De Rújula & S.L.Glashow, Phys. Rev. Lett., Vol.37, P.398, 1976

GLASHOW70: S.L.Glashow, J.Iliopoulos & L.Maiani, Phys. Rev., D2, 1970, P.1285

HOLMES85: S.D.Holmes, Ann. Rev. Nucl. Part. Sci., 35, 1985, P.397

IWASAKI77: Y.Iwasaki, Phys. Rev. D, Vol.17, 1977, P.765

JAMES80: F.James, CERN CC/80/6, 1980

JAMES68: F.James, CERN DD/68-15, 1968

JONES78: L.M.Jones & H.W.Wyld, Phys. Rev. D, Vol.17, 1978, P.759

KALBFLEISCH/1: J.G.Kalbfleishc, "Probability and Statistical Inference", V.1: "Probability"

KALBFLEISCH/2: J.G.Kalbfleishc, "Probability and Statistical Inference", V.2: "Statistical Inference"

KALMUS82: G.Kalmus, RL-82-090, 1982

References

LEADER: E.Leader & E.Predazzi, "An Introduction to Gauge Theories and the New Physics"

LIKHODED81: A.K.Likhoded, S.R.Slabospitsky & A.N.Tolstenkov, IFUE 81-110, Serpukov, 1981

LOHRMANN: E.Lohrmann, DESY report. "Introduction to Photoproduction"

LÜTH85: V.Lüth, CERN-EP/83-142

KÖLBIG83: K.S.Kölbig & B.Schorr, CERN-DD/83/5, 1983

NASH83: T.Nash, In: 1983 International Lepton/Photon Symposium, Cornell University

NIU78: K.Niu, In: Proc. 19th Int. Conf. High Energy Physics, Tokyo 1978, P.371

PALMONARI84: F.Palmonari, Riv. Nuovo Chim., 9, 1984

PAUL85: E.Paul, CERN-EP/85-130, 1983

PERKINS: D.H.Perkins, "Introduction to High Energy Physics"

PETERSON: J.O.Peterson, July 1983. "An Introduction to CAMAC - Hardware and Software Aspects . Notes for Summer Students"

POINTING: P.J.Pointing, CERN-EP/80-01

PRENTICE79: J.D.Prentice, In: Proc.Int.Symp. Lepton & Photon Interactions in HEP, 1979. P.563

REEDER79: D.D.Reader, In: Proc.Int.Symp. Lepton & Photon Interactions in HEP, 1979. P.553

ROBERTS86: K.Roberts, Ph.D. Theseis, Liverpool University. 1986

ROSSI52: B.Rossi, "High-Energy Particles", 1952, P.50

SACTION78: J.Saction, In: Proc. 19th Int. Conf. High Energy Physics, Tokyo, 1978, P.374

SCHINDLER81: R.H.Schindler *et al* ., Phys. Rev. 24D, 1981, P.78

SEEBRUNNER84: H.Seebrunner, In: Proc. Nineteenth Rencontre De Moriond, Vol. 2, 1984

References

STODOLSKY67: L.Stodolsky, Phys. Rev. Lett. N°18, 1967, P.135

TRILLING81: G.H.Trilling, Phys. Rep., 75, N^0.2, 1981, P.57

USHIDA80: N.Ushida *et al* ., Phys. Rev. Lett., 45, 1980, P.1049 & 1053

USHIDA82/1: N.Ushida *et al* ., Phys. Rev. Lett., 48, 1982, P.844

USHIDA82/2: N.Ushida *et al* ., In: Int. Conf. High Energy Physics, Paris 1982

VAVILOV57: P.V.Vavilov, Zch, Für Expr. Teor. Fiz. V.32, 1957

VOYVIDIC79: L.Voyvidic, In: Proc.Int.Symp. Lepton & Photon Interactions in HEP, 1979. P.569